This dissertation has been
microfilmed exactly as received 67-3977

MERRITT Jr., Harry Warner, 1934-
GAS ABSORPTION INTO THIN WAVY LAMINAR LIQUID FILMS FALLING DOWN INCLINED PLANES.

The University of Oklahoma, Ph.D., 1967
Engineering, chemical

University Microfilms, Inc., Ann Arbor, Michigan

Downloaded from SHAREOK. Persistent Handle URL: https://hdl.handle.net/11244/2134

THE UNIVERSITY OF OKLAHOMA

GRADUATE COLLEGE

GAS ABSORPTION INTO THIN WAVY LAMINAR LIQUID FILMS FALLING DOWN INCLINED PLANES

A DISSERTATION

SUBMITTED TO THE GRADUATE FACULTY

in partial fulfillment of the requirements for the degree of

DOCTOR OF PHILOSOPHY

BY

HARRY WARNER MERRITT JR.

Norman, Oklahoma

1966

GAS ABSORPTION INTO THIN WAVY LAMINAR LIQUID

FILMS FALLING DOWN INCLINED PLANES

APPROVED BY

Orrin K. Crosser

C. M. Sliepcevich

W. J. Saucier

F. Mark Townsend

M. L. M. Irvine

DISSERTATION COMMITTEE

ACKNOWLEDGEMENTS

I wish to express my appreciation to Dr. O. K. Crosser who gave so freely of his time, particularly in the latter stages of this work, when he was burdened with other commitments. His advice and confidence have been a valuable encouragement to me during the course of this endeavor.

I also wish to express my thanks to Dr. C. M. Sliepcevich for his assistance during the completion of my thesis and to the other members of my doctoral committee, Drs. C. P. Colver, M. L. McGuire and W. J. Saucier.

I am indebted to the other faculty members at the University of Oklahoma, as well as my fellow graduate students, particularly F. E. Merliss and L. E. Trimble, whose interest was of great benefit to me during this investigation.

I am grateful to the various industrial and governmental organizations who provided partial financial assistance over the course of this research and wish to acknowledge their support. Among these are the Continental Oil Company and Cities Service Research and Development Company who each contributed a fellowship toward my support. The support of the National Science Foundation, through the summer fellowships for teaching assistants and grant, GP-527, was indispensable.

TABLE OF CONTENTS

Page

LIST OF TABLES v

LIST OF ILLUSTRATIONS. vi

Chapter

I. SUMMARY 1

II. INTRODUCTION. 3

III. THEORETICAL DEVELOPMENT 23

IV. APPARATUS AND OPERATING PROCEDURE 49

V. EXPERIMENTAL RESULTS AND DISCUSSION 64

VI. CRITICISM OF PREVIOUS WORK FROM THIS LABORATORY. 106

VII. CONCLUSIONS 115

VIII. SUGGESTIONS FOR FURTHER WORK. 117

NOMENCLATURE 119

BIBLIOGRAPHY 121

APPENDICES

A. DERIVATION OF THE SHAPE OF A MENISCUS AT A VERTICAL WALL WHICH IS WETTED BY THE FLUID 126

B. CORRECTION TO LEVICH'S ESTIMATE OF INCREASE IN MASS TRANSFER IN WAVY FILM FLOW. 134

C. EXAMPLES OF CAPACITOMETER TRACES. 140

D. EXAMPLES OF INTERFERENCE PROFILES 147

LIST OF TABLES

Table | Page

1. Percent Increase in Mass Transfer in Wavy Surface Films 40

2. Average Bulk Concentration of Dissolved CO_2 in Water Films at 24°C 89

LIST OF ILLUSTRATIONS

Figure		Page
1.	Coordinate System for Smooth Surface Problem . .	26
2.	Coordinate System for Wavy Surface Problem . . .	26
3.	Theoretical Concentration Profiles Used in Pohlhausen Analysis.	30
4.	The Dependence of the Bulk Concentration on the Penetration Height for Theoretical Concentration Profiles	32
5.	Comparison Between Theoretical Concentration Profiles for CO_2 Diffusion into Water at 24° C and an Angle of 5°, Re = 926, and Contact Lengths of 22 and 28 Inches.	44
6.	The Dependence of Total Diffusion Coefficient on Film Height for Theoretical Concentration Profiles	46
7.	Sketch of Gas-Liquid Contacting Cell	50
8.	Schematic Diagram of Experimental Apparatus . .	52
9.	The Experimental Relation Between Total Reynolds Number and Film Reynolds Number for Water at 24° C	66
10.	The Experimental Effect of Volumetric Flow Rate on the Percent of Total Water Occupying the Meniscus Regions on Glass Walls at 24° C	67
11.	The Experimental Effect of Film Reynolds Number on Mean Film Thickness of Water at 24° C and an Angle of 1°	70
12.	The Experimental Effect of Film Reynolds Number on Mean Film Thickness of Water at 24° C and an Angle of 2°	71

LIST OF ILLUSTRATIONS--Continued

Figure		Page
13.	The Experimental Effect of Film Reynolds Number on Mean Film Thickness of Water at 24° C and an Angle of 3°	72
14.	The Experimental Effect of Film Reynolds Number on Mean Film Thickness of Water at 24° C and an Angle of 5°	73
15.	The Experimental Effect of Film Reynolds Number on Mean Film Thickness of Water at 24° C and an Angle of 10°	74
16.	The Experimental Effect of Film Reynolds Number on Mean Film Thickness of Water at 24° C and an Angle of 15°	75
17.	The Experimental Effect of Film Reynolds Number on Mean Film Thickness of Water at 24° C and an Angle of 25°	76
18.	The Experimental Dependence of Average Wave Frequency on Film Reynolds Number for Water at 24° C	82
19.	The Experimental Dependence of Average Wave Amplitude on Film Reynolds Number for Water at 24° C	84
20.	Comparison Between Lu's Interference Profiles and Theoretical Concentration Profiles for CO_2 Diffusion into Water at 24° C and an Angle of 5°, Re = 926, and Contact Lengths of 22 and 28 Inches	112
21.	Force Balance on Liquid Surface for Determination of Meniscus Shape	128
22.	Water Meniscus Shape in the Vicinity of a Vertical Glass Wall	133
23.	Capacitometer Calibration Curve for Angles of 1°, 2°, and 3°	141
24.	One Second Capacitometer Traces at an Angle of 2°	142
25.	One Second Capacitometer Traces at an Angle of 3°	143

LIST OF ILLUSTRATIONS--Continued

Figure Page

26. Capacitometer Calibration Curve for Angles of 5°, 10°, 15°, and 25° 144

27. One Second Capacitometer Traces at an Angle of 15° 145

28. One Second Capacitometer Traces at an Angle of 25° 146

29. Example Interference Profiles from Quiet Pool Studies 148

30. Example Interference Profiles from Flowing Film Studies at an Angle of 2° and a Position 19 Inches from Liquid Feed Point 149

31. Example Interference Profiles from Flowing Film Studies at an Angle of 2° and a Position 25 Inches from Liquid Feed Point 150

GAS ABSORPTION INTO THIN WAVY LAMINAR LIQUID FILMS FALLING DOWN INCLINED PLANES

CHAPTER I

SUMMARY

Gas absorption into thin laminar liquid films with both smooth and wavy surfaces falling down inclined planes was investigated for angles of 1°, 2°, 3°, 5°, 10°, 15°, and 25° from the horizontal at Reynolds numbers varying between 140 and 1940. In a flat plate diffusion cell, experimental measurements were made of the mean thickness of the films, the characteristics of the surface disturbances, the bulk concentration of dissolved gas, and the light interference patterns that formed as a result of the diffusion of CO_2 into the water films. A theoretical study was made of the molecular diffusion process into the thin films when the surface was both smooth and wavy.

Results indicate that wall effects can have a significant bearing on the flow and mass transfer into the films. When the wall effects are accounted for, the Nusselt laminar flow theory appears to predict the mean thickness of the films, and the laminar flow diffusion

theory of Pigford predicts, within about ten percent, concentrations in the films, whether waves are present on the surface or not. The interference profiles formed as a consequence of the CO_2 diffusion seem to represent other properties in addition to the solute distribution, and suggest a need for further development with the interferometric technique. Theoretical analysis using only the molecular diffusivity results in a prediction of significant increases in mass transfer, depending on the amplitude of the surface disturbances.

CHAPTER II

INTRODUCTION

Mass transfer is an important phenomenon which is relied upon in the chemical industries as a unit operation, a process closely associated with molecular diffusion. Since molecular diffusion is a relatively slow process, one of the more challenging goals for the chemical engineer is to accomplish the desired mass transfer both rapidly and economically.

Certainly the amount of mass transferred by diffusion between two phases is proportional to the interphase contact area. In an attempt to understand better the diffusion process, considerable effort has been devoted to studies in apparatus that provides an easily calculable interphase surface area. Among these are wetted-walled columns and flat plate apparatus. In most cases the flat plate equipment is operated in a vertical orientation.

Pigford (34) presented the solution of the differential equation describing the concentration of a system in which a liquid with a smooth surface is allowed to flow viscously down a vertical flat surface, while molecular diffusion is occuring across the gas-liquid interface. From his

integrated solution for the bulk concentration, he was able to determine a Height of a Transfer Unit (HTU) that showed an increase with increasing Reynolds number. In this same work he presented the data of Childress (8) for the absorption of pure sulfur dioxide, oxygen, chlorine, and carbon dioxide in falling water films on a wetted-walled column at flows corresponding to Reynolds numbers varying from 100 to 500. The data indicated no dependence of the HTU on the Reynolds number. At low values of the Reynolds number the experimental mass transfer was greater than the theory predicted and, at higher values, this behavior was reversed. At the higher Reynolds numbers studied (about 100), disturbances were noticed on the liquid surface that resembled waves. It was suggested that the lower values of the experimental HTUs were associated with the presence of waves. He further suggested that if the waves could be eliminated with surface active agents, considerably better agreement with his theory might be expected.

Grimley (18), working with a wetted-walled column for CO_2 absorption, had noted an improved performance when ripples were present on the liquid surface. He had also added a surface active agent to the flowing liquid and observed both the elimination of the waves and a decrease in the mass transferred; however, whether the decrease in the mass transfer was a result of the absence of the waves or the presence of the surface active agent contaminant was not established.

When Emmert and Pigford added wetting agents to their flowing liquid, climinating the surface ripples over a range of Reynolds numbers, they noted a much closer agreement with Pigford's theory. In fact, for CO_2 absorption in water, they found 3 to 15 percent decrease in absorption as compared to the theory. They also noted in these studies that there was apparently an optimum concentration of wetting agent for the elimination of the ripples.

Finally, in order to determine the retardation effect of the surface active agent contaminant on the absorption process, they studied the same systems on very short wetted-walled columns. Residence times on these columns were of such short duration that no ripples were formed when the surface active agent was not present. They found only an 11 percent decrease in dissolved gas concentration when the wetting agent was present and concluded that the effect, independent from the elimination of ripples, was minor.

Lynn, Straatemeier, and Kramers (31) studied the absorption of SO_2 into water falling down wetted-walled columns of lengths varying from 12 to 22 cm. They found that when wetting agents were present, the experimental results agreed well with their penetration theory, except at the higher values of Reynolds number where negative deviations were encountered. They attributed this negative deviation from theory to be a result of entrance effects associated with the liquid acceleration and wave

inception. As flow rates increased, the wave inception point moved closer to the bottom of the column. Their studies, when wetting agents were not present, showed about a 50 percent increase in absorption rates as compared to theory for the lower values of Reynolds number. At the higher Reynolds numbers, waves never appeared on the liquid surface, and the absorption rates reduced to those predicted by the penetration theory.

Stirba and Hurt (41) examined the absorption of CO_2 into water films falling down wetted-walled columns and calculated effective diffusivities based on the bulk concentrations. The effective diffusivities were higher than the molecular diffusivities by about 50 percent at low values of Reynolds number, around 150 percent higher in the vicinity of the generally accepted transition point and about 450 percent higher well into the turbulent range. They also dissolved solid coating from the column walls and found increases in effective diffusivity of 600 percent and greater.

Reiss and Hanratty (39) have obtained interesting results for a diffusion-controlled electrolytic reaction in a fluid flowing through a full tube. At a liquid Reynolds number of 2340 they report fluctuations in the diffusion process that vary 40 percent from the mean diffusion rate. A single fluctuation existed over a 5-second interval, suggesting that steady state diffusion is not possible over short time intervals.

Jepsen (23) used an interferometer to view the concentration profiles of dissolved CO_2 in water films falling down flat plates inclined from the horizontal at angles of 25° and less. From his results, assuming a parabolic velocity profile, he calculated the total diffusivity which included the eddy component. He found the diffusivity to reach a maximum in the central portion of the film, and to take on values up to 70 times the molecular diffusivity. His calculated local values of the total diffusion coefficient are at all points larger than the molecular diffusion coefficient. His bulk concentration measurements indicate equivalent HTUs to be only about half of those predicted by the Pigford theory previously mentioned.

Lu (30) extended the interferometric work of Jepsen to other angles of inclination, still less than 25°, and found essentially the same type of behavior of the total diffusivity with position in the film. A maximum was not found in all cases though an increasing diffusivity with height above the solid boundary was reported. The magnitude of the total diffusivity reached 50 times that of the molecular diffusion coefficient and was, at all depths, in excess of it. Comparison of Lu's bulk concentration data with that predicted by the Pigford smooth surface film theory indicated 5 to 10 percent increases in the total amount of mass transferred. The slopes of the theoretical and experimental concentration as a function of

contact distance curves are not the same and appear to cross one another upstream from where the data were taken.

Thus, although there does not appear to be any complete definition available from the data, most investigators report enhanced mass transfer when ripples are present on the surface of falling liquid films. Experimental evidence seems to show a connection between the waves on the liquid surface and the higher mass transfer rates. The elimination of the waves with wetting agents and the subsequent decrease in mass transferred across the interface tends to support these inferences. Thus, much work, both experimental and theoretical, has been expended toward properly describing the dynamics of film flow.

One of the earliest efforts at mathematical representation of the flowing film is attributed to Nusselt (32). He is credited with deriving and solving the equations for laminar viscous flow, from which expressions for the film thickness, shear stress, and velocity profile may be obtained. Experimental efforts to verify his predicted values of film thickness have occupied many investigators, most of whom conclude that Nusselt's representation is relatively sound. Pigford assumed this profile to exist in deriving his theory for the mass transfer. However, his theory assumes no bulk flow normal to the gas-liquid interface. Some kind of normal flow is necessary to account for the increased rates of mass transfer reported by experimental

investigators. Kapitsa (25) studied theoretically the vertical flow of liquid films with capillary waves distributed on the surface. Portalski (35) reviewed this work (in English) while refining the calculations. Both of these investigators neglected a term in the basic equations which was comparable in magnitude to others that were retained. Bushmanov (7) corrected the error and the proper solution appears in Levich (28). These solutions indicated that in the laminar flow regime the expected mean film thickness should be 93 percent of that predicted from the Nusselt theory. Lu (30) has subsequently modified the theory in Levich to apply to falling films at angles less than the vertical.

Dukler and Bergelin (10) have proposed an alternate theory. Von Karman (44) had suggested the existence of a universal velocity profile for turbulent flow which was verified by the data of Nikuradse (31) for flow in full cylindrical pipes. By assuming that the same equation that applied for full pipes was applicable to two phase film flow, Dukler was able to develop an expression for the film thickness as a function of the Reynolds number. His data were found to be in good agreement with the proposed theory. The theory yielded film thicknesses corresponding to experimental data in both laminar and turbulent flow regimes and suggested a transition Reynolds number of 1080.

Dukler (11) extended this work to predict mean film thicknesses in the presence of interfacial shear, such as that resulting from co- and counter- current gas flows.

Other approaches to the problem of wavy laminar flow have been directed toward describing the stability of the free liquid-gas interface. The equations of motion are subjected to a small perturbation from which the Orr-Sommerfelt equation results. The conditions for neutral stability (i.e. the conditions at which a disturbance neither grows nor damps) are obtained and usually related to Reynolds number. Such work has been performed by Lin (29) and Benjamin (2, 3). The results indicated wave formation at very low values of Reynolds number when flow was on a vertical surface. Benjamin concluded that there was no lower limit on the Reynolds number for wave formation when surface tension was a factor. However, both the amplification factor and disturbances were very small until a Reynolds number of 16 was achieved; disturbances do not grow rapidly below this value. While this type of theory may predict the wave formation and phase velocity, it does not provide the mechanism for the increased mass transfer noticed by investigators in experimental work. It is seen, however, that waves or disturbances may be present on a liquid film surface when the flow is essentially in the laminar regime.

Much of the experimental work associated with falling liquid films has been directed toward the measurement of the

mean thicknesses of films flowing on vertical surfaces. Probably the earliest attempts were made using micrometers to locate the surface. When surface disturbances of any appreciable size were present, this method gave only a value of a maximum film thickness and, as such, provides little assistance in choosing among the various theories.

A common method employed by many investigators was to measure the volume of liquid hold-up on the surface at some instant. This measurement was accomplished by simultaneously eliminating the feed to the flow surface and redirecting the surface efflux. It was essential that the height of fluid above the distribution weir was eliminated to prevent collection in the surface efflux. The residual fluid adhering to the surface was usually collected on tared toweling. The total volume of fluid was then divided by the area of the flow surface to calculate the mean film thickness. A disadvantage of this method was that the volume of fluid that was undergoing acceleration was included in the hold-up from the surface, indicating a larger thickness than the fluid would have in fully developed flow. The use of a large surface would, of course, reduce this distorting effect on the measurements. Another disadvantage is that nothing can be learned about the characteristic shape of the free liquid surface.

Many investigators have used this technique on vertical surfaces. Among those who have reported experimental

results from wetted-walled columns are Fallah, Hunter, and Nash (14), Friedman and Miller (15), and Thomas and Portalski (42). Portalski (37) has worked with a vertical flat plate, and Fulford (16) has made similar measurements both on vertical and inclined flat plates. All of these authors have found the mean liquid film thicknesses to be within 10 percent of those predicted by the Nusselt and Kapitsa theories. Thomas and Portalski showed a laminar-turbulent transition Reynolds number of 1080 with the slope of the film thickness as a function of Reynolds number being much steeper in the turbulent regime than in the viscous regime. Fulford's work, at lower angles than the vertical, indicated a slight upward trend in film thickness around a Reynolds number of 1200, but the break in the curve was not sufficient to suggest the onset of turbulence.

Kamei and Oishi (24) used a similar technique and weighed both the column and the fluid during operation. Their experiments were also carried out with and without gas flow. Counter-current gas flows caused their wetted-wall column to oscillate and complicated their experimental procedure.

Jackson (21) used a method which involved the counting of radioactive emissions from liquids flowing inside vertical tubes. He studied a variety of fluids having densities both larger and smaller than that of water. For those fluids less dense than water he found that viscous theory described the film thicknesses adequately up to

Reynolds numbers of 5000. He did note, however, a greater scatter in his data at Reynolds numbers above 2000 than below. For the fluids more dense than water he noted a negative deviation from viscous theory at the higher flow rates. The only real objection to his technique was that his calibration assumed viscous flow at very low flow rates. If viscous flow did not exist for the regions of his calibrations, then he would have to shift his curves accordingly, leaving their trends the same, however. It is interesting that he noted no transition to turbulent flow up to Reynolds numbers of 5000. Jackson reported his measurements to be accurate to within 0.0005 inches.

Belkin et al. (1) used a photographic technique to determine film thicknesses of water flowing down the surface of vertical one-inch diameter rods. By photographing both the dry and wet rods from the same position and using identical magnifications, he claimed to measure the film thicknesses to within 0.003 inches. His Reynolds number range varied from 200 to 30,000. From the results presented in his paper the transition from laminar to turbulent flow was in the vicinity of a Reynolds number of 2200. His experimental film thickness as a function of Reynolds number curves were similar to those of Dukler and Bergelin (10), yielding a steeper slope in the turbulent than in the laminar regime.

Dukler and Bergelin (10) have developed a capacitometer for the measurement of instantaneous values of the

film thickness. This device measured the change in capacitance of the air gap located between the surface of a metal plate, suspended above the liquid, and the flow surface. Accuracy in determination of surface location was claimed to be within 0.001 inches. In addition, information about the frequency and amplitude of surface disturbances was obtained. Calibration curves presented in the article indicated that the closest approach of the metal plate of the capacitometer to the flowing liquid surface was about 0.094 inches. Experimental data taken with this device agreed well with the theory (already referred to) presented by these authors in the same publication. This same type of device has been utilized by Portalski (37) as a check against his hold-up measurements and by Jepsen (23) and Lu (30) with modifications for a visicorder readout. Jepsen's measurements, of which further comment will be made later, yielded film thicknesses from 20 to 35% greater than laminar theory predicted. Lu reported film thicknesses greater than predicted by laminar theory and the slope of his data, when plotted logarithmically against liquid Reynolds number, was greater than the predicted value of 1/3.

Van Rossum (43), working with water films flowing in horizontal channels, has used a resistance measurement for determination of film thicknesses. The resistance between two parallel platinum strips, mounted with their major axes in the direction of flow, varied depending on

the height of fluid located above them. Calibration with known film thicknesses allowed the determination of the fluid depth through the resistance measurement. It is interesting to note than van Rossum found a maximum film thickness at the center of his channel, which was six inches wide. He claimed that his film thickness measurement technique was accurate to within 5 to 10 percent of the true value.

Velocity profile data in falling films has been difficult to obtain because the films are so thin (0.001 to 0.04 inches). Some work in the viscous sublayer of full conduits yields interesting information which should be considered in the film flow studies. Fage and Townend (13) have used an untramicroscope to detect "sinusoidal" fluctuations in the motion of small suspended dust particles flowing in liquids very close to the walls of a square pipe. Similar fluctuations of dye traces have been photographed by Rundstadler, Kline and Reynolds (40) in their studies near the bottom of a horizontal channel.

Grimley (18) had succeeded in using an ultramicroscope to determine velocities of small colloidal particles suspended in falling water films. The particles were assumed to travel with the velocity of the surrounding fluid. His measurements indicated that when waves flow on the liquid surface, the profile does not correspond to the Nusselt theory, but reaches a maximum somewhat below the free surface of the liquid. These peak velocities are

reported to be occasionally three times the maximum velocity calculated for a film of comparable thickness flowing with the Nusselt profile. When the surface active agents were added to the flowing fluid, however, the surface disturbances were damped out and the experimentally measured velocity profiles approached the parabolic distribution predicted by the Nusselt theory.

Wilkes and Nedderman (46) have used stereoscopic photography of small air bubbles moving with the fluid at very low Reynolds numbers (eg. 0.5 to 4.1) in vertical developed flow. For the lower Reynolds numbers studied, the surface of the liquid remained smooth and the measured profiles coincided with the laminar theory. However, at a Reynolds number of 4, disturbances appeared on the liquid surface, and the measured local velocities varied $\pm$ 20 percent from the parabolic profile. When surface active agents were added to the fluid at this flow rate, the disturbances dissappeared, and the experimentally determined profiles once again approached the laminar parabola.

Instead of measuring the velocity profiles, some investigators have accepted a determination of the surface velocity and the film thickness, reasoning that from a volumetric flow rate, an average thickness and an absolute velocity at a point, a profile could be fitted to the results. A simple technique for measuring surface velocity is to clock the time of traverse of dye particles or some floating body, such as a hair or piece of paper or plastic

confetti over a measured course. Friedman and Miller (15) have clocked the velocity of dye drops over a two foot course on a vertical column. Although the film thicknesses agreed with laminar theory up to values of Reynolds number of 1000, the surface velocity was only consistent with laminar theory to Reynolds numbers of 30. The theoretical value for the ratio of surface velocity to average velocity when a laminar flow prevails is 1.5. However, these investigators measure ratios of 2.0 to 2.25 for several fluids flowing at Reynolds numbers varying from 30 to 150. Above 150, the authors felt that their technique was less precise because the dye dispersed considerably and the time intervals became too short to be measured accurately by a stopwatch.

Binnie (4) had measured surface velocities by timing a small hair over a measured distance at very small angles of inclination from the horizontal. Although no film thicknesses were measured, he found surface velocities up to twice as great in the vicinity of his vertical retaining walls as in the center of his channel. The measured bulk flows were larger than those calculated from his surface velocities measured at the center, and this difference increased as the angle of inclination increased.

Jackson, Johnson, and Ceaglski (22) have obtained results similar to those of Friedman and Miller by measuring pressure drop (i.e. interfacial shear) of a counter-current flowing gas stream. Their data revealed a transition between the surface velocity to average velocity ratio to occur

between Reynolds numbers of 25 and 80. Below Reynolds numbers of 25 the ratio was the laminar theoretical value of 1.5, while above 80, the experimental values clustered around 2.0.

Portalski (38) used an unusual technique to measure surface velocities. He used a vertical surface over which he first allowed the flow to reach steady state; then he redirected the flow while the surface was allowed to drain to a "just wetted" condition, and finally again allowed the liquid to flow anew over the surface. The assumption was made that the wave front moved with its maximum velocity, and the velocity ratio was calculated. A value close to 1.5 was obtained for a range of Reynolds numbers varying from 4 to 1200. At the point where laminar-turbulent transition was expected, the surface velocity to average velocity ratio began to decline and then to level off at a value of 1.15 at a Reynolds number of 2500.

Fulford (16) has measured the surface velocity of falling films at not only the vertical angle, but also angles of $7\frac{1}{2}^{\circ}$, 24°, 43°, and 62° from the horizontal. He has used a technique described in Lamb (25), in his discussion of the Lord Rayleigh fishline problem, in which the wave lengths of stationary waves formed upstream from a point just pricking the surface of the liquid are determined. His measurements over a range of Reynolds numbers from 420 to 3600 gave values of the velocity ratio of 1.5.

Thus it is seen that, depending upon the technique that is chosen for measurement, the investigator may determine values for the surface velocity to average velocity ratio of 1.5 to 2.25, while still measuring mean film thicknesses that correspond to laminar flow theory. Those experimenters reporting ratios of 1.5 claim that ratios of 2.0 are high due possibly to a pumping action of the surface waves. The surface waves reportedly travel at velocities up to 2.0 times the liquid surface velocity as predicted by laminar theory. However, it is interesting to note that in the range of Reynolds numbers studied by Fulford (16) the wave velocities determined experimentally fall below 1.34 times the surface velocities and in some cases the ratio falls below 1.0.

The laminar theory of Nusselt has assumed a fluid of infinite width where wall effects can have no influence. It is reported that Hopf (20) has supplied the theory for the lateral velocity profiles where vertical retaining walls are present, but without capillary effects. Fulford has included capillary forces by numerically calculating the velocity profiles in a falling liquid film flowing parallel to a vertical retaining wall that is wetted by the fluid. For an inclination angle of 30° and a laminar flowing constant surface film 1/3 mm thick, his calculations predict velocities about 20 times greater adjacent to the wall than at great distances from the wall. It will be remembered that Binnie (4), in his study of falling

water films at angles not greater than 2 3/4° from the horizontal, reported surface velocities near his wood retaining walls twice as great as those in the center of his channel. These results are very important in the interpretation of the results of Jepsen (23) and Lu (30).

As in the experimental confusion that exists over the ratio of surface velocity to average velocity described above, another uncertainty exists in the fate of a dye drop placed on the surface of a falling film. Friedman and Miller (15) reported limitations in their method of surface velocity determination due to rapid dispersion of the dye. Stirba and Hurt (41) also noticed a rapid dispersion of dye drops placed on the liquid surface as long as waves were present, but when a wetting agent was added, the surface disturbances damp out and the dye drop remained in a thin thread. Davies (9) on the other hand presented photographs of dye drops in falling films that remained in thin threads.

Several authors have commented on the characteristics of the surface ripples. Fulford (17) has a very good account of the appearance of a falling film surface as Reynolds number is gradually increased from small to large values. Benjamin (2) has reported an amplification factor that increases very rapidly with Reynolds number. Portalski (37) shows exponential type increases in surface area with Reynolds number, but whether it resulted from a higher frequency of disturbances or a greater amplitude

was not established. Belkin et al. (1), who have studied the surfaces of falling films photographically, reported decreases in disturbance amplitude with increases in Reynolds number. Lu (30) has likewise reported a decrease in disturbance amplitude with increases in Reynolds number, though his theory predicts increases with increasing Reynolds number.

Thus, it may be concluded that although the behavior of falling liquid films has been broadly studied, there is much conflicting evidence presented in the literature. A few basic observations may be made, however. In general, mean film thicknesses tend to agree within 5 to 10 percent of the Nusselt laminar theory, at least up to Reynolds numbers of 1200. Surface disturbances on films in vertical flow appear at very low values of Reynolds number, around 10. As long as the surface is smooth, the velocity profiles in the film are parabolic.

The mass transfer rates into falling liquid films increase with the appearance of spontaneously occurring surface disturbances. The surface ripples may be suppressed, but not totally eliminated, by the addition of wetting agents to the liquid. With the disappearance of the surface disturbances, the mass transferred approaches more closely the values predicted by the Pigford theory for smooth-surface, laminar-flowing, falling-liquid films.

Jepsen and Lu have had some success in defining the concentration profiles of diffusing gas into falling liquid

films. Their work, however, has been limited to angles less than 25°, primarily as a result of the small film thicknesses encountered at higher inclinations. Since surface disturbances limit the visible portion of the film in interferometric work, it was thought that the most profitable area of attention was that of the nearly smooth surface films at small angles of inclination.

Several advantages were offered by the study of the mass transfer and flow down slightly inclined planes. First, the film thickness was expected to be relatively large when compared to those encountered at the higher angles studied by Lu and Jepsen. Second, with thicker films, the velocities encountered would be lower and consequently would result in residence times sufficient to allow significant penetration of the diffusing gas into the body of the film. Third, at low velocities and small angles of inclination, the smooth surface film theory of Pigford must apply. Comparison of the concentration profiles determined experimentally and those calculated from this theory would establish the interferometric technique.

Therefore, the proposed study was the investigation of the flow of, and gas absorption into, smooth-surface, laminar, liquid films at small angles of inclination and a range of rates to include the laminar and laminar transition flow regimes.

CHAPTER III

THEORETICAL DEVELOPMENT

Considerable theoretical work has been directed toward describing the dynamics of liquid film flow and the stability of film surfaces, but few results have been presented that account for the increases in mass transfer that are reported as experimental results (8, 12, 18, 23, 30, 31, 34, 41). Pigford has obtained theoretical concentration profiles resulting from diffusion of a gas into a smooth-surface, developed, laminar-flowing film. His solution is an infinite series of exponential terms, which converges slowly for small values of the argument. This renders his solution technique unwieldy in application to the wavy surface problem.

Levich (28) has modified the theoretical film dynamics of Kapitsa (25) and has obtained an approximation to the amount of mass transfer expected as a result of the wavy surface. His solution is valid only for slight penetrations since he has found it necessary to eliminate the velocity profile from his analysis. Unfortunately, his work contained arithmetic errors, which when corrected (see

Appendix B) result in a prediction of a 1.52 percent decrease instead of the reported 15 percent increased mass transfer when waves were present.

Bird (5) presents the theory for concentration profiles of gas diffusing into films with smooth surfaces with a uniform velocity. This solution is a complementary error function and is perfectly correct for only slight penetrations into laminar flowing films.

Portalski (38) has calculated circulations that exist in the fluid beneath the troughs of the Kapitsa waves, but no quantitative prediction of the increase in mass transfer that accompanies these circulations was offered.

Apparently no theory is available for mass transfer into laminar flowing wavy surface films in which the entire velocity profile is considered. In the past it has been necessary to disregard either the surface disturbances or the velocity profile in order to obtain a solution to the convective diffusion equation.

The important features of the problem can be retained in a solution obtained using the method of Pohlhausen (35). The Pohlhausen approach requires that a concentration profile be assumed. In order to see whether so violent an approach was advisable, the smooth-surface, developed, laminar-flow case was solved first, and these results compared with the closed form for the average concentration given by Pigford. The results seemed acceptable and the technique was extended to accommodate a film

with surface waves. This technique gives an estimate of solute penetration from a theory in which three essential features are combined: the parabolic velocity profile, the wavy surface, and the molecular diffusion.

Smooth Surface Problem

The differential equation that Pigford solved is:

$$u \frac{\partial C}{\partial x} = D \frac{\partial^2 C}{\partial y^2}$$

$$C(0,y) = C_o$$

$$C(x,h) = C_s \qquad (1)$$

$$\frac{\partial C}{\partial y}(x,0) = 0$$

where D is a constant molecular diffusion coefficient, C the concentration of dissolved solute, C_o the initial concentration of solute in the feed liquid, C_s the solute concentration at the liquid surface (the saturation value), and where u, the local velocity, is obtained from the momentum equation assuming viscous flow:

$$\nu \frac{\partial^2 u}{\partial y^2} + g = 0$$

$$u(x,0) = 0 \qquad (2)$$

$$\frac{\partial u}{\partial y}(x,h) = 0$$

In equation (2), ν is the kinematic viscosity and g is the acceleration of gravity. The coordinate system for the flow problem is found in Figure 1.

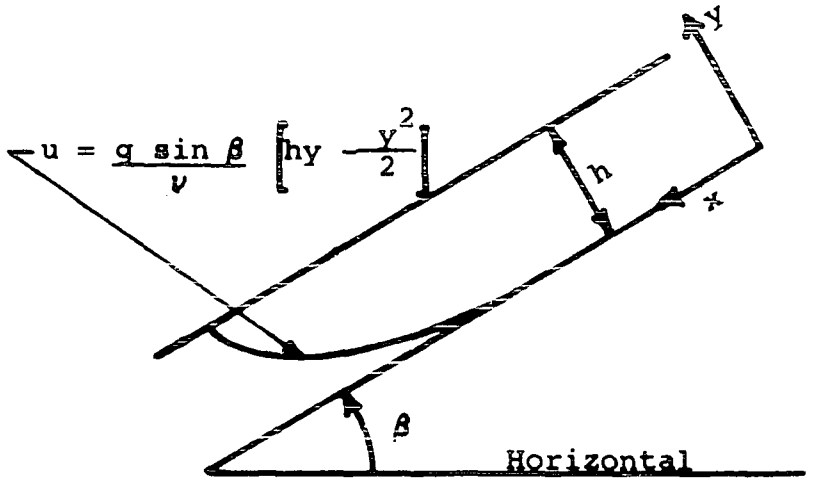

Figure 1

Coordinate System for
Smooth Surface Film Problem

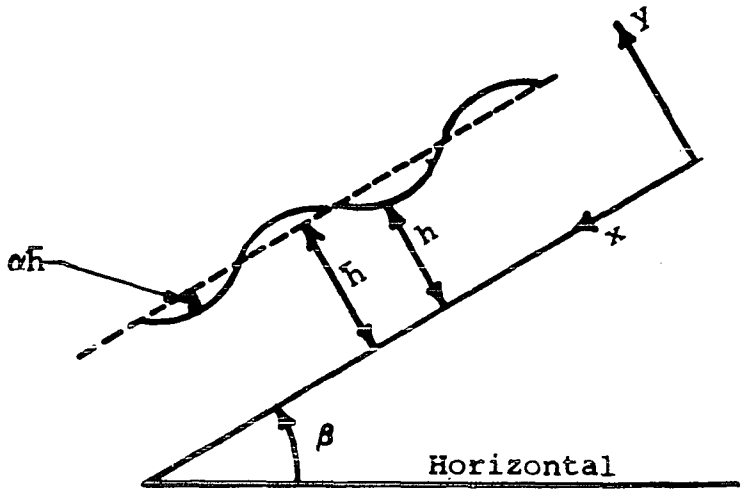

Figure 2

Coordinate System for
Wavy Surface Film Problem

If β is the angle from the horizontal of the surface down which the liquid flows, the solution to the momentum equation is:

$$u = \frac{g \sin \beta}{\nu} \left[hy - \frac{y^2}{2} \right] \tag{3}$$

which may now be substituted into equations (1) with the result:

$$\left[hy - \frac{y^2}{2} \right] \frac{\partial C}{\partial x} = \frac{D\nu}{g \sin \beta} \frac{\partial^2 C}{\partial y^2}$$

$$C(0,y) = C_o$$

$$C(x,h) = C_s \tag{4}$$

$$\frac{\partial C}{\partial y}(x,0) = 0$$

In the application of the Pohlhausen technique to this problem, the existence of a diffusion boundary layer, δ, is assumed and the appropriate boundary conditions adjusted to apply at this point. If new dimensionless variables are defined as:

$$\underline{C} = \frac{C - C_o}{C_s - C_o}$$

$$Y = y/h \tag{5}$$

$$\Delta = \delta/h$$

then equations (4) may be rewritten as:

$$\left[Y - \frac{Y^2}{2} \right] \frac{\partial \underline{C}}{\partial x} = \frac{K}{h^4} \frac{\partial^2 \underline{C}}{\partial Y^2} \tag{6}$$

$$\underline{C}(0,Y) = 0$$

$$\underline{C}(x,1) = 1$$

$$\frac{\partial \underline{C}}{\partial Y}(x,\Delta) = 0$$

where $K = (D\nu)/(g \sin \beta)$.

Integration with respect to Y over the diffusion boundary layer yields

$$\int_{\Delta}^{1}\left[Y - \frac{Y^2}{2}\right]\frac{\partial \underline{C}}{\partial x}\, dY = \frac{K}{h^4}\left[\frac{\partial \underline{C}}{\partial Y}(x,1) - \frac{\partial \underline{C}}{\partial Y}(x,\Delta)\right] \qquad (7)$$

which upon use of Leibnitz's rule for differentiation under an integral sign, and $\underline{C}(x,\Delta) = 0$ yields

$$\frac{\partial}{\partial x}\int_{\Delta}^{1}\left[Y - \frac{Y}{2}\right]\underline{C}\, dY = \frac{K}{h^4}\frac{\partial \underline{C}}{\partial Y}(x,1) \qquad (8)$$

Assuming as an approximate solution to the set of equations (6), the second order polynomial

$$\underline{C} = \left[\frac{Y - \Delta}{1 - \Delta}\right]^2 \qquad \Delta \leq Y < 1 \qquad (9)$$

$$\underline{C} = 0 \qquad Y < \Delta$$

which has been constructed such that the boundary conditions in equation (6) and $\underline{C}(x,\Delta) = 0$ are satisfied, and integrating equation (8) after substituting equation (9) for $\underline{C}$

$$\left[-7 + \Delta + 9\,\Delta^2 - 3\,\Delta^3\right]\frac{d\Delta}{dx} = 120\,\frac{K}{h^4} \qquad (10)$$

is obtained.

Equation (10) is an ordinary differential equation in Δ and x, in which the variables are separable. Integration over indefinite limits with respect to x yields

$$-7\Delta + \frac{\Delta^2}{2} + 3\Delta^3 - \frac{3}{4}\Delta^4 = \frac{120\ Kx}{h^4} + C_1 \qquad (11)$$

C_1 is evaluated at the entrance to the diffusion section where $\Delta = 1$ at $x = 0$.

$$C_1 = \frac{17}{4} \qquad (12)$$

Substituting the value of C_1 into equation (11) and rearranging, an expression for the diffusion boundary layer is obtained.

$$\Delta^4 - 4\Delta^3 - \frac{2}{3}\Delta^2 + \frac{28}{3}\Delta - \frac{17}{3} + \frac{160Kx}{h^4} = 0 \qquad (13)$$

Equation (13), being a quartic equation in Δ has four roots. The root of interest in this analysis is the one lying between 0 and 1. There is only one such root to equation (13), and this root exists only when $-17/3 + (160Kx/h^4)$ lies between $-17/3$ and 0.

The preceding development is applicable provided contact times are not sufficient to allow penetration to the bottom of the flowing film, i.e. $\Delta \geq 0$. In order to evaluate $\underline{C}$ for any particular value of x, the root of equation (13) lying between 0 and 1 must be determined and substituted into equation (9). A parabolic concentration profile is thus established, examples of which appear in Figure 3.

The bulk concentration in the flowing film is determined by multiplying equation (9) by the velocity profile, integrating from the edge of the boundary layer to the surface (i.e. from Δ to 1) and dividing the result by the volume of fluid flowing.

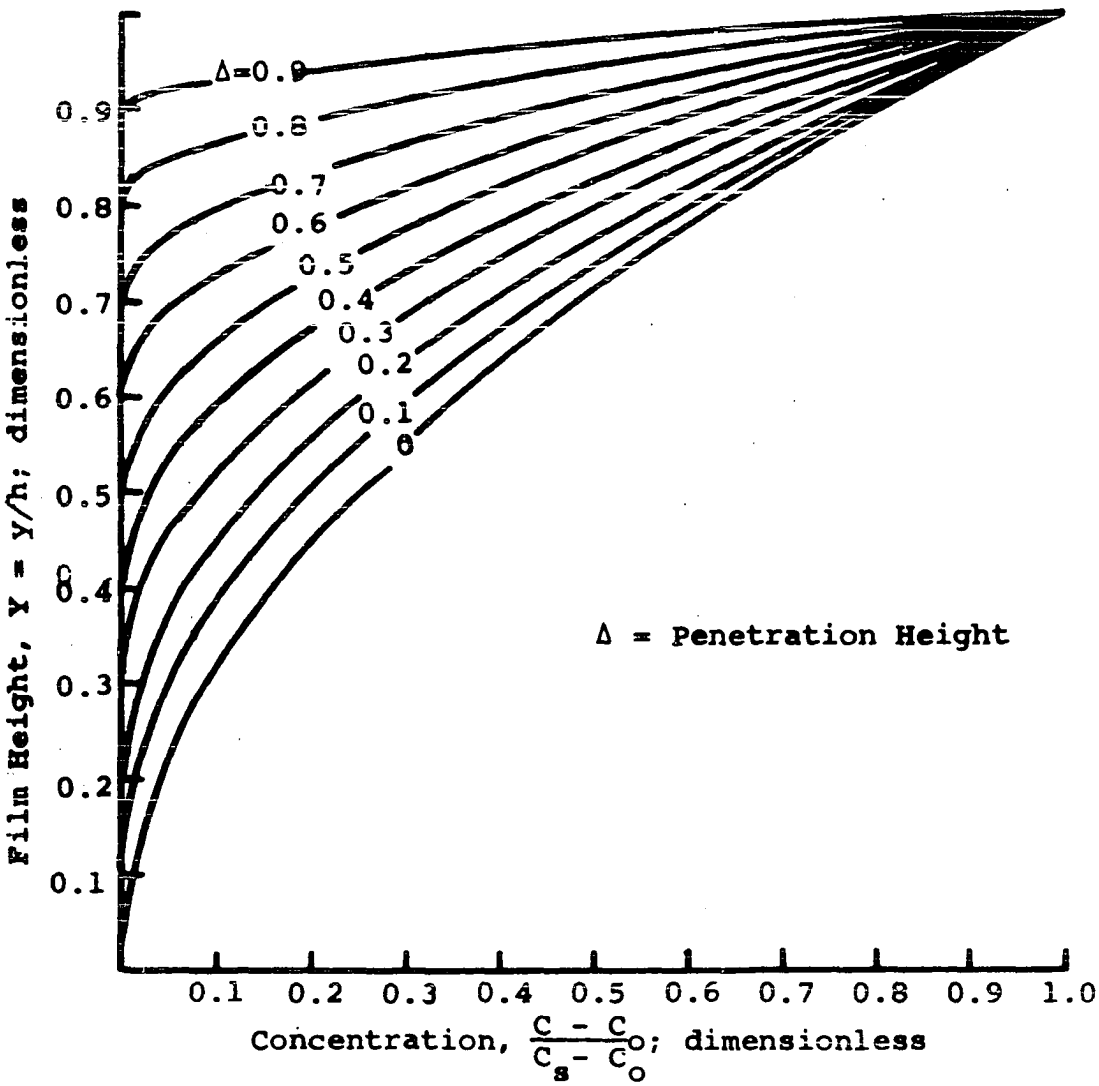

Figure 3

Theoretical Concentration Profiles
Used in Pohlhausen Analysis

$$\underline{C}_{avg} = \frac{\int_{\Delta}^{1} \left[\frac{Y - \Delta}{1 - \Delta}\right]^2 \left[Y - \frac{Y^2}{2}\right] dY}{\int_{\Delta}^{1} \left[Y - \frac{Y^2}{2}\right] dY} \tag{14}$$

$$\underline{C}_{avg} = \frac{1}{(1-\Delta)^2} \left[\frac{\Delta^5}{20} - \frac{\Delta^4}{4} + \Delta^2 - \frac{5\Delta}{4} + \frac{9}{20}\right] \tag{15}$$

A plot of equation (15) is found in Figure 4.

The above procedure has also been followed using two, third order and one, fourth order polynomial approximation for the dependent variable, $\underline{C}$. When the boundary conditions of equation (6) plus

$$\frac{\partial^2 \underline{C}}{\partial Y^2} (x, \Delta) = 0 \tag{16}$$

are used, an expression

$$\underline{C} = \left[\frac{Y - \Delta}{1 - \Delta}\right]^3 \qquad \Delta < Y < 1 \tag{17}$$

is obtained which results in an expression for Δ

$$\Delta^4 - 4\Delta^3 - 16\Delta - 9 + \frac{480Kx}{h^4} = 0 \tag{18}$$

The bulk concentration for any value of x is obtained by solving equation (18) where the particular value of x is substituted and evaluating from

$$\underline{C}_{avg} = \frac{1}{(1-\Delta)^3} \left[\frac{\Delta^6}{60} + \frac{3\Delta^5}{20} - \Delta^3 + \frac{15\Delta^2}{8} - \frac{27\Delta}{20} + \frac{7}{20}\right] \tag{19}$$

Similarly if a third order polynomial is determined from using the boundary conditions of equation (6) plus

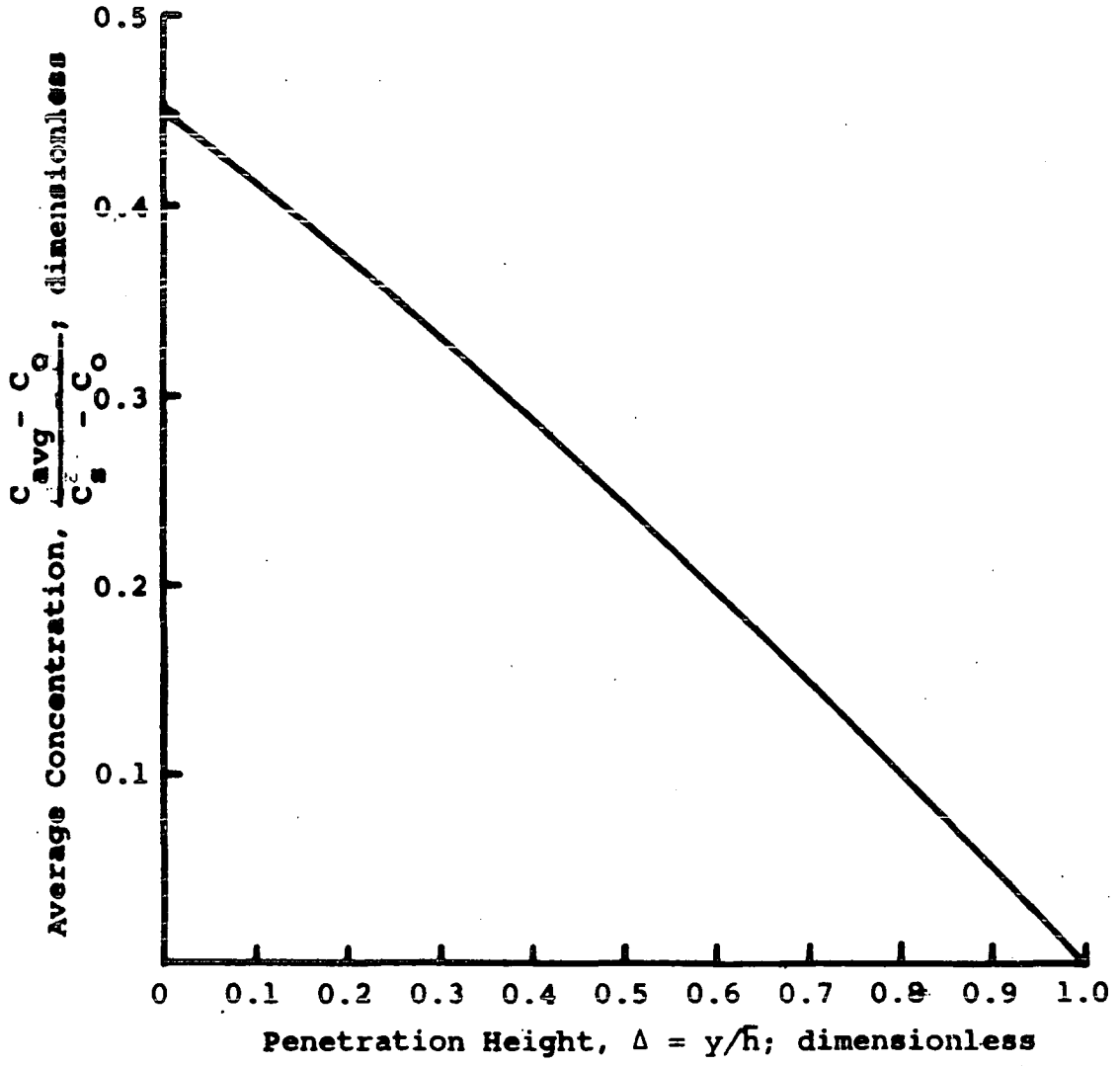

Figure 4

The Dependence of the
Bulk Concentration on the Penetration Height
for the Theoretical Concentration Profiles

$$\frac{\partial^2 \underline{C}}{\partial Y^2}(x,1) = 0 \qquad (20)$$

the expression for Δ is

$$\Delta^4 - 4\Delta^3 + 8\Delta - 5 + \frac{96Kx}{h^4} = 0 \qquad (21)$$

and for $\underline{C}_{avg}$ is

$$\underline{C}_{avg} = \frac{1}{(1-\Delta)^3}\left[-\frac{\Delta^6}{16} + \frac{3\Delta^5}{8} - \frac{3\Delta^4}{8} - \Delta^3 + \frac{39\Delta^2}{16} - \frac{15\Delta}{8} + \frac{1}{2}\right] \qquad (22)$$

Finally, if the boundary conditions of equation (6) plus equations (16) and (20) are used to determine a quartic equation for $\underline{C}$,

$$\underline{C} = \frac{1}{(1-\Delta)^4}\left[-Y^4 + (2+2\Delta)Y^3 - 6\Delta Y^2 + (6\Delta^2-2\Delta^3)Y - 2\Delta^3 + \Delta^4\right] \qquad (23)$$

results. Δ is obtained from

$$\Delta^4 - 4\Delta^3 - \frac{12\Delta^2}{5} + \frac{64\Delta}{5} - \frac{37}{5} + \frac{224Kx}{h^4} = 0 \qquad (24)$$

The value of the bulk concentration is calculated from

$$\underline{C}_{avg} = \frac{1}{(1-\Delta)^4}\left[\frac{\Delta^7}{28} - \frac{\Delta^6}{4} + \frac{3\Delta^5}{10} + \Delta^4 - \frac{13\Delta^3}{4} + \frac{15\Delta^2}{4} - 2\Delta + \frac{29}{70}\right] \qquad (25)$$

The average concentrations to be expected after a contact length of 88.59 cm have been calculated using equations (15), (19), (22), and (25) and have been compared with those determined from Pigford's integrated exact solution.

The angles of inclination studied were 1°, 2°, and 3°. At the low flow rates where sufficient contact time is allowed to make Pigford's solution applicable, equation (15) is within 3 percent of Pigford's solution, equation (19) is within 9 percent, equation (22) is within 9 percent and equation (25) is within 5 percent. At the higher flow rates Pigford's solution does not apply, as contact times are too short to allow convergence for the number of terms he has presented in his series. His values disagree with those obtained by assuming a constant velocity over the penetration depth. The Pohlhausen determined concentrations at these higher Reynolds numbers agree much better with the constant velocity solution, equation (15) agreeing to within 3 percent, equation (19) agreeing to within 8 percent, equation (22) agreeing to within 6.5 percent and equation (25) agreeing to within 3 percent.

Wavy Surface Problem

The Pohlhausen technique, using a second order polynomial, is now applied to a modification of the smooth surface problem to obtain an estimate of the penetration expected in the wavy surface problem. Examination of equation (3) shows that as h is increased for a constant value of y, the velocity at y increases. Similarly, if h is decreased, a lower value of local velocity is obtained at a constant value of y. Thus, if a film thickness varying with x is substituted for h in equation (3), a line of

constant velocity will alternately plunge closer to the bottom of a film or toward the surface, depending on whether the new surface is located farther from or closer to the bottom of the film than was the mean film thickness.

By replacing h in equation (3) with

$$h = \bar{h} (1 + \alpha \sin kx) \tag{26}$$

where $\bar{h}$ is the mean film thickness, α is the dimensionless amplitude, and $k = 2\pi/\lambda$, λ being the wavelength, a periodically increasing and decreasing velocity is obtained for constant values of y. This method effectively places a standing wave on the surface of the laminar flowing film. The continuity equation may be written as before as

$$\frac{\partial u}{\partial x} + \frac{\partial v}{\partial y} = 0 \tag{27}$$

but now v, the vertical component of velocity, is no longer zero. Using equation (3) with equation (26) substituted for h, v may be determined from equation (27) as

$$v = \frac{-g \sin \beta}{\nu} \frac{y^2}{2} \frac{\partial h}{\partial x} = \frac{-g\bar{h}\alpha k \sin \beta \cos kx}{2\nu} \tag{28}$$

With two components of velocity, the convective diffusion equation, where x direction diffusion is neglected when compared with the bulk flow, becomes

$$u \frac{\partial C}{\partial x} + v \frac{\partial C}{\partial y} = D \frac{\partial^2 C}{\partial y^2} \tag{29}$$

where u is defined by equation (3) and (26) and v by equation (28). When the boundary conditions are adjusted to apply at the edge of the diffusion boundary layer, they appear as

$$C(0,y) = C_o$$

$$C(x,h) = C_s$$

$$C(x,\delta) = C_o \qquad (30)$$

$$\frac{\partial C}{\partial y}(x,\delta) = 0$$

Equations (29) and (30) may be rewritten in dimensionless form with the dimensionless variables of equation (5) being modified for h defined by equation (26) as

$$\left[Y - \frac{Y^2}{2}\right]\frac{\partial \underline{C}}{\partial x} = \frac{Y^2}{2h}\frac{\partial h}{\partial x}\frac{\partial \underline{C}}{\partial Y} + \frac{K}{h^4}\frac{\partial^2 \underline{C}}{\partial Y^2}$$

$$\underline{C}(0,Y) = 0$$

$$\underline{C}(x,1) = 1 \qquad (31)$$

$$\underline{C}(x,\Delta) = 0$$

$$\frac{\partial \underline{C}}{\partial Y}(x,\Delta) = 0$$

where as before $K = (D\nu)/(g \sin \beta)$.

Equation (31) is now integrated once with respect to Y across the diffusion boundary layer, that is from Δ to 1, which yields

$$\int_\Delta^1 Y \frac{\partial \underline{C}}{\partial x}\, dY - \int_\Delta^1 \frac{Y}{2}\frac{\partial \underline{C}}{\partial x}\, dY = \frac{K}{h^4}\int_\Delta^1 \frac{\partial^2 \underline{C}}{\partial Y^2}\, dY + \frac{1}{h}\frac{\partial h}{\partial x}\int_\Delta^1 \frac{Y^2}{2}\frac{\partial \underline{C}}{\partial Y}\, dY \qquad (32)$$

Again resorting to Leibnitz's rule for differentiation under an integral sign, the first term in equation (32) is written as

$$\int_{\Delta}^{1} Y \frac{\partial \underline{C}}{\partial x} dY = \frac{d}{dx} \int_{\Delta}^{1} \underline{C}\, Y\, dY + \frac{1}{h} \frac{\partial h}{\partial x} \int_{\Delta}^{1} Y\underline{C} dY \qquad (33)$$

and the second term in equation (32) becomes

$$\int_{\Delta}^{1} \frac{Y}{2} \frac{d\underline{C}}{\partial x} dY = \frac{d}{dx} \int_{\Delta}^{1} \frac{Y^2}{2} \underline{C} dY + \frac{1}{h} \frac{\partial h}{\partial x} \int_{\Delta}^{1} Y^2 \underline{C} dY \qquad (34)$$

Substituting equations (33) and (34) into equation (32) yields

$$\frac{d}{dx}\int_{\Delta}^{1}\left[Y\underline{C} - \frac{Y^2}{2}\underline{C}\right] dY = \frac{K}{h^4} \frac{\partial \underline{C}}{\partial Y}(x,1) + \frac{1}{h} \frac{dh}{dx} \int_{\Delta}^{1}\left[\frac{Y^2}{2}\frac{\partial \underline{C}}{\partial Y} - Y\underline{C} + Y^2\underline{C}\right] dY \qquad (35)$$

Assuming as before a second order polynomial approximation to the dependent variable, equation (9) is substituted into equation (35). When the requisite mathematical operations are performed, and like terms collected, equation (35) becomes

$$[-7 + \Delta + 9\Delta^2 - 3\Delta^3]\frac{d\Delta}{dx} + \frac{1}{h}\frac{dh}{dx}[-12 - 2\Delta + 8\Delta^2 + 8\Delta^3 - 2\Delta^4] = \frac{120K}{h^4} \qquad (36)$$

Equation (36) is the differential equation that determines the diffusion boundary layer depth as a function of x. The equation is non-linear and difficult to integrate. However, a first approximation to Δ is obtained if all elements containing a Δ in the second term of equation (35) are dropped. Multiplying by dx and integrating over indefinite limits,

$$\int[-7 + \Delta + 9\Delta^2 - 3\Delta^3]d\Delta - 12\int\frac{dh}{h} = \int\frac{120K}{h^4}dx \qquad (37)$$

is obtained.

Carrying out the integrations, with the help of Bois's (6) integral tables,

$$-7\Delta + \frac{\Delta^2}{2} + 3\Delta^3 - \frac{3\Delta^4}{4} - 12 \ln \bar{h} = C_1 + \frac{120K}{k\bar{h}^4} \left\{ \frac{\alpha \cos kx}{3(1-\alpha^2)(1+\alpha \sin kx)^3} \right.$$

$$+ \frac{5\alpha \cos kx}{6(1-\alpha^2)^2(1+\alpha \sin kx)^2} + \frac{(11\alpha+4\alpha^3)\cos kx}{6(1-\alpha^2)^3(1+\alpha \sin kx)} + \frac{6+14\alpha^2-5\alpha^4}{3(1-\alpha^2)^{3/2}}$$

$$\left. \arctan\left[\frac{\tan\left(\frac{kx}{2}\right) + \alpha}{(1-\alpha^2)^{1/2}} \right] \right\} \qquad (38)$$

The integration constant, C_1, is evaluated at the entrance to the contacting section where at $x = 0$, $\Delta = 1$.

$$C_1 = -12 \ln \bar{h} - \frac{17}{4} - \frac{120K}{k\bar{h}^4} \left[\frac{18\alpha-5\alpha^3+2\alpha^5}{6(1-\alpha^2)^3} + \frac{(6+14\alpha^2-5\alpha^4)}{3(1-\alpha^2)^{7/2}} \right.$$

$$\left. \arctan\left(\frac{\alpha}{(1-\alpha^2)^{1/2}}\right) \right] \qquad (39)$$

Substituting equation (39) into equation (38) and rearranging

$$\Delta^4 - 4\Delta^3 - \frac{2}{3}\Delta^2 + \frac{28\Delta}{3} - \frac{17}{3} + 16 \ln(1+\alpha \sin kx) + \frac{160K}{k\bar{h}^4}$$

$$\left\{ \frac{\alpha \cos kx}{3(1-\alpha)^2(1+\alpha \sin kx)^3} + \frac{5\alpha \cos kx}{6(1-\alpha^2)^2(1+\alpha \sin kx)^2} \right.$$

$$+ \frac{(11\alpha+4\alpha^3)\cos kx}{6(1-\alpha^2)^3(1+\alpha \sin kx)} - \frac{18\alpha-5\alpha^3+2\alpha^5}{6(1-\alpha^2)^3} + \frac{(6+14\alpha^2-5\alpha^4)}{3(1-\alpha^2)^{7/2}}$$

$$\left. \arctan\left[\frac{\tan\left(\frac{kx}{2}\right)+\alpha}{(1-\alpha^2)^{1/2}}\right] - \arctan\left[\frac{\alpha}{(1-\alpha^2)^{1/2}}\right] \right\} = 0 \qquad (40)$$

Equation (40) must be solved for Δ to obtain a first approximation of the penetration depth of solute in the wavy surface problem. The root of equation (40) that lies between 0 and 1 is the desired diffusion boundary layer depth. This value of Δ may be substituted into equation (9) for an approximation of the concentration profile or into equation (15) for the bulk concentration in the falling film. Since the depth of the diffusion boundary layer varies due to the presence of a wave trough or peak, the bulk concentration should be determined as an average over an entire wavelength. The oscillation in the diffusion boundary layer depth may be eliminated by discarding the logarithm term in equation (40), which merely gives a deeper penetration depth under a crest and a shallower one under a trough.

When the logarithm term is removed from equation (40), the remaining dominating term in the determination of the constant term in the polynomial for Δ is the arctan $\left[\frac{\tan(\frac{kx}{2}) + \alpha}{(1-\alpha^2)^{1/2}}\right]$ term. It is seen that the results depend heavily on the value of α chosen for the wave amplitude. Using 1.5 as the ratio of the surface velocity to the average velocity, and Kapitsa's (25) value of 2.4 for the ratio of the wave velocity to the average velocity in the laminar flowing film, the values of Δ have been calculated for α's ranging from 5 percent to 50 percent of the film thickness. The wave number, k, has been determined from experimental data. An average frequency of disturbances which have amplitudes greater than 0.0005" is used, except at the lower angles

where 0.0001" amplitude is the criterion for a disturbance. Using the values of Δ determined from equation (4) the values of $\underline{C}_{avg}$ determined from equation (15) are compared with those determined using the Δ from equation (13) for the comparable smooth surface problem. The results indicate that the percentage increase in mass transfer at a constant dimensionless wave amplitude does not change significantly with angle of inclination. The results appear in Table 1.

TABLE 1.

PERCENT INCREASE IN MASS TRANSFER
IN WAVY SURFACE FILMS

Amplitude, Percent of Mean Film Thickness	Percent Increase in Bulk Concentration	Angles in Comparison, degrees
5	0.7	1, 2, 3
10	3.0	5, 10, 15, 25
20	12.	5, 10, 15, 25
30	28.	5, 10, 15, 25
40	56.	5, 10, 15, 25
50	101.	5, 10, 15, 25

Of course, the amplitude of the disturbances changes with the angle of inclination, but this dependence has not been determined analytically. Lu (30), in his modification of the Kapitsa (25) theory to lower angles of inclination than the vertical, predicts relatively constant wave amplitudes at around 60 percent of the mean film thickness. Had amplitudes of 60 percent been used in the above comparison, increases in mass transfer should have been higher. The most recent measurements of Wicks (45) shows comparable wave

amplitudes for vertical films.

The predicted increases in mass transfer shown in Table 1 are definitely not the result of increases in surface area. At a wave amplitude of 50 percent of the mean film thickness for the thickest films measured, and the shortest wave lengths, the increase in surface area is around 0.6 percent. These are the severest conditions encountered in the analysis, and thus the increase in surface is very slight in comparison to the predicted increases in gas absorption.

This analysis has been performed on a laminar flowing film whose surface is described by a standing wave. If it is desired to cause the wave to move with time, the arguments of the trigonometric functions in equation (40) should be altered to $k(x - ct)$, where ct is the wave velocity.

Discussion

There are features of this wavy convective diffusion model that are interesting. First, the proposed velocity profile is parabolic as derived by Nusselt (33) and measured by Wilkes and Nedderman (46) and to a certain extent by Grimley (18) for smooth surface films. As the experimental investigators noticed, when disturbances form on the liquid surface, the local velocities at a constant height above the flow surface fluctuated around the value determined for the smooth surface film in laminar flow. This observation is analogous to the plunging and rising of the streamlines

alternately as a wave crest or trough passes over a particular position along the bottom surface. Thus, in a sense, this flow model is consistent with the experimental velocity profiles.

Second, the introduction of the oscillating character to the free surface has resulted in a net increase in the penetration depth of solute into the film. As the amplitudes of the surface waves are increased, the penetration depth of the solute into the film is increased. The increase in mass transfer is accomplished merely as an increase in penetration depth rather than by the addition of an eddy diffusivity or a bulk mixing term.

The wavy problem has been solved to a first approximation, for a regular, periodic wave. Jepsen (23) has reported that the distribution of both wave lengths and amplitudes on the surface of falling films is random in nature. An interesting extension of this theoretical treatment would be the effect of a random wave pattern on the gas absorption process.

If the approximate solution to the smooth surface laminar convective diffusion equation obtained in this study is substituted into the partial differential equation, equation (6), it is found that the equation is not satisfied. This result is no surprise because of the methods used to obtain the approximate solution. However, because the integrated bulk concentrations determined from the approximate solution and Pigford's exact solution agree to within 3 percent, it is expected that the approximate profiles give

sufficiently accurate representation of the true profiles for design purposes.

It is noted that for short contact times only slight penetrations into the film are expected. With slight penetrations, the complementary error function solution of Bird (5) is also expected to provide an approximation to the correct profile since there are only small differences in the film velocity pattern in the surface region. Therefore the parabolic profiles of this study should also fit rather closely with Bird's complementary error function solution in the region of very small penetrations. Numerical solution of equation (6) by Jepsen (23) reveals that for slight penetrations (into one-quarter of the film thickness beneath the surface) the numerical and complementary error function solutions coincide.

A comparison of the parabolic profiles predicted for diffusion of CO_2 into a water film 0.0925 cm (Re = 926) thick at 24°C falling down a 5° inclined plane with contact lengths of 22" and 28" appears in Figure 5. Also appearing in Figure 5 are the concentration profiles predicted for a film of infinite depth flowing at a constant velocity equal to the surface velocity of the finite film. Though agreement between the profiles is close, the deviation is the reason for the 3 percent difference in bulk concentrations reported earlier. As penetration becomes deeper, the deviation of the parabolic profiles from those of the complementary error function solution

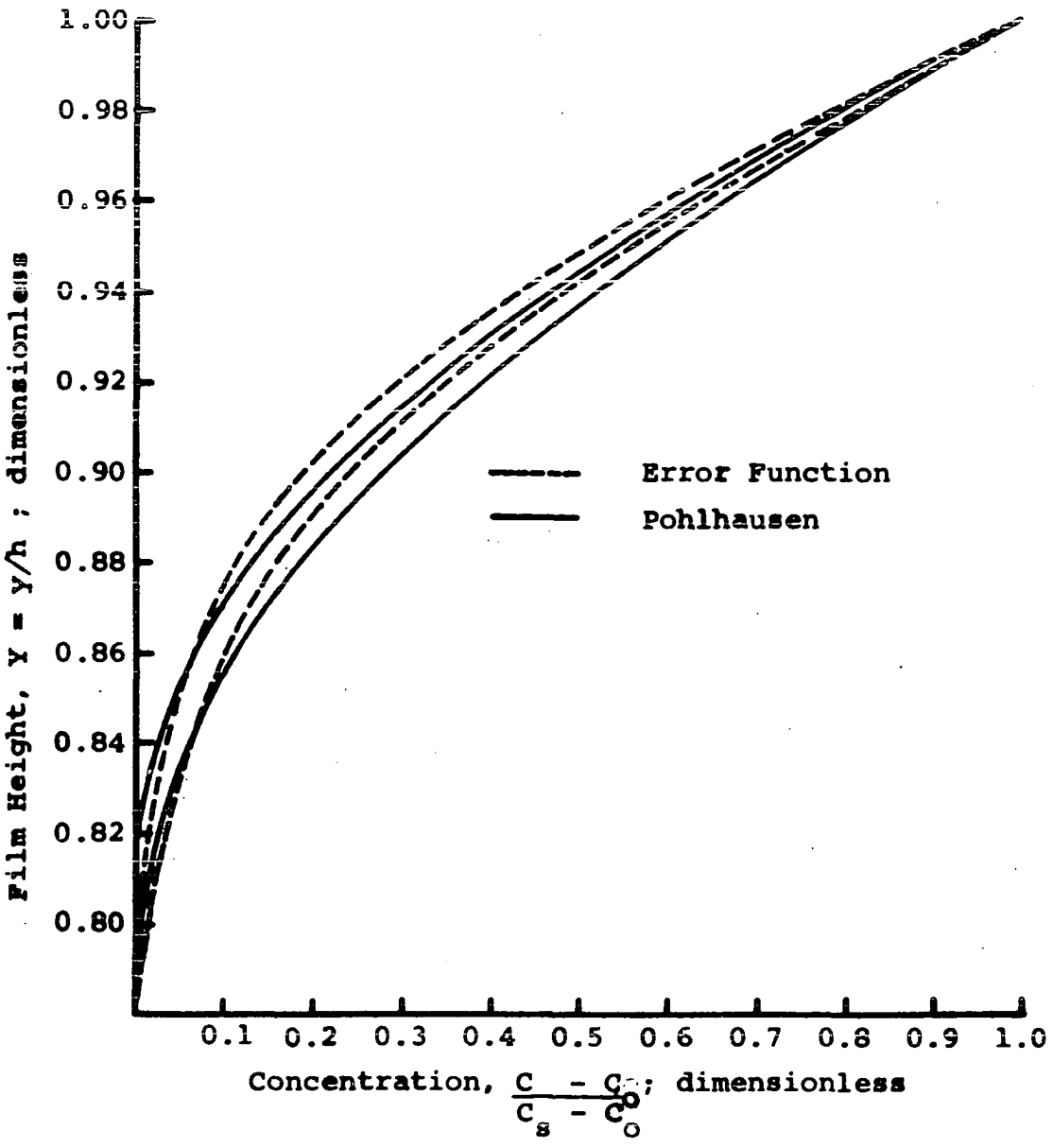

Figure 5

Comparison Between Theoretical Concentration Profiles for CO_2 Diffusion into Water at 24°C, an Angle of 5°, Re = 926, and Contact Lengths of 22 and 28 Inches

are seen to be in the proper direction. Because of the parabolic velocity profile, local velocities below the surface in the finite film are less than the surface velocity which results in longer residence times for the fluid traveling below the liquid surface. With extended contact times the solute penetration is expected to be deeper, so the deviations between the two corresponding curves is in the right direction. This condition is true except at the low values of concentration where the curves cross. The finite film concentration profiles must go to zero at some finite film depth while the error function profiles only go to zero at an infinite film depth.

If the total diffusion coefficient for the parabolic concentration profile is calculated as a function of film depth from equation (41)

$$D+\epsilon = \frac{h^2 \int_o^Y u[\underline{C}(x_2,Y) - \underline{C}(x_1,Y)]dY}{[x_2-x_1]\left.\frac{d\underline{C}}{dY}\right|_{avg}} \qquad (41)$$

an estimate of the deviation of the parabolic solution from the exact solution is obtained. The results of this calculation for the concentration profiles of Figure 5 are found in Figure 6. Also appearing in the figure is the same clacula-tion using equation (41) with $u = u_s$ for the error function profiles when 1.) the solute below Y = 0.75 is assumed negligible; 2.) all solute below the liquid surface is included; and 3.) only additional solute is added to case 1

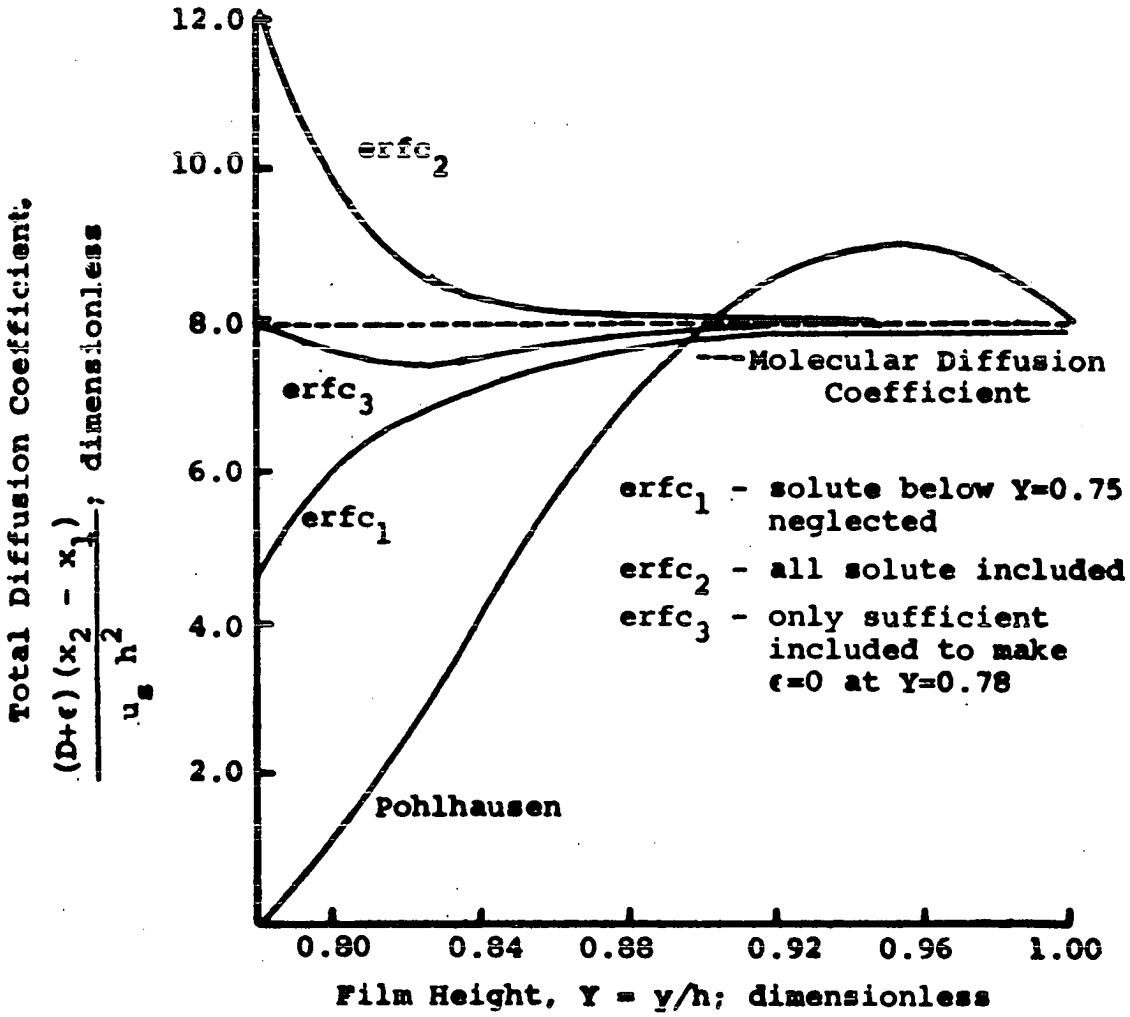

Figure 6

The Dependence of Total Diffusion Coefficient on Film Height for Theoretical Concentration Profiles

to permit the calculation to yield the molecular diffusion coeffecient at $\bar{Y} = 0.78$. All the integrations were made by graphical integration. The average value of $d\underline{C}/dY$ was determined from a graphically integrated average $d\underline{C}/dy$ between x_1 and x_2.

The total diffusion coefficients determined from the complementary error function concentration profiles demonstrate the sensitivity of the calculational procedure to inaccuracies in the reduction of experimental data. For the error function curves, Case 1 shows the result of interpreting an absence of solute at a depth where some is present, Case 2 shows the effect of determining a penetration that is too deep into the liquid, and Case 3 shows what may occur as a result of the graphical integration procedure. These results are further distorted if an arithmetic average value of $d\underline{C}/dY$ is used in equation (41) instead of an integral average. The curve for the parabolic concentration profile shows the diffusion coefficient obtained when slight deviation (3 percent) from the exact solution to the differential equation is encountered.

The wavy problem analysis also points up a difficulty that might be encountered in interpretation of experimental data. The oscillating character of the diffusion boundary layer depth, combined with an always parabolic concentration profile, would cause instantaneous values of the profile to be inappropriate for determination of the bulk concentrations.

Specifically, the high value (16) of the exponent in the logarithm term in equation (40) would cause much greater apparent penetrations under wave crests than under troughs. In the comparison of two profiles, one obtained under a trough and the other obtained under a peak, it might be inferred that a much larger change in total concentration occurred than actually existed. Thus, determination of effective diffusion coefficients from instantaneous concentration profiles not having the same surface configuration might lead to erroneous conclusions.

In summary, then, there are three useful features resulting from this theoretical model. The first is the prediction of sizable increases in gas absorption when waves are present on the surface of the film. The increase in mass transfer has been obtained without the introduction of an eddy diffusivity or a bulk mixing term. The second contribution of this theory is that it shows the sensitivity of the calculation procedure used by previous investigators for the determination of total diffusion coefficients. Slight deviations in profile shape can have rather large effects on diffusion coefficient determinations. The third contribution is the observation that the concentration profiles are of a time varying character due to the motion of the waves, and thus, they will cause calculations of diffusion coefficient values to scatter widely.

CHAPTER IV

APPARATUS AND OPERATING PROCEDURE

The equipment used in this experimental study was the same as that used by two previous investigators, Jepsen (23) and Lu (30). Only minor modifications were necessary. Three separate types of experimental measurements were made. These included the determination of the various gross liquid film characteristics, largely from capacitance measurements, the determination of average concentration of solute in the efflux from the experimental apparatus by titration procedures, and the measurement of concentration profiles from photographs of light interference patterns.

All of the experimental measurements were associated with the various transport processes occurring interior to the gas-liquid contacting cell (see Figure 7) which was previously described by Jepsen. This cell was constructed from two aluminum plates 0.438" x 2.95" x 35.33". Upon the bottom aluminum plate was cemented a glass plate measuring 0.0625" x 2.95" x 34.83". The original glass plate became cracked due to the compression from the vertical sides and was replaced by placing another glass plate,

SIDE VIEW

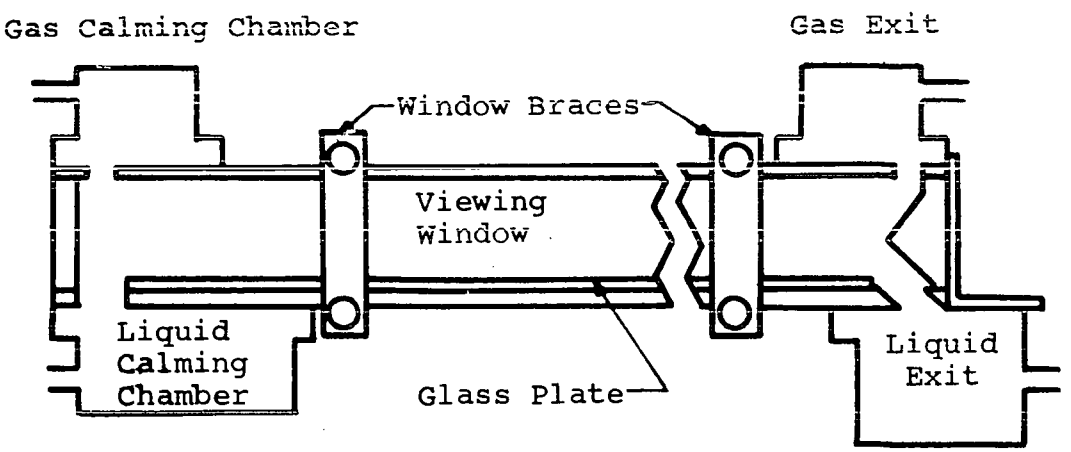

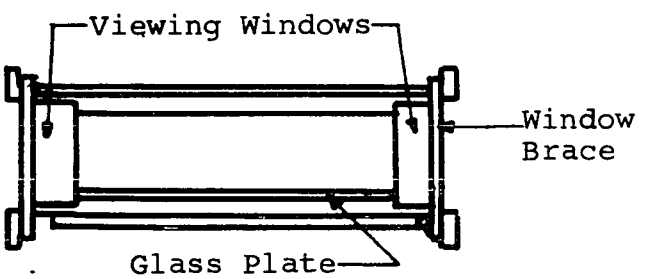

END VIEW

Figure 7
Sketch of Gas-Liquid Contacting Cell

0.0625" x 2.98" x 34.83" over it. The latter glass plate was used only in compartmented flow determinations.

The lateral liquid retaining walls were provided by 0.4" x 1.0" x 36.0" optically-flat, glass, viewing windows. One window was shattered early in the experimental studies at a position 26" from the feed end of the cell. The cracks in the window were plugged with glue and the experiments continued, as no replacement window was available.

Gas and liquid entered the cell through separate calming chambers and flowed out of the cell through separate slots located in the top and the bottom at the downstream end of the cell.

Temperature and flow control were provided on both the gas and liquid streams and have been previously described by Jepsen. Operating temperature was at 24.0° C, $\pm$ 0.1°. Water flow rates were measured constant to $\pm$ 2 percent. Lu's schematic diagram of the experimental apparatus arrangement is applicable to this study except that the ion exchange column and filter were removed, the centrifugal pump was replaced by two 1/4 horsepower gear pumps mounted in parallel, and the liquid flow lines were 1/2" nominal galvanized pipe instead of tygon tubing. The schematic diagram of the apparatus is found in Figure 8.

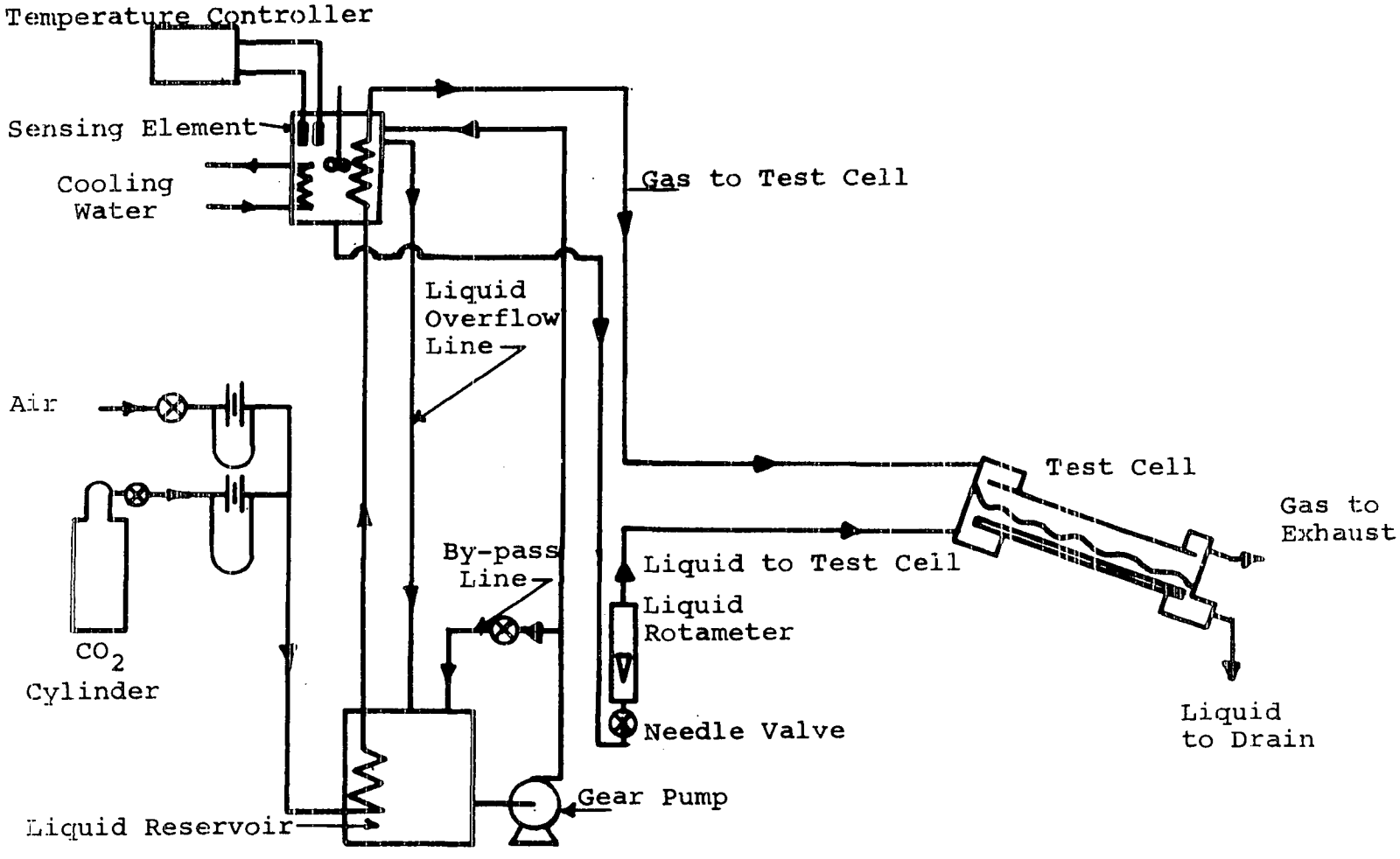

Figure 8

Schematic Diagram of Experimental Apparatus

Studies of Film Characteristics

The gross film characteristics were obtained as the output from a capacitometer and recorded on light-sensitive paper by a Minneapolis-Honeywell 906C Visicorder with a mechanically damped galvanometer whose maximum frequency response was 270 cps ± 10 percent. The capacitometer was a device designed by Dukler and Bergelin (10) and modified by Jepsen. This device was employed in the measurement of the instantaneous values of the capacitance of the air gap that existed between the surface of the liquid film and a 6 x 8 mm aluminum plate mounted on a depth micrometer. The flowing fluid in these experiments was tap water. Calibration studies on quiescent liquid layers showed this water to be a sufficiently good conductor to act as the other capacitor plate, independent of its depth. The capacitometer was capable of detecting surface fluctuations of 0.0001" but uncorrectable instrument drift prevented absolute determination of film thickness to closer than 0.001". Correction for drift was attempted by repeating the measurements from four to five times and averaging the results.

The most satisfactory method of instrument adjustment, calibration, and operation was found to be as follows. The contacting cell was oriented horizontally, and a thin layer of tap water was admitted, sufficient to provide a distance of 0.07" between liquid surface and the bottom. The metal plate probe was located at a large distance,

about 0.12", above the quiescent liquid surface. The variable capacitor and the discriminator current control were adjusted so that a small change in the variable capacitor, whose output was registered on the milliammeter, produced a large deflection of the current of the microammeter. These adjustments were continued until the capacitometer was in its most sensitive condition. Next, the galvanometer was brought onto the visicorder scale by adjustment of the visicorder current control. The micrometer-mounted metal plate was then advanced toward the liquid surface to determine the extent of the scale sweep of the galvanometer. Minor adjustments to the variable capacitor, when the capacitometer was in this most sensitive adjustment, had large effects on the sweep of the visicorder galvanometer. Usually the micrometer-mounted metal plate would cease to produce deflection of the visicorder galvanometer while an air gap of 0.003" still existed. This type of adjustment was satisfactory for operation at low angles of inclination where disturbance amplitudes were slight. For work at the higher angles of inclination where disturbance amplitudes were greater, it was necessary to sacrifice capacitometer sensitivity to gain a non-deflecting galvanometer position at a larger terminal air gap by adjusting the capacitometer sensitivity to gain a non-deflecting galvanometer position at a larger terminal air gap. This requirement was accomplished by adjusting the capacitometer in the same fashion as described above, but upon obtaining a zero galvanometer

deflection when a small air gap existed, the variable capacitor was adjusted slightly so that the galvanometer moved back to visicorder readings corresponding to larger air gaps. It was found that this technique reduced both the capacitometer sensitivity and the breadth of full scale galvanometer sweep. Also, the air gap of zero galvanometer deflection was found to be larger than that of the most sensitive adjustment.

With the capacitometer adjusted to the desired sensitivity, the calibration procedure could be carried out. Micrometer settings and the corresponding galvanometer position on the visicorder scale were recorded. The micrometer reading for the case where the metal plate rested on the bottom glass plate of the contacting cell had been previously recorded. By advancing the metal plate toward the liquid surface in small increments, it was possible to obtain the necessary visicorder and micrometer readings. When the air gap became sufficiently small to eliminate further deflection in the visicorder galvanometer, the metal plate was extended until it just touched the liquid surface and the appropriate micrometer reading was recorded. Thus, with micrometer readings for the film bottom, surface, and at various positions above the surface, it was possible to determine the magnitude of each air gap and its corresponding visicorder reading.

In order to be certain that the actual capacitance measured represented only the air gap and not also the tap

water layer, the calibration procedure was repeated several times on liquid layers of various depths but with no further adjustment of the capacitometer controls. It was found that the various air gaps as a function of visicorder reading curves did not coincide, but no definite trend was established with changing film thickness. Usually the calibration curves for the different depth layers fell within 0.001" of the mean. No attempt was made to eliminate instrument drift as a small change in the variable capacitor often produced drastic changes in capacitometer sensitivity.

After the capacitometer was calibrated by this procedure, film measurements could be made. This measurement was accomplished by inclining the cell to the desired angle, setting the liquid flow rate at the desired level with the needle valve and rotameter, and placing the micrometer mounted metal plate in a position sufficiently close to the liquid surface to insure adequate deflection with wave passage, but not so close as to allow wetting of the probe surface by high amplitude disturbances. The visicorder paper drive was then started and was run for approximately fifteen seconds. With a known micrometer reading for the metal plate probe, the calibration curve, and the wave trace, it was possible to determine instantaneous values of the liquid surface location.

At the termination of a series of runs, the calibration procedure was again repeated for several liquid layer depths to determine the amount of instrument drift

over the duration of the experiment. The mean of the initial calibration curves was used for the reduction of data taken during the earlier experiments, and the final calibration curves were used in the analysis of the later experiments.

From each visicorder trace it was possible to determine the frequency of disturbances, a lower limit on the disturbance amplitude, and, through various methods of calculation (see Experimental Results), an estimate of the mean film thickness.

Studies of Gas Absorption in the Falling Film

The gas absorption studies were carried out in the contacting cell previously described. Pure CO_2 diffused into a falling film of distilled water in these studies. At the low angles of inclination of this study, it was not possible to use the technique of Jepsen and Lu to determine the bulk concentration of solute at various downstream positions from the liquid inlet without obviously altering the flow pattern over a large portion of the contact surface. Therefore bulk concentration measurements were made only at the exit end of the contacting cell. The analytical procedure for determining the concentration of the dissolved pure CO_2 in the distilled water was essentially as follows. A 250 ml sample of the contacting cell efflux was collected in a clean Erlenmeyer flask that had been previously filled with nitrogen. The sample was collected

through a funnel whose neck extended into the flask. Liquid was allowed to overflow the flask for approximately one minute after the flask had filled. Aliquots of 51.562 ml were taken with a sample-rinsed, hypodermic syringe and needle and placed in another clean Erlenmeyer that contained a measured amount of standardized NaOH, sufficient $BaCl_2$ solution to precipitate a 50 ml CO_2 saturated water sample, and phenolphthalein indicator. The $BaCl_2$ precipitated dissolved CO_2 as $BaCO_3$ in the basic solution, and the NaOH neutralized the hydrogen ion present. The excess NaOH was then back titrated to the phenolphthalein endpoint with standardized HCl solution. Separate aliquots from the same sample could generally be reproduced to within 1 percent. Titrations on aliquots from separate samples varied up to $\pm$ 15 percent.

During every run at each angle of inclination, a blank was titrated on the system distilled water. This measurement established initial dissolved CO_2 concentration or carbonate ion content of the feed water. Initial CO_2 concentrations were generally less than 0.01 gm/liter.

As has been mentioned previously, due to the increased flows in the meniscus that formed adjacent to the vertical windows, it was necessary to compartment the contacting cell efflux to determine the proper flows to which the film thickness measurements corresponded. In addition, due to differences in residence times, the flow compartmentation was necessary to prevent the relatively dilute solution of the meniscus region from distorting the bulk

concentrations of the film flow region. The compartmenting of the cell was accomplished by forming dividers constructed from cut microscope slides. The leading edge of each partition was ground to a sharp "V". In the compartmented flow studies, each partition was 12" long and located about 1/4" inside each viewing window. The partitions were glued to the bottom glass plate and extended upstream from the exit of the contacting cell from which the flow for a particular rotameter reading was collected over a measured time interval. The flows in each meniscus region were also collected over measured time intervals as a check on the total volumetric flow. Since the adjusted volumetric flow over a known plate width was determined experimentally, it was possible to calculate the appropriate Reynolds number for the capacitance measured film thickness.

The twelve-inch partitions occupied about 1/3 of the total cell length. As the liquid passed the tips of the partitions, two new menisci were formed from the central region fluid, producing a thinner film. Had this effect been ignored, distorted values of the bulk concentration might have resulted. Thus, in an effort to maintain a constant film thickness over as much of the cell length as possible, the partitions were shortened to 3" for the concentration studies and placed about 0.4" inside each vertical viewing window. This provision left a free space of 2.19" in the central section of the cell.

For the central section, bulk flows per unit of width agreed well with those obtained in the compartmented flow studies.

In order to collect the divided flows in separate containers, it was necessary to remove the end from the contacting cell. This operation left one end open to the atmosphere and created difficulty in maintaining a 100 percent pure CO_2 atmosphere above the liquid surface during the concentration studies.

Interferometric Studies

The third phase of the experimental studies was performed on the Mach-Zehnder interferometer that was designed and built by Jepsen and is completely described in his thesis. Light from a 1000 watt, DC, high pressure, mercury vapor lamp was passed through condensing lenses and a green filter. This beam was focused on a slit to provide a point source of monochromatic light. The beams issuing from the slit were collimated and directed toward the first beam splitter plate of the interferometer. Here, half of the incident light beam reflects at a 60° angle from its incoming path and the other half is transmitted to a full mirror, where it, too, is reflected at a 60° angle from its incident path. The initially reflected beam is again reflected at 60° and passed through the test section of the contacting cell while the transmitted beam from the initial beam splitter, after reflection, is passed through glass compensating plates that provide a change in optical path

length equivalent to the test section of the contacting cell when it is filled with pure water. The two light beams are recombined by a second beam splitter plate which is aligned parallel to the initial splitter but at the opposite corner of the parallelogram. Here half of the beam from the test section is reflected and lost while the other half is transmitted. Also on this plate, the beam from the compensating plates is half transmitted and lost while the other half is reflected and recombined with the transmitted portion of the test section beam. Due to a slight divergence of the two beams issuing from the final splitter plate, light interference patterns (fringes) are formed. The fringe pattern is passed through a photographic objective lens and onto the lens system of a 35 mm camera. Photographs of the light interference patterns were taken at 1/30 second shutter speed on Type 1-D Kodak spectroscopic plates and developed for 10 to 15 minutes in Kodak D-19 developer solution. The photographic plates while being exposed were mounted in suitable holders and located one foot behind the camera lens. The camera was focused at the approximate center of the contacting cell.

In the operation of the interferometer and flow system the distilled water was brought to 24.0° C $\pm$ 0.1° C by temperature control in the constant head tank. The liquid was then allowed to flow at the desired rate through the contacting cell with a quiescent air atmosphere, and a photograph of the fringe pattern was made. Partially

obstructing the photographed light pattern was a cross hair arrangement mounted independent of the interferometer and test section in order to provide a reference point. After the photograph of the air-water fringe pattern was made, pure CO_2, also at 24.0° C $\pm$ 0.1° C, was allowed to flow into the test section. As a result of the change in refractive index of the distilled water containing the CO_2 solute, the fringe pattern distorted in proportion to the concentration profile in the liquid film. When no further change in the profile could be noted, except for fluctuations due to surface disturbances, a by-pass valve was opened on the CO_2 line which allowed a quiet CO_2 atmosphere to exist above the liquid. A photograph was then taken of the fringe pattern of the CO_2 - water system. Upon completion of this routine, the contacting cell was purged of CO_2 with air (evident when the fringe patterns indicated no varying profile in the film) and the water rate set at the next desired level. This procedure was repeated at liquid flow rates corresponding to film Reynolds numbers (i.e. determined from central compartment flows which excluded the meniscus flows) ranging from 140 to 1940. A photograph of the air-water system was taken for each Reynolds number studied up to 1100. Above this Reynolds number, the CO_2 - water fringe patterns were compared with the air-water photographs at a Reynolds number around 1000. Photographs of the concentration profiles were taken at positions

located 10, 19, 22, 25, 28, and 30" from the liquid feed point. The angles of inclination studied were 1°, 2°, and 3° from the horizontal.

In order to be able to locate the bottom glass plate in each fringe pattern, it was necessary to photograph the base of the depth micrometer as it extended into the flowing film at a known distance above the bottom plate. The micrometer was extended to the bottom glass plate and read. It was then lifted from the bottom until light could be seen beneath the tip of the micrometer shaft, and another reading made. A photograph was then made of the fringe pattern and the micrometer tip and another made with the green filter removed from the light path and with the light beam that passed through the compensating plates obscured. Since the magnification ratio was established from a photograph of a 1/2 cm scale with 100 divisions placed in the center of the cell, it was possible to locate the glass plate surface at the top of striations that existed in each photograph. In order to see the maximum available fringe pattern, the contacting cell was rotated laterally until the thickest light band possible appeared before the bottom location procedure was begun.

CHAPTER V

EXPERIMENTAL RESULTS AND DISCUSSION

Film Characteristics

Experimental measurements associated with the characteristics of the falling liquid films included determinations of bulk liquid flows and various properties of the film. The bulk liquid flows were determined in the compartmented contacting cell which allowed the elimination of flows in the meniscus regions located at the sides of the glass plate. The properties of the film were determined from capacitance studies in the center of the cell. From the capacitance measurements it was possible to obtain average values of the film thickness, average frequencies of the surface ripples and estimates of the ripple magnitude.

Flow Measurements

Because of the increased depth of fluid in a meniscus region, local velocities adjacent to a vertical boundary, which is wetted by the liquid, are greater than in the film (4, 16, 17). In order to establish an appropriate Reynolds number in a region far from the cell walls, it was necessary to eliminate flows in the vicinity of the

wall. This requirement was accomplished by dividing the efflux from the cell as it flowed from the end of the bottom glass plate. The measurements were carried out at angles of 1°, 2°, 3°, 5°, 10°, 15°, and 25° at flow rates ranging from 4.6 to 33.3 $cm^{3}/sec.$ in the 7.5 cm width diffusion cell. These flows corresponded to total Reynolds numbers, i.e. those determined from the total volumetric flow rates distributed over the total cell width, that varied from 272 to 1917. The film Reynolds numbers, which were based on the flow per unit width in the center compartment of the cell, were of course, less than these values because of the exclusion of the meniscus flows.

The results of the compartmented flow measurements are presented in Figures 9 and 10, where the film Reynolds number is plotted as a function of the total Reynolds number, and the fractional meniscus flows are plotted as a function of volumetric flow rate. Also shown are the results of Binnie's (4) studies on a flat plate with teakwood sides.

The figures show that at a given total Reynolds number, the film Reynolds number differs more as the angle of inclination increases. This result is attributed to the film becoming thinner at the higher angles, while the relative height of the meniscus on the vertical wall remains essentially the same.

When the volumetric flow rate is increased at a particular inclination angle, one expects the film Reynolds

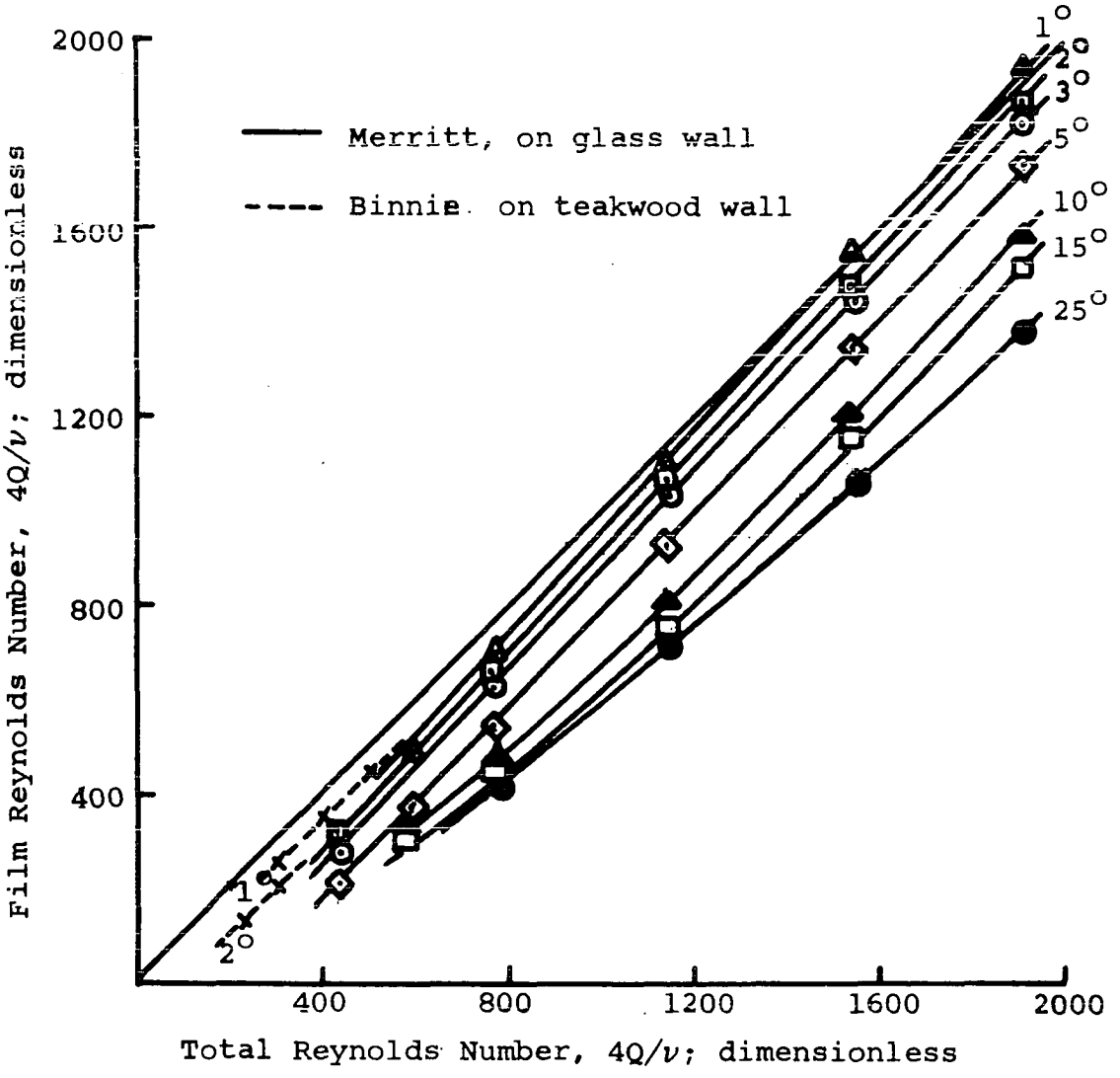

Figure 9

The Experimental Relation Between
Total Reynolds Number and Film Reynolds Number
for Water at 24° C

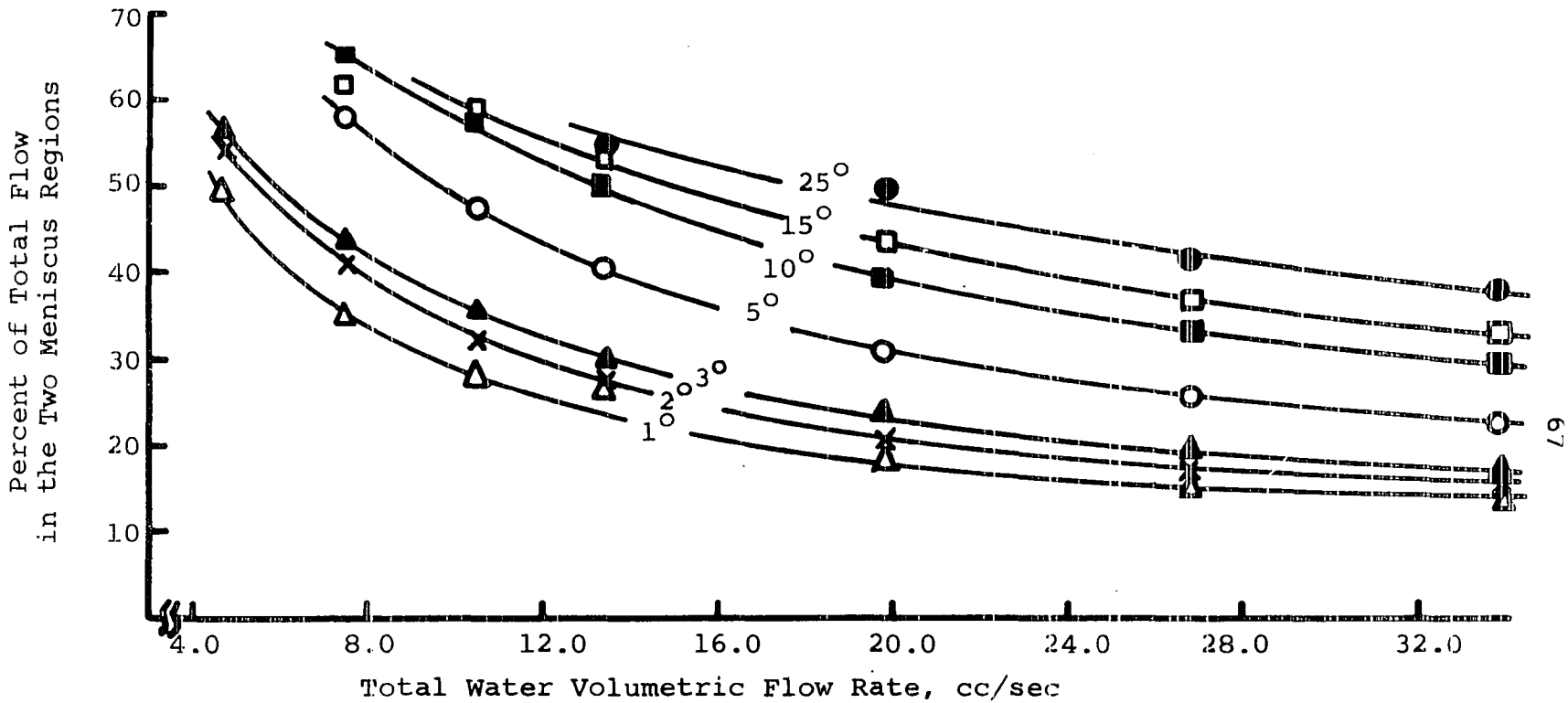

Figure 10

The Experimental Effect of Volumetric Flow Rate on the Percent of Total Water Occupying the Meniscus Regions on Glass Walls at 24° C

number to tend towards the total value. This observation is the result of a proportionately larger increase in the film thickness than in the meniscus height. Accordingly, the slopes of the experimental curves are greater than unity at the higher Reynolds numbers.

Figures 9 and 10 show rather graphically the hazards that may be encountered at low Reynolds numbers if the lateral distribution of the flowing fluid is ignored. Basing film characteristic correlations on total bulk flows can lead to serious error in the designation of the appropriate Reynolds number. It is obvious from the figures that the wall effects become more pronounced as the angle of inclination is increased.

Several experimental difficulties were encountered in these investigations. As the liquid flow rate was decreased to film Reynolds numbers around 200 at a constant inclination angle, the films became so thin that it was no longer possible to maintain a continuous film laterally across the plate. The film would break near the bottom end of the inclined plate, and the tear in the liquid surface would propagate up the plate, leaving liquid to flow out the two corners where the bottom plate joined the side walls. The initial break in the film may have resulted from a small bow in the glass plate due to compression from the walls.

At the leading edge of the dividers, which separated the flow, circular indentations were noticed in the

liquid surface, approximately 3/8" in diameter. The tip of the divider was located half way along the radius toward the center of the indentation. The indentation extended into about the middle of the film. It was assumed that no redistribution of the flow resulted from these indentations in the surface. Because of the formation of additional menisci on the flow dividers, the liquid depth decreased in the side compartments downstream from the divider tips.

Film Thickness

The thickness of the falling tap water films was measured with the capacitometer at angles of inclination of 1°, 2°, 3°, 5°, 10°, 15°, and 25°. The liquid flow rates were varied over a range of film Reynolds numbers from 140 to 1940. This range was originally assumed to include the transition region between laminar and turbulent flow. The upper limit of Reynolds number for the laminar flow region has been reported in the literature (10, 42) as between 1000 and 1200 when flow is down a vertical surface.

The average experimental film thicknesses as a function of film Reynolds number are shown in Figures 11 to 17. Because the capacitometer yields instantaneous values of the liquid surface height, an average film thickness may be determined in several ways. Three different averages are reported in the figures. The three methods of calculating the average film thicknesses

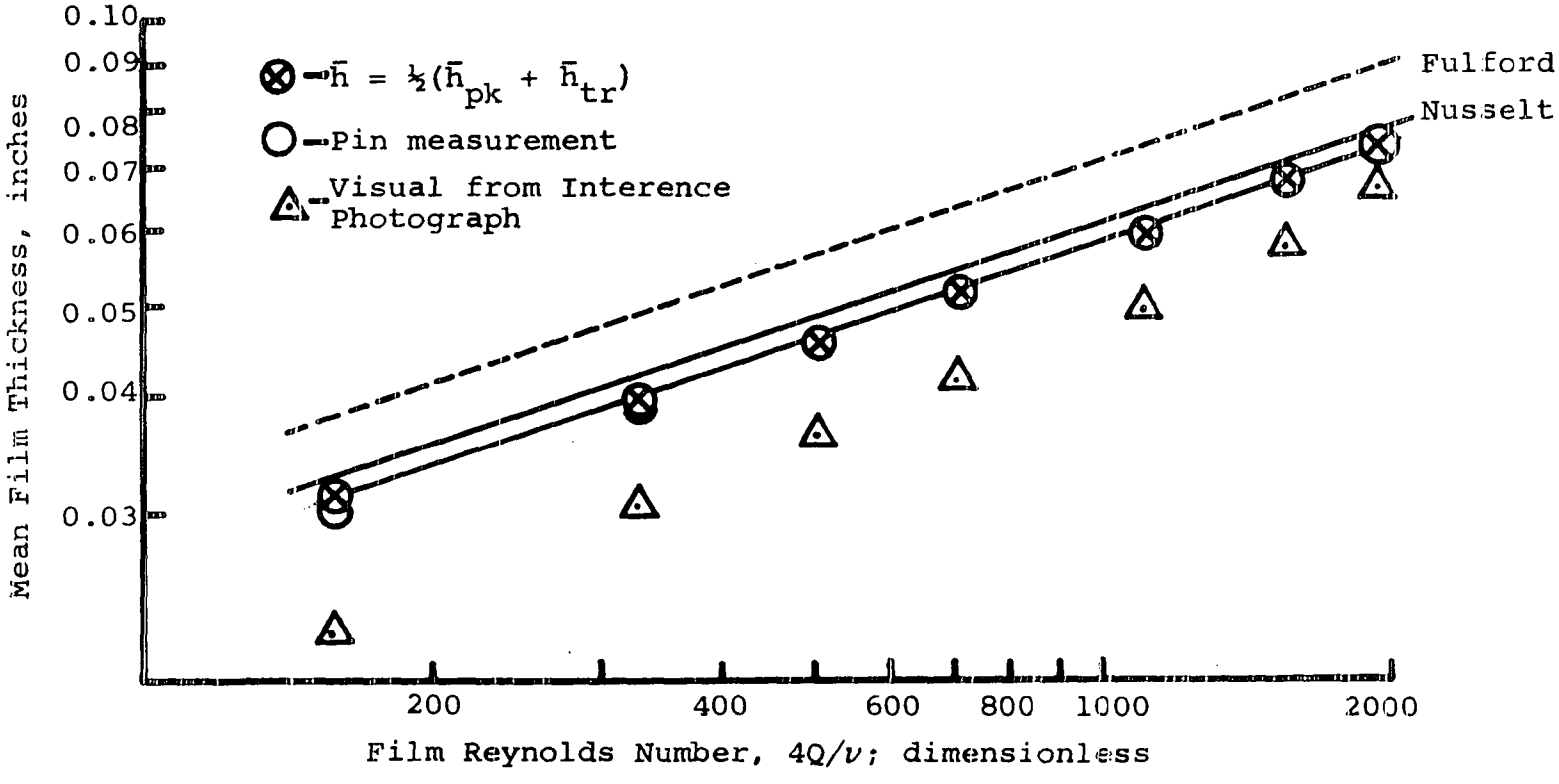

Figure 11

The Experimental Effect of Film Reynolds Number on Mean Film Thickness of Water at 24°C and an Angle of 1°

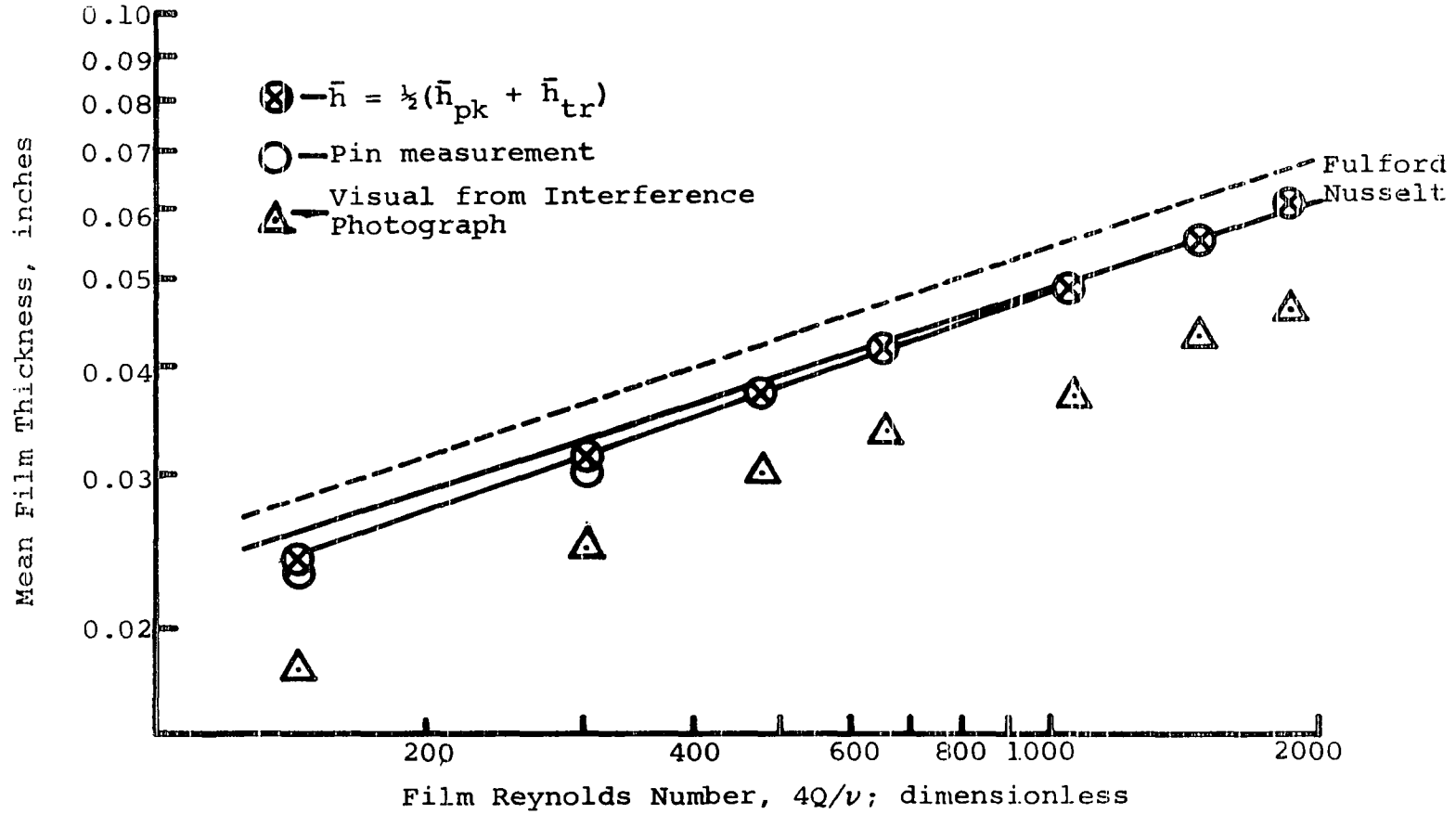

Figure 12

The Experimental Effect of Film Reynolds Number on Mean Film Thickness of Water at 24°C and an Angle of 2°

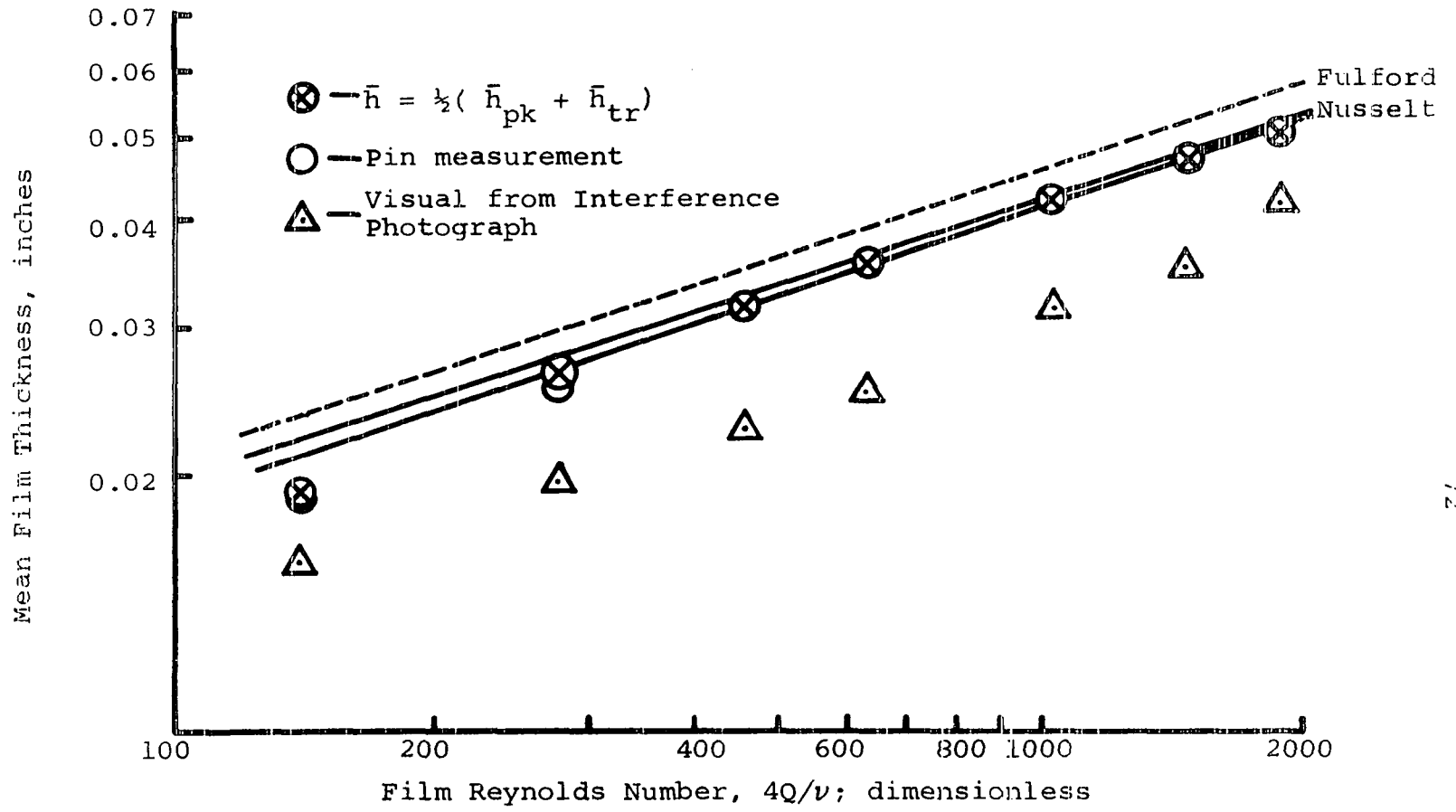

Figure 13

The Experimental Effect of Film Reynolds Number on Mean Film Thickness of Water at 24°C and an Angle of 3°

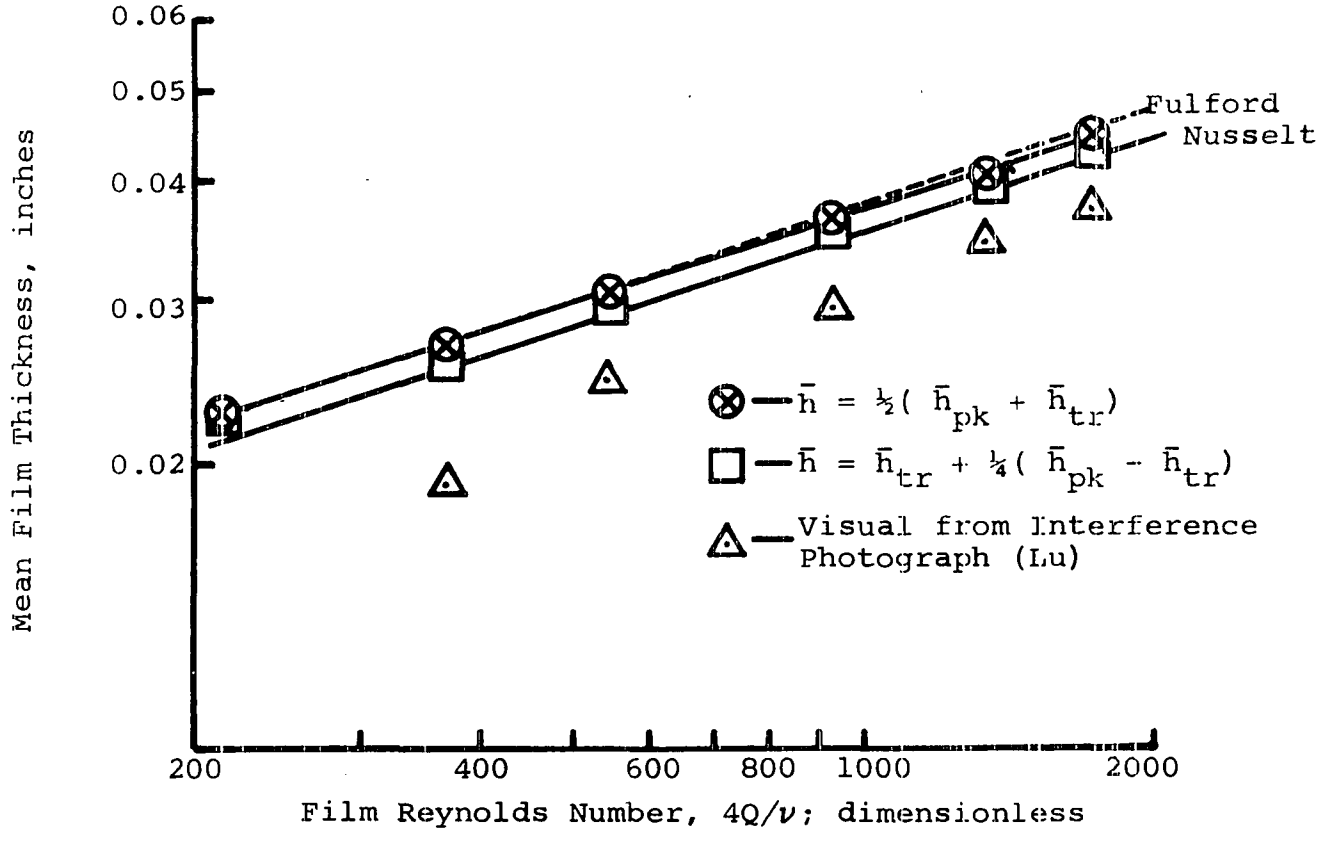

Figure 14

The Experimental Effect of Film Reynolds Number on Mean Film Thickness of Water at 24°C and an Angle of 5°

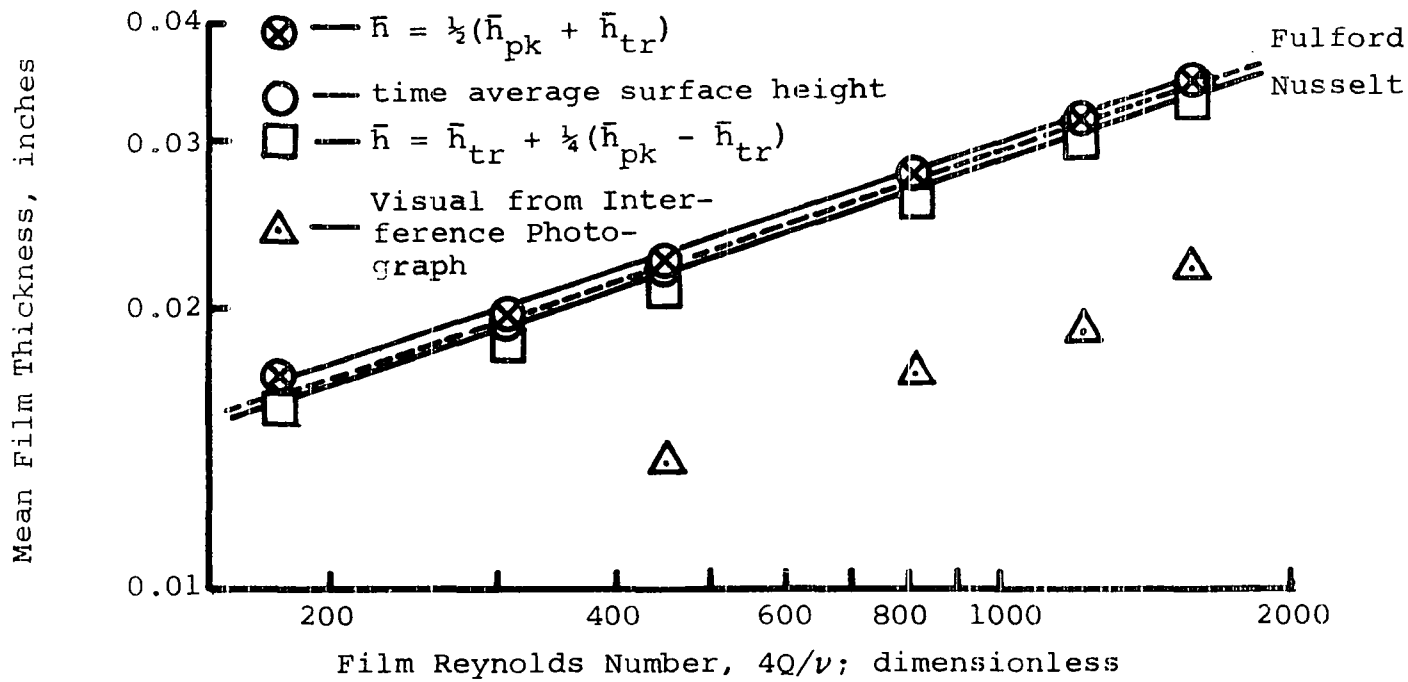

Figure 15

The Experimental Effect of Film Reynolds Number on Mean Film Thickness of Water at 24°C and an Angle of 10°

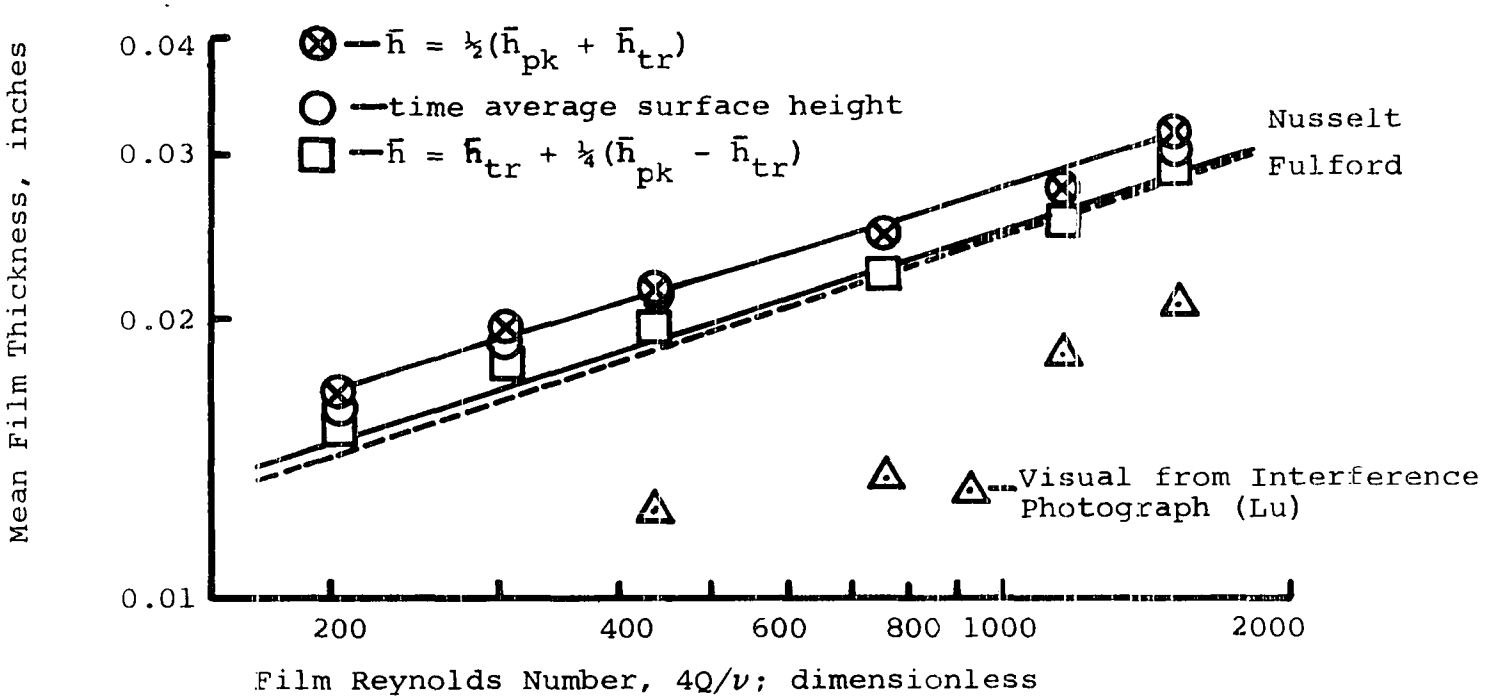

Figure 16

The Experimental Effect of Film Reynolds Number on Mean Film Thickness of Water at 24°C and an Angle of 15°

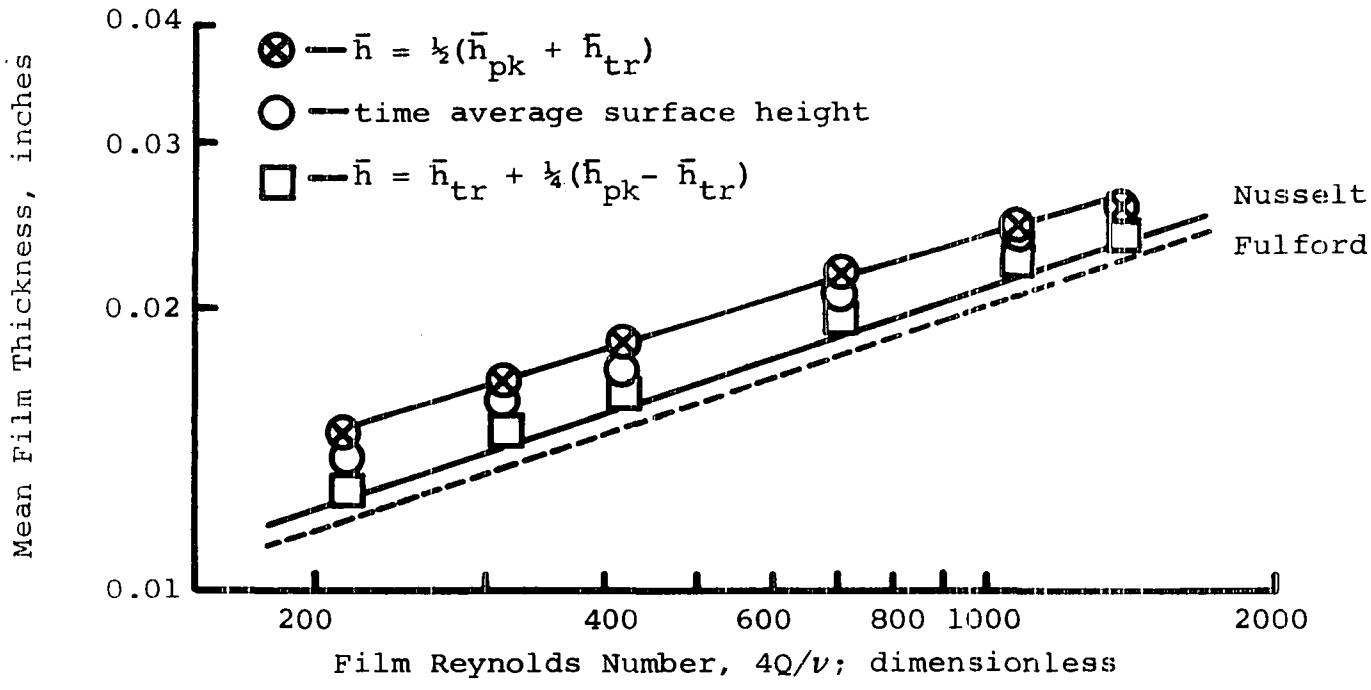

Figure 17

The Experimental Effect of Film Reynolds Number on Mean Film Thickness of Water at 24°C and an Angle of 25°

were 1.) an arithmetic average of the mean peak and trough heights of the surface disturbances; 2.) a point located one-fourth of the vertical distance from the mean trough to the mean peak height; and 3.) an average of the surface locations determined at equally spaced time intervals. Included in Figures 11 to 17 for comparison, are the corresponding curves for the Nusselt film thickness and the extrapolated empirical correlation of Fulford (17). The experimental film thicknesses presented are the averages of all the data taken at a particular flow rate and angle of inclination. In the instances where the surface was free of disturbances, checks on the capacitance measured film thicknesses were made with a micrometer mounted pin. These data are also reported in Figures 11 to 13.

Of the three methods mentioned for determining an average film thickness, the average of the mean peak and trough heights is the most readily obtainable. However, the problem is to decide which peaks and troughs are due to actual irregularities in the surface as opposed to spurious disturbances. As will be explained in a subsequent section, Wave Amplitude, a minimum amplitude criterion was selected. Examination of the capacitometer traces shows that the wave profiles are irregular in shape and suggests that the mean surface height is located somewhere beneath the average of the mean peak and trough heights. For comparison the second average surface height,

located one-fourth of the vertical distance from the trough height to the mean peak height, was determined. Finally if the wave pattern is truly random, as suggested by Jepsen (23), a time average of the surface height would yield a good estimate of the mean film thickness. The values obtained from the time averaging of the surface heights are seen to fall closer to the average of the mean peak and trough heights than to the thickness located at one-fourth of the vertical distance from the mean trough to the mean peak height.

Examination of Figures 11 to 17 shows that the mean film thickness agrees well with the Nusselt theory up to angles of 10°, and that the slopes of the film thickness as a function of Reynolds number curves are close to the theoretical value for laminar flow of 1/3. Above 10°, the data indicate thicker mean films than the theory predicts though the slopes of the curves are still in the vicinity of the theoretical value of 1/3. At the higher angles, the surface agitation becomes more violent, and it is here that the mean thickness determined at one-fourth of the vertical distance from the mean trough height to the mean peak height is still found to yield good agreement with the Nusselt theory. Since the hold-up data of Fulford (17) also agree with the Nusselt theory, it is felt that it is safe to conclude that Nusselt type flow exists in the mean, up to 25° of inclination. At about 5°, Fulford's extrapolated empirical correlation

crosses the curve representing the Nusselt film thickness. Films thicker than those of the Nusselt theory at angles less than 5° are not physically satisfying, and hence disagreement with the Fulford correlation at these conditions is not considered disturbing.

Film thickness measurements were made at positions 10", 19", and 25" from the liquid inlet to the diffusion cell. No significant deviation is observed in the data as the distance from the inlet is changed, indicating that the flow is fully developed into its parabolic profile before it has traveled 10" down the inclined plate. In addition, capacitance measurements of the average liquid film thickness were made to within 1/4" of the sides. No detectable difference in liquid film thickness is observed, indicating the essentially uniform depth of the film to within 1/4" of the walls.

Figures 11 to 17 do not show any tendency of the film thickness toward the turbulent regime as is demonstrated by the results of Dukler (10) and Thomas (42). Both Dukler and Thomas were studying films in vertical flow, however, where local velocities reach much higher values than are encountered at the low angles of this study. Apparently the Reynolds number alone is not sufficient criterion for determining the transition point of laminar to turbulent flow in inclined flow, but it must in some way reflect the angle of inclination. Fulford's correlation also recognizes this point and

relates film thickness directly to the cube root of the Reynolds number and inversely to the cube root of the sine of the angle of inclination.

A difficulty encountered in the treatment of the data arises in deciding how large a surface disturbance must be before it is properly classified as a wave. This decision is further complicated by noise generated in the capacitometer as well as the effect of the virtually stationary waves emanating from the edge of the cell. In addition, the capacitometer traces (see Appendix C) indicate that the waves are triangular in appearance (pointed at their peaks) and spaced with irregular intervals between their bases. The bases or troughs of the waves when compared with the peaks appear wider and more rounded. This observation suggests that the mean film thickness is located nearer to the average trough height than to the average peak height, but just how much nearer is not readily determined without an integration of the areas under the traces. Because of the equipment and expense involved, as well as the complicating factors of the irregular nature of the free surface, the non-linearity of the capacitometer calibration curve, and the uncertainty of the velocity profiles beneath the liquid surface, an integral average was not obtained.

Wave Frequency

The surface fluctuations on falling liquid films have been described as both ripples and waves. Certainly

the larger amplitude fluctuations, those readily visible with the eye, are properly named, and may be characterized by their frequency and amplitude. However, when the free surface of a falling film is observed by capacitance measurements, a large number of smaller disturbances is also detected.

If the surface waves have an effect on mass transfer rates into falling films, it might be reasonable to consider those with large amplitudes as more important than those that are barely detectable. On the other hand, if a surface were merely the observable manifestation of some internal dynamic action, then all surface disturbances should be considered to contribute to an overall characteristic frequency. Because of the complex pattern of wave lengths and amplitudes that appear on the capacitometer traces (see Appendix C), the average wave frequency is defined in this study as the total number of surface disturbances, both large and small, that appear on a trace, divided by the time period over which the trace was obtained. To complete the definition, the number of disturbances is considered to be half the number of changes in direction on a capacitometer trace.

Wave frequencies were determined from the capacitometer traces at angles of inclination of 1°, 2°, 3°, 5°, 10°, 15°, and 25° at a range of flow rates that corresponded to film Reynolds numbers that varied between 140 and 1940. The frequencies are reported in Figure 18

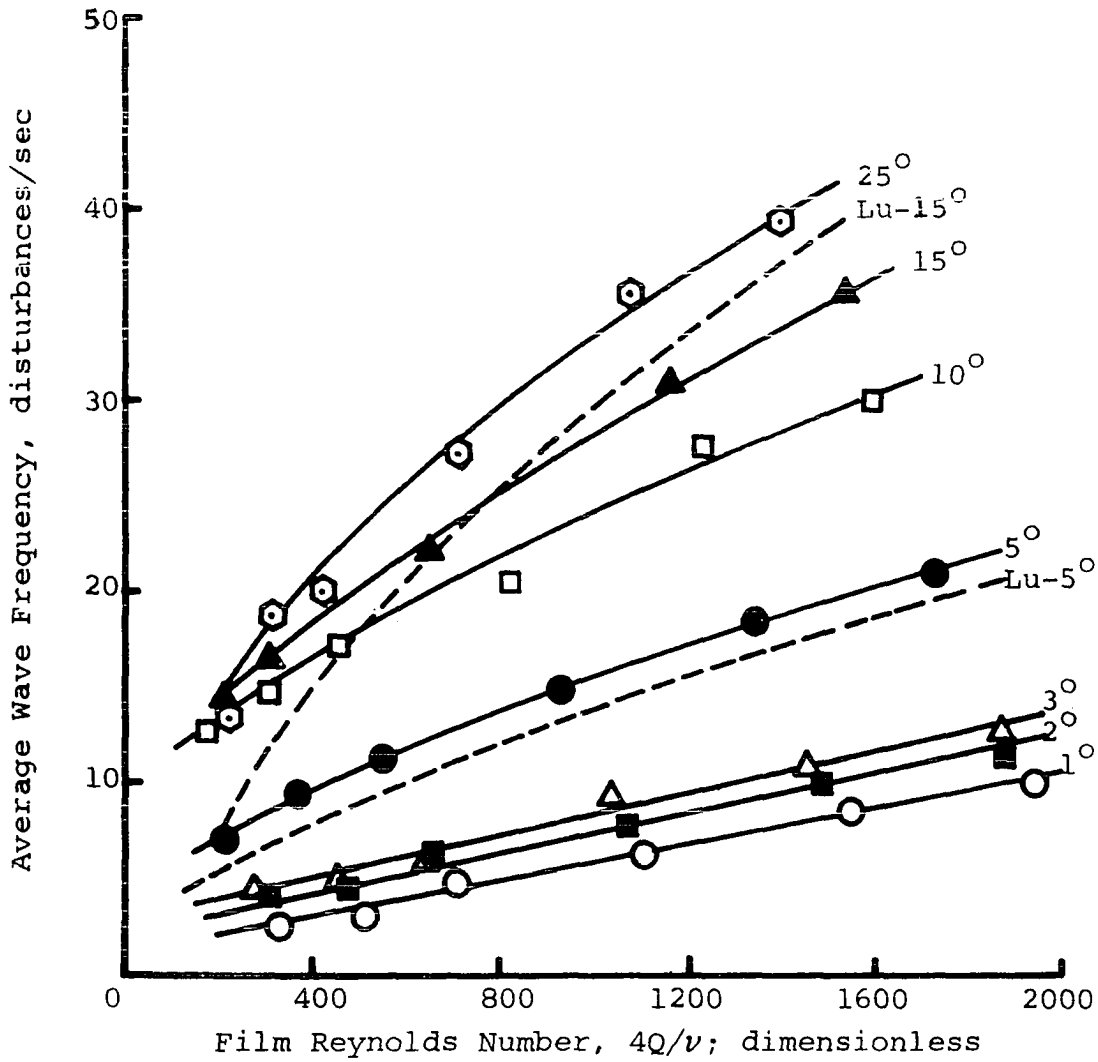

Figure 18

The Experimental Dependence of
Average Wave Frequency on Film Reynolds Number
for Water at 24° C

as averages of all the data and are plotted as a function of the film Reynolds number with the angle of inclination as a parameter. For comparison, the frequency data of Lu (30) at angles of 5° and 15°, and over the same range of film Reynolds numbers, are also plotted in Figure 18.

The data indicate an increase in surface disturbance frequency with increases in both film Reynolds number and angle of inclination. At the higher Reynolds numbers, the increase in frequency is less rapid than at the lower values. The data at an angle of 5° compare well with those of Lu, the curves having the same slope, though the absolute magnitudes determined by Lu are slightly less than those determined in this study. Lu's data at 15°, while deviating from the results here, do demonstrate the same trend.

Wave Amplitude

Since capacitometer traces yield a continuous record, it is possible to obtain an estimate of the average amplitude of the disturbances that travel on the surface of falling films. In this study, the mean wave amplitude is defined as one half the difference between the mean peak and trough heights of the surface disturbances. Mean wave amplitudes are reported in Figure 19 as a function of film Reynolds number for angles of inclination of 1°, 2°, 3°, 5°, 10°, 15°, and 25° and flow rates that correspond to Reynolds numbers which vary between 140 and

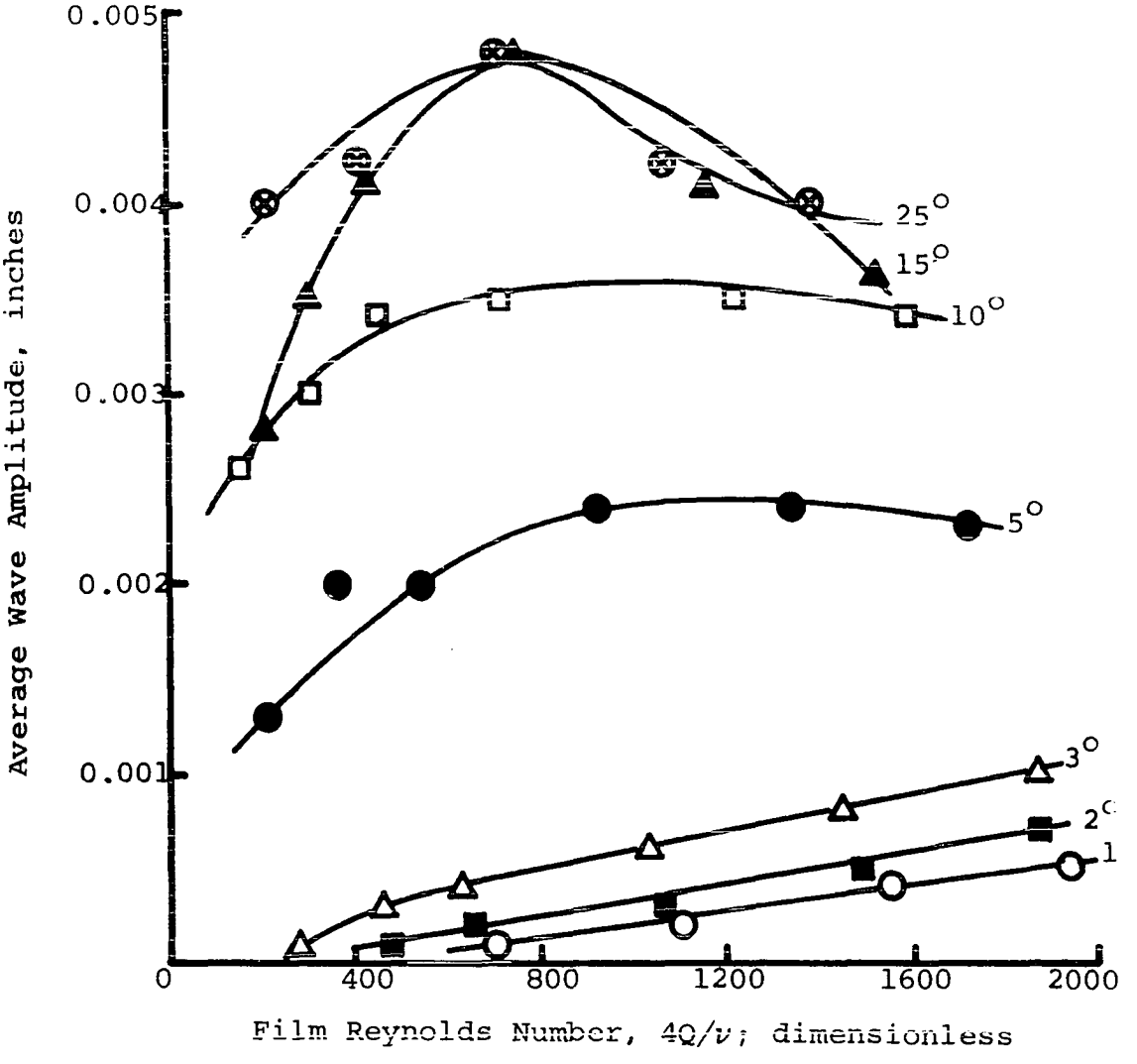

Figure 19

The Experimental Dependence of
Average Wave Amplitude on Film Reynolds Number
for Water at 24° C

1940. The results are presented as arithmetic averages of all the data obtained from the several runs.

The data in Figure 19 indicate increases in average wave amplitude with increases in angle of inclination. As the Reynolds number increases at angles above 3°, the average amplitude increases rather rapidly at low values of Reynolds number, passes through a maximum, and decreases gradually at the higher Reynolds numbers. Belkin (1), who has studied photographically the surfaces of films falling down vertical rods, also reports decreasing amplitudes with increases in Reynolds number.

For values of Reynolds number below 200 at angles of inclination between 1° and 5°, no disturbances were detected on the surfaces of the films. At angles greater than 5°, the capacitometer traces indicated surface fluctuations at all values of Reynolds number studied. The minimum surface fluctuation detectable at angles of 5° and above was about 0.0005", while at the lower angles capacitometer adjustment permitted the detection of fluctuations down to 0.0001".

Future investigators, who wish to use a capacitometer for determination of surface characteristics of liquid films, should be aware of the averaging properties that result from the dimensions of the probe, particularly with respect to the smaller length disturbances. Capacitometer traces reflect an average capacitance for the air gap between the metal probe and the liquid surface. If

probes are designed with dimensions comparable to half wavelengths of the disturbances, the surface position will not be determined accurately.

While operating at the higher angles (15° and 25°) some difficulty was encountered with wetting of the capacitance probe during studies at Reynolds numbers above 1000. In order to operate along the linear portion of the calibration curve, the probe was placed as close to the liquid surface as possible. The visicorder indicated that the probe was no closer than 0.015" from the liquid surface, yet advance of the probe position of 0.001" usually resulted in its wetting. With the probe in the more remote position, there was no indication that waves with amplitudes sufficient to wet the probe were present.

Dye Studies

In studies to determine whether the fluid traveled faster at the sides than at the center of the contacting cell, the cell was oriented at an angle of 2° and the flow was set at a film Reynolds number of 655. Red ink was dropped from an eye-dropper onto the surface of the liquid at a point about two feet from the exit end of the cell. The time required for the ink to pass out of the cell was determined with a stopwatch. Dye dropped at the wall required one to two seconds to exit the cell while that dropped into the center of the cell required 1.5 to 3 seconds.

The most interesting result of these studies was the behavior of the drops in the center of the cell. The dye on the surface dispersed rapidly toward the walls and passed out of the cell with a conical appearance, the dye that migrated to the wall passing out faster than that at the center. The undispersed dye that passed through the liquid surface to the bottom of the film, persisted in a long thin thread. It took approximately 15 seconds for this thread to be carried out of the cell by convection, though after the initial spreading on the liquid surface no further dispersion was detected.

These observations indicate a secondary flow on the fluid surface toward the vertical sides. However, no return flow was detected; the dye dropped adjacent to the wall did not indicate a similar lateral movement. Jackson (21) had proposed a film model in which the surface waves possessed a turbulent flow pattern. These turbulent waves were traveling over a sublayer that was in laminar flow. This condition might explain dye dispersion from the central region except that no such dispersion was noticed in the drops that were introduced into the fluid traveling at the cell walls.

The results of the dye studies give some insight into the complicated nature of flat plate, film flow and the effects that must be explained before a complete definition of the phenomena is accomplished.

Bulk Concentration Studies

Measurements of the bulk carbon dioxide concentration in the falling liquid film as it flowed from the end of the diffusion cell were made for angles of inclination of 1°, 2°, 3°, 5°, 10°, 15°, and 25° at flow rates corresponding to film Reynolds numbers that varied between 140 and 1940. Because of the distorted velocity pattern across the diffusion cell, concentrations were determined adjacent to the walls as well as in the central compartment of the cell.

The experimental routine was carried out in runs, which were considered to consist of all of the samples taken at the various flow rates at a particular angle of inclination. Thus, on a particular day, if seven flow rates were studied at one angle of inclination, the seven samples obtained, or more if several of the flow rates were repeated at the same angle, comprised a single run.

Titrations on successive 50 ml aliquots from the same 250 ml sample usually agreed to within 2 percent. However, titrations of aliquots from separate samples obtained under the same operating conditions on the same or on different runs varied as much as 15 percent. The average of all the concentration data obtained at a particular flow rate and angle of inclination is tabulated in Table 2. Also included in the table are the results of the average concentration determinations of the fluid in the meniscus region.

TABLE 2

AVERAGE BULK CONCENTRATION OF DISSOLVED CO_2 IN WATER FILMS AT $24^{\circ}C$

Angle of Inclination, degrees	Film Reynolds Number	Avg. Concentration in Meniscus, gm/liter	Avg. Concentration in Film, gm/liter	Avg. Concentration Pigford Theory, gm/liter
1	157	.2036	.4367	.4910
1	328	.1646	.3052	.3060
1	507	.1303	.2399	.2340
1	701	.1226	.2081	.1865
1	1103	.1123	.1525	.1380
1	1550	.1087	.1241	.1077
1	1940	.0976	.1012	.0885
2	143	.1880	.4175	.6090
2	304	.1473	.3325	.3545
2	477	.1383	.2383	.2525
2	655	.1334	.1957	.2022
2	1069	.1212	.1570	.1462
2	1480	.1108	.1238	.1136
2	1870	.1002	.0989	.0949
3	140	.2014	.5200	.7600
3	278	.1690	.3397	.4100
3	458	.1595	.2588	.2795
3	630	.1553	.2297	.2200
3	1032	.1290	.1664	.1580
3	1452	.1208	.1347	.1270
3	1870	.1115	.1174	.1092
5	214	.1941	.3964	.4310
5	368	.1705	.2939	.3010
5	541	.1538	.2484	.2370
5	926	.1389	.1905	.1720
5	1340	.1199	.1555	.1440
5	1725	.1143	.1215	.1280
10	176	.2414	.4179	.5460
10	307	.1961	.3630	.4200
10	450	.1851	.3171	.3265
10	815	.1481	.2179	.2080
10	1220	.1283	.1715	.1650
10	1587	.1082	.1377	.1429

TABLE 2--Continued

Angle of Inclination, degrees	Film Reynolds Number	Avg. Concentration in Meniscus, gm/liter	Avg. Concentration in Film, gm/liter	Avg. Concentration Pigford Theory, gm/liter
15	204	.2404	.4415	.5530
15	304	.2026	.3745	.3970
15	434	.1893	.3482	.3360
15	756	.1686	.2454	.2580
15	1160	.1325	.1864	.2000
15	1526	.1235	.1661	.1622
25	313	.2554	.3437	.4420
25	419	.2255	.3048	.3720
25	703	.1993	.2589	.2640
25	1072	.1650	.2249	.2035
25	1385	.1620	.1996	.1975

For comparison, an estimate of the expected concentration according to the Pigford theory is included in Table 2. Because of the short residence times of fluid in the diffusion cell, the equation used to estimate the exit concentration is the short form of the Pigford equation,

$$\frac{C_{avg} - C_o}{C_s - C_o} = \left[\frac{6Dx}{\pi \bar{h}^2 u_{avg}}\right]^{\frac{1}{2}} \qquad (42)$$

In using this equation C_o, the initial concentration, was assumed at zero; C_s, the saturation concentration of CO_2 in water, is 1.44 gm/liter; x, the contact length is 88.59 cm; D, the molecular diffusion coefficient for CO_2 into water, is 1.79×10^{-5} cm^2/sec; $\bar{h}$, the mean film

thickness, is the Nusselt film thickness corresponding to the film Reynolds number being considered; and u_{avg} is the Nusselt average velocity for the film Reynolds number being studied.

There are two prominent features of the experimental data. First, there is a significant difference between the CO_2 concentrations in the meniscus region and the film flow region. At the lower values of Reynolds number, where the compartmented flow studies have shown the wall effects to be most drastic with respect to the lateral velocity distribution, the concentrations in the meniscus fluids are only about 50 percent of the film region concentrations. This concentration level can have a very noticeable effect on bulk concentration measurements if wall effects are ignored. As the Reynolds number is increased, the concentrations of the two regions approach one another. It is remembered that under these same conditions the lateral velocity distribution becomes more uniform. In addition, as the angle of inclination is increased, the approach to equality of the concentrations in the two regions becomes less rapid with increases in Reynolds number.

The explanation for this behavior lies in the effective residence times in the two regions of flow. The fluid adjacent to the sides is traveling more rapidly than that in the central region and thus its surface has a shorter exposure time to the diffusing gas. As the liquid flow rates are increased, the velocities in the central region

begin to approach those of the region adjacent to the sides. The effect is to bring the contact times closer together with a result of equalizing the concentrations. It was shown in the compartmented flow studies that only at the lowest angles did the total and film Reynolds numbers become equal at the bulk flow rates investigated. In the vicinity of the vertical walls, the free surface area per unit volume of fluid is much less than in the film flow region. Even though a dynamic action may be accounting for enhanced absorption adjacent to the windows, the small surface area per unit volume tends to counteract this effect.

It should be observed that the comparison of the concentrations in the two regions depends on the size of the two regions compared. Had the wall compartments been made larger, some of the more concentrated central region fluid would have been mixed with the dilute meniscus fluid and would have resulted in an apparently higher wall region concentration. A comparison based on the ratios of the concentrations of the two regions thus reveals only a trend and not an absolute difference. As long as the meniscus region fluid contains any fluid from the uniform thickness region, the concentration ratios determine only an upper bound on the real values.

The second important observation resulting from the data is the agreement of the measured concentrations with the predicted bulk concentrations of the Pigford theory. The data indicate the laminar flow, molecular

diffusion theory predicts within 10 percent the experimental concentrations in the film flow region, whether waves are present on the surface or not. True, agreement between experiment and theory is not so good at the very low Reynolds numbers studied at any angle of inclination, but it is at these flow rates that the most difficulty was experienced in acquiring samples. It was difficult to maintain a continuous film across the plate at these low flow rates, and it is not surprising that the discrepancy is so large at these conditions. As the flow rates are increased, wetting of the plate is accomplished more easily, and the data appear to support Pigford's theory. Even at the lowest angles studied, waves were present on the liquid surfaces at Reynolds numbers above 500, and it is noted that slight increases in concentration are reported in comparison with the theory.

At angles of 10°, 15°, and 25° for the reported mean wave amplitudes, the present theory (equation (15) and (40) of Chapter III) predicts increases in concentration of about 10 to 15 percent above those of the smooth film theory. The data do not indicate consistent increases of this magnitude, but because of the scatter experienced in the experimental results, the data certainly do not disprove the theory. Slight increases in gas absorption, however, do occur in more cases than not under conditions when waves are present. It does seem that the Pigford theory quite adequately predicts the experimental

concentrations to within about 10 percent whether waves are present or not. Since the Pohlhausen solution was found earlier to agree to within 3 percent of the smooth surface Pigford theory, it too may be considered as experimentally verified.

Because it was necessary to open the bottom end of the diffusion cell in order to obtain the compartmented flows, precautions were taken to obtain a pure CO_2 atmosphere above the surface of the falling film. A positive gas flow was begun through the diffusion cell 5 to 10 minutes prior to taking the first sample and was maintained over the duration of the experiment. It was felt that the positive gas flow combined with the slight interfacial drag on the gas phase was sufficient to provide a saturated condition at the gas-liquid interface.

Interferometric Studies

Interferometry is a sensitive experimental technique that permits the calculation of changes in optical path length of a light beam as it passes through a transparent medium. Since the optical path length through a body is defined as the product of the physical path length times the refractive index of the medium through which the beam travels, the technique provides a means of determining the refractive index of the medium. Because the refractive index of a material is proportional to its density and, therefore, changes with composition, temperature, and

pressure, the interferometric technique may also be adaptable to the study of such transport processes as heat and mass transfer in either quiescent or convective systems. If a system is of uniform density, the light interference patterns, called fringe patterns, appear as straight lines. As the composition or temperature of the system changes, the fringes will show either the increases or decreases in density by their distortion.

Harvey (19) used a Mach-Zehnder interferometer to study the absorption of CO_2 into quiescent pools of water. He found that the refractive index of the water pool changed linearly and in direct proportion to the changes in CO_2 concentration. The Handbook of Chemistry and Physics (19a) values for the refractive index of water as a function of temperature shows an inverse proportionality, though the relationship is linear over small temperature ranges. Thus, if both heat and mass transfer are present in a study of the CO_2-water system, the opposing effects might introduce complications into the interpretation of the fringe distortion or shape.

Quiet Pool Studies

Essential to any interferometric determination of absolute concentration is a knowledge of the dependence of the solution refractive index on concentration. Since Harvey showed the relationship to be linear for the CO_2-water system, it is sufficient to establish the number of

fringe shifts associated with the saturated concentration. This method was chosen as a means of calibration of the equipment in this study of the diffusion of CO_2 into flowing water films. When the water is saturated throughout with air, the fringe patterns are straight lines, indicating a uniform density. As the solute gas is admitted to the diffusion cell, the surface of the liquid rapidly saturates and the interference fringes deflect accordingly. Thus, with a saturated concentration at the interface and an essentially zero concentration at the bottom of the liquid, the number of fringe shifts corresponding to saturation is easily established.

This technique was applied to a quiescent water pool with CO_2 gas diffusion at a temperature of 24° C. Photographs of the fringe patterns obtained during the calibration appear in Appendix D for the air-saturated, water pool, and the system after exposure to pure CO_2 for time periods of 1.5, 2.5, and 3.5 minutes. The scale presented in the appendix shows the photographic magnification where 100 divisions is equivalent to 0.5 cm.

Notice in the air-saturated pool photograph the deflection of the fringes in the vicinity of the surface, and in the photographs of the partially CO_2-saturated pools, the difficulty in locating the terminus of a fringe near the liquid surface. Notice also in the 3.5 minute exposure time photograph the collapse of the fringes when solute penetration is apparently to the bottom of the pool. The

deflection near the surface of the air-water system is felt to be a distortion of the light beams, since a raising and lowering of the interferometer light source was found to shift the direction of this portion of the fringe. This distortion band was present in all photographs of the fringe patterns, as can be seen by examination of those for the flowing systems which are also found in Appendix D. The difficulty of locating the terminus of the fringe is associated with both the distortion band close to the surface and the uncertainty of the precise location of the gas-liquid interface.

Bird (5) has presented the solution to the problem of transient state diffusion into a pool of infinite depth as a complementary error function. For short contact times into a pool of finite depth, the complementary error function solution should be satisfactory as an estimate of the solute distribution since with only slight penetration the solute cannot "know" how deep the pool is. Comparison of the fringes in the photographs with the complementary error function curves corresponding to the measured exposure times indicated disagreement with the theory. The penetrations were not so deep as the theory indicated and the discrepancy became larger as contact time increased. Because of this disagreement between theory and experiment, attempts were made to extrapolate the straight portions of the experimental profiles near the surface of the fluid to see if a profile could be obtained which coincided with

the theoretical one for the appropriate contact time. This effort was unsuccessful.

Harvey (19) has reported the change in refractive index of water upon saturation with CO_2 at 20° C to be 0.00003. If this value is assumed to apply at 24° C (the temperature of this study) the expected fringe shift at saturation in the 7.49 cm width diffusion cell, using 5460 Å wavelength light from the mercury vapor lamp, is calculated as 4.0. The photographs of the quiet pool for the shorter contact times in Appendix D show about a 3.0 fringe shift at saturation, creating doubt as to whether the gas-liquid interface is visible or not. How much of the experimental fringe shift is attributable to the distortion shown in the air saturated pool photograph is not known.

Jepsen (23) and Lu (30) allowed their quiescent water pools to saturate with CO_2 over a period of 45 minutes, determining the total number of fringe shifts at complete saturation of the liquid pool. Jepsen reports a saturation fringe shift of 2.67 at 22° C and Lu obtained 2.85 at 24° C in the same contacting cell used in this study. Both investigators titrated samples of the liquid from the CO_2 saturated pools to see that they contained the equilibrium concentration for a CO_2 atmosphere. As a result of the difficulty interpreting quiet pool photographs in this study, a reasonable value of 2.8 fringe shifts at saturation is assumed as the calibration to be used in the reduction of the experimental profiles obtained in the flowing systems.

Because the emphasis in this investigation was on the convective system, the quiet pool study in this thesis was not extensive, and therefore the experimental results cannot be considered as sufficient evidence to disprove the theory. It does suggest, however, that more development work might be performed on the interferometric technique to explain the anamolous results obtained.

Flowing Liquid Film Studies

In an effort to determine the distribution of the diffusing CO_2 in laminar flowing water films, photographs were made of the light interference patterns formed when the contacting cell was inclined at angles of 1°, 2°, and 3°, and the liquid flow rates were varied over a range corresponding to film Reynolds numbers from 140 to 1940. The downstream positions at which the photographs were taken were located 10", 19", 22", 25", 28", and 31" from the liquid inlet. In order to provide a reference or zero point against which to compare the profiles affected by the CO_2, photographs were also made of the interference patterns formed when the water films were saturated with air. Examples of the profiles obtained are found in Appendix D.

The method of reducing the experimental data was to measure the deviation of the CO_2 fringes from the position of the corresponding air fringe. Since CO_2 penetration into the flowing films was expected to be slight, the base of a CO_2 fringe should not deviate from that of an

air fringe. As comparison is made at points closer to the liquid surface, the effect of the diffusing CO_2 became greater and the CO_2 and air fringes began to deviate more noticeably. It is expected that the greatest difference between the two profiles is at the free surface.

The deviation between the CO_2 and air fringes at a point may be converted to concentration by dividing the number of fringe shifts of deviation between the two fringes by the number of fringe shifts corresponding to CO_2 saturation, and then multiplying the quotient by the saturation concentration of CO_2 in water. The number of fringe shifts at saturation is not known precisely, as was discussed previously, but a reasonable value of 2.8 was assumed from the experience of previous investigators. The saturation concentration used was 1.44 gm/liter; it was obtained by correcting the handbook value of 1.49 to prevailing atmospheric conditions.

Close examination of the profiles for the CO_2- and air-water systems shows a shift in the base of the profiles upon diffusion of CO_2. Because theoretical calculations involving the Pohlhausen solution to the smooth surface films indicated much less penetration than is shown in the photographs, the CO_2 profiles were corrected by shifting the base of each profile to a zero CO_2 concentration. Had this correction not been made, bulk concentration calculation from the interference profiles would have been much higher than the experimental titrations showed. Figure 4

shows that significant changes in bulk concentration are encountered from only slight changes in penetration depth.

Experimental work presented earlier in this thesis indicates that the mean film thicknesses encountered in this study correspond to those predicted by the Nusselt laminar flow theory. The visual film thicknesses determined from the interference photographs, however, only measure about 80 percent of those reported from the capacitance studies described elsewhere. The average values of the visual film thicknesses obtained in this study, as well as those reported by Jepsen (23) at 10° and Lu (30) at 5° and 15° are plotted in Figures 11 to 16.

In order to determine whether the full thickness of the film was being seen, a pin, mounted on a micrometer, was advanced until it just pricked a non-wavy liquid surface from above. The top of the pin was not observable in the interferometric field of view. When the pin was advanced until it was just visible in the field of view, it was found that a difference of from 0.0018" to 0.0045" existed between the point of contact with the liquid surface and the point where the pin just entered the observable fringe pattern. The results of this experiment tend to support the belief that the observed fringe pattern did not extend to the free surface.

Interruption of the light path through the film by waves is not a satisfactory explanation for the invisible portion of the film. From Figures 11 to 16 it appears that

about the top 20 percent of the film is obscured. Wave amplitudes for the films at these low angles rarely measured as much as 4 percent of the mean film thickness. In addition, the pin studies described above were performed on films where there were no waves present on the surface.

With the top 20 percent of the film obscured in the interference photographs, two important goals of the study cannot be realized. First, the distribution of a major portion of the solute in the film is not determinable as it lies out of the field of view of the interferometer. Secondly, with such a large portion of the solute distribution unknown, it is not possible to obtain a meaningful estimate of the bulk concentration of the solute in the film. This second feature prevents comparison of the bulk concentrations calculated from interference profiles and the titration measurements.

It was seen in the discussion of the theoretical development in Chapter III that the concentration profiles resulting from the Pohlhausen solution to the smooth surface convective diffusion problem, using a second order polynomial, agreed favorably with the numerical profiles obtained for the same problem. When the penetration depths calculated from the Pohlhausen solution for the conditions of this study were compared with the apparent penetrations in the interference photographs based on the capacitance-determined, mean film thicknesses, it was found that the photographs indicated a much deeper penetration

into the film than the theory predicted. In addition, for the experimental conditions when the film surface was smooth, the interference profiles indicated a higher concentration than the approximate theory predicted. This experimental result based on the interference profiles conflicts with the titration measurements of bulk concentration for the smooth surface conditions.

In an attempt to compare the interference profiles with the theoretical profiles based on the apparent penetration in the interference photographs and the capacitance film thicknesses, it was found again that the two sets of profiles disagreed. In this case the ultimate penetrations were the same, but the interference profiles indicated less solute than the theory predicted at points between the minimum penetration depth and the liquid surface.

From the results of the two preceding comparisons, it appears that the shapes of the interference profiles are not the same as those of laminar convective diffusion theory, under conditions where the theory could reasonably be expected to apply. It is suggested therefore that the interference profiles may be reflecting changes in other properties in addition to changes in CO_2 concentration.

Previous investigators have calculated the deviations of the interference profiles from those satisfying the laminar convective diffusion equation and reported

their results as local values of a total diffusion coefficient as a function of position in the film. Their data reveal a maximum in the total diffusion coefficient in the central portion of the film. It was seen in Chapter III, that although the approximate solution obtained from the Pohlhausen technique gave a close approximation to the exact profile, the deviation was sufficient to yield a maximum in the total diffusion coefficient. Experimental attempts to reproduce interference profiles at an angle of 2° and for flow rates corresponding to Reynolds numbers from 200 to 1900 showed differences sufficient to produce a maximum in a calculated total diffusion coefficient. Thus, it appears that the current reproducability of the profiles is not precise enough to permit a meaningful calculation of the local total diffusion coefficient.

In summary, the results of the interference studies may be stated as follows. The experimental interference profiles do not agree with those resulting from the theory, for either the quiet pool or the flowing system. On the other hand, bulk concentration measurements tend to indicate concentrations corresponding to molecular diffusion. Because only a limited portion of the solute is visible in the photographs, a meaningful comparison between the calculated concentrations from the interference profiles and the bulk concentration studies is not at present possible. Consequently, it appears that the

information contained in the interference photographs is sufficiently obscured by other effects that accurate and conclusive remarks concerning the solute distribution, and its implications, cannot be made until further development work with the interferometric technique has been accomplished.

CHAPTER VI

CRITICISM OF PREVIOUS WORK FROM THIS LABORATORY

Previous investigators in this laboratory experienced difficulty in reconciling differences in results obtained from independent measurements of the same variable. For instance, film thicknesses measured by Jepsen (23) using the capacitance technique were greater than the film thicknesses calculated from laminar theory for the experimentally determined volumetric flow rates. In addition, the visual film thicknesses determined from the photographs of the light interference patterns also disagreed with the theoretically determined film thicknesses. Jepsen attributed the differences in capacitance and photographic measurements to inaccuracies in the application of the capacitometer.

Lu (30) also determined film thicknesses and plotted them as a function of Reynolds number. He found that the slopes of his curves were greater than predicted by laminar theory, and that a transition existed around a Reynolds number of 1000, where the slopes of the experimental and theoretical curves became more nearly equal. The transition encountered was opposite to that expected for the laminar-turbulent transition. Lu's photographically determined film thicknesses also disagreed with his capacitance determined values.

Binnie (4) and later Fulford (16) have recognized the existence of increased flows in the vicinity of a vertical boundary. For this reason experiments were made by the techniques developed in this study under the same conditions used by both Jepsen and Lu. The results obtained indicated that the mean film thicknesses for the conditions of Jepsen and Lu correspond to the laminar theory. The values obtained in the present study do not always agree with those determined by Jepsen and Lu, but this discrepancy may be attributed to their experimental techniques.

It is evident, then, that once the experimental film thicknesses are checked with laminar theory, and are verified by independent measurements (such as location of the surface with a micrometer mounted pin when waves are not present), film thicknesses determined visually appear to be in error. The disagreement of the visually determined film thicknesses with the laminar theory may be seen in Figures 14 to 16. The values presented in the figures are averages of the maximum values of film thickness reported among the data in the earlier theses. It appears in the figures that generally only about 70 percent of the total film thickness is present in the photographs. This difference might be attributed to the surface fluctuations except that the same measurements at very low angles of inclination indicate the same trend when wave amplitudes are much reduced.

The existence of the disproportionately high meniscus flows also explains the peculiar transition encounted by Lu.

As the film thickness in the central region becomes very thin, the flow adjacent to the vertical windows makes up a greater fraction of the total volume, since local velocities vary with the square of the depth, and the height of wetting is relatively constant. As the flows in the central region become greater, there is a more uniform lateral distribution of fluid across the flat plate. Under these conditions, collection of the total flow for determination of Reynolds number is more appropriate than in the low flow situations.

Recognition of the meniscus flows will certainly alter Lu's c/v_o (ratio of wave velocity to average velocity) ratios and may well yield better agreement between his theory and his experimental measurements. Lu's v_o was determined from his total volumetric flows and his capacitance measured film thicknesses. Since at the lower flow rates the film Reynolds numbers for Lu's measured film thicknesses are only about half his reported values, his average velocities in reality are only half his reported values and thus his reported ratio should practically double.

Another difficulty encountered by Lu and Jepsen was the disagreement of bulk concentration measurements with integrated concentrations from the interference photographs. Both attributed the difference to pressure fluctuations in the contacting cell, causing misalignment of the viewing windows, and a consequent shift in the fringe base. Since Jepsen contended that as soon as waves formed, penetration

to the bottom of the film was immediate, he was justified in shifting the fringes himself until agreement could be obtained between bulk concentration and the interference determined concentration. Of course, if only 70 percent of the film is visible, the integrated bulk concentration is understated, since the faster flowing, more concentrated portions of the film are not included. Indeed, if all of the film were visible, it might be possible to account for all of the solute without allowing the base of the fringe to shift.

Lu carried out experiments by sampling the bottom portion of a film flowing under conditions similar to those of Jepsen's study. His concentration measurements revealed virtually no solute in the bottom portion of the film and thus, he refrained from shifting the base of the fringes unless he could detect an other than zero gradient to the concentration profile at its base. He, therefore, did not shift the fringe base and was not able to obtain agreement for the two methods of determining an average concentration.

Both Jepsen and Lu have compared their experimental bulk concentrations with those predicted by the exact solution to the smooth surface, laminar, convective diffusion equation of Pigford (34). Jepsen made his comparison through an HTU, in which he determined the theoretical HTU, attributed to Pigford, necessary to absorb an equivalent amount of solute. Lu made his comparison on the basis of his capacitance determined film thicknesses, some of which are thicker than

the theoretical laminar films corresponding to the volumetric flows. Both investigators measured increases in gas absorption as compared to laminar theory, Jepsen reporting as much as 100 percent and Lu's values only slightly greater than theory. If Jepsen's extrapolated bulk concentrations are compared with the theoretical values obtained by using the film thicknesses reported in this thesis, his measured concentrations are at most 30 percent greater than theory. If the diluting contribution of the meniscus region flows had been considered in his work, it is evident that his values would have been greater. Nevertheless, Jepsen's higher values of bulk concentration imply increases in mass transfer with waves.

Lu similarly reports higher concentrations than laminar theory predicts. When the theoretical values are corrected to correspond to film thicknesses measured in the current study, Lu's data appear less than theory at 5° and 15°, but greater than theory by 15 percent at 25°. It must be observed that Lu's concentrations include the dilute material obtained from the meniscus regions, which possibly explains his negative deviations from laminar theory.

Both Jepsen and Lu consider as a significant contribution the observation of a maximum of the total diffusion coefficient in the central portion of the film when plotted as a function of film depth. Lu's total diffusion coefficients are from 10 to 200 times as large as the molecular diffusion coefficient. Jepsen reports values of diffusion coefficient varying from 5 to 60 times the molecular diffusivity. Both

of these investigators report values in the mentioned ranges for up to 50 percent of the film thickness, yet bulk concentration measurements indicate at best a 50 percent increase over the value obtained for molecular diffusion into a laminar film.

It is possible to get curves similar to those of Jepsen by using a constant concentration, equal to the amount of shift of the base of his fringes, multiplied by the integral of the velocity profile over the film thickness. If this integrated concentration is then divided by the average derivative between the two points being considered, a maximum of magnitude at least as large as Jepsen's average values is obtained.

Lu reports the same type of behavior of total diffusion coefficient while in most cases using a common base for the two fringes being compared. One such set of fringes (G7-4 and G2-6) which were obtained at an angle of 5°, a Reynolds number of 926, and for contact lengths of 22" and 28" are found reproduced in Figure 20. Also appearing in the figure are the theoretical profiles resulting from the Pohlhausen solution to the smooth surface problem with the same operating conditions. It is seen that Lu's profiles indicate much deeper penetration into the film than is predicted by the molecular diffusion theory. For comparison, it is noted that Lu's measured bulk concentrations for these two conditions are about 5 percent less than the molecular diffusion theory predicts. Thus, Lu's work poses

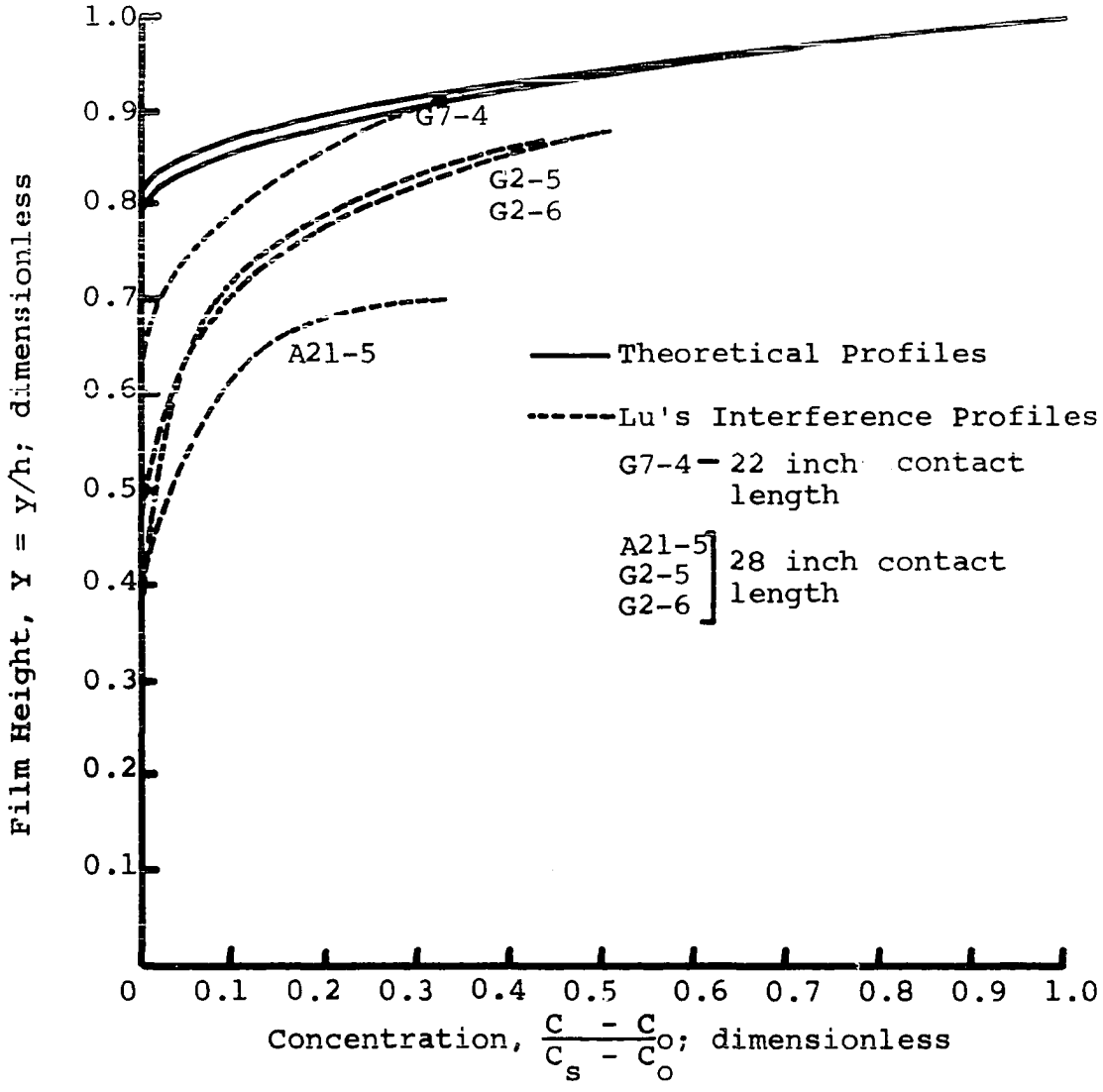

Figure 20

Comparison Between Lu's Interference Profiles and Theoretical Concentration Profiles for CO_2 Diffusion into Water at 24° C and an Angle of 5°, Re=926, and Contact Lengths of 22 and 28 inches

an anamoly in that his interference profiles indicate significantly deeper penetration into the film than theory, yet his bulk concentration measurements indicate less penetration into the film than the theoretical curves show.

It was shown in Chapter III that the deviation of the theoretical profiles from those that satisfy the convective diffusion equation was sufficient to produce a maximum in the total diffusion coefficient calculations. It is easy to see that Lu obtained significant differences from the molecular diffusion coefficient while working with these profiles. The main question that arises is whether the interference profiles represent only the concentration in the film. It is the conclusion of this thesis that they do not, and therefore the results of calculations involving the profiles are of questionable significance.

High speed moving pictures from the present study showed that when waves were present on the surface of the films, the profiles fluctuated over short time intervals. A photograph of an interference profile necessarily freezes it in time. Because of the time varying character of the profiles, it is difficult to reproduce the data at any set of operating conditions. Presented in Figure 20 are three different profiles obtained by Lu at an angle of 5° , a Reynolds number of 926 and a position 28" from the liquid inlet, demonstrating Lu's difficulty in reproducing his profiles. G2-5 and G2-6 were obtained within 30 seconds of one another while A21-5 was obtained on a different day

of operation, but at the same operating conditions. Agreement of the profiles is not very good. It is interesting to consider that had one of these profiles satisfied the convective diffusion equation exactly, comparison with one of the other profiles instead would have caused deviations large enough to introduce a maximum into the total diffusion coefficient calculations.

CHAPTER VII

CONCLUSIONS

The following conclusions have been drawn as a result of the work included in this thesis.

Mass transfer into falling liquid films is severely changed by meniscus effects at solid boundaries. Particularly in flat plate cells, the velocity structure is distorted and local bulk concentrations will be much smaller near the walls for a liquid that wets the walls. The velocity distortion becomes even more noticeable at higher angles of inclination, up to 25°.

Experimental measurements which exclude the flow affected by these wall effects, show that water film thicknesses agree with the Nusselt theory for Reynolds numbers up to 1900 and angles of inclination up to 25°.

Mass transfer is described by the theory of Pigford which predicts within about 10 percent the bulk concentrations of CO_2 diffusing into water films up to angles of 25° and Reynolds numbers up to 1900. The concentration predictions are very sensitive to the film thickness used; a mean value determined from a time average of the surface height seems sufficient. The equation obtained using the Pohlhausen technique for the non-wavy surface predicts experimental results as well.

Uncertainties arise in the interpretation of the light interference patterns for the CO_2-water system. These appear because of the lack of agreement with diffusion theory of the interferometer profiles in both the quiescent and flowing systems; the variation among profiles obtained from identical experimental conditions; and the limitations which restrict visibility to a portion of the liquid film. It is not possible to consider the profiles to represent only the solute distribution in the liquid until further development of the technique has been accomplished.

Gas diffusion into films flowing with wavy surfaces and parabolic velocity profiles, can be described analytically for small penetrations using the Pohlhausen technique. The resulting equation predicts large increases in mass transfer without requiring a large eddy diffusivity or the addition of bulk mixing terms.

Levich's approximate solution to the problem of mass transfer in wavy films is incorrect; based on the previous work of Lu it has been possible to present the correct solution which predicts a decrease, rather than an increase in mass transfer as compared to smooth surface film, molecular diffusion theory.

CHAPTER VIII

SUGGESTIONS FOR FURTHER WORK

The results obtained in this thesis suggest the need for further development work with the interferometric technique in order to establish the relationship between the interference patterns and the concentration profiles. Useful information might result from more extensive quiet pool studies on a system from which the menisci had been eliminated. Simultaneous monitering of the liquid surface location is necessary in order that a knowledge of the portion of the quiet pool appearing in the interference patterns is obtained.

The quiet pool work could be extended into a similar study with creeping flow, once the technique had been established. After completion of the creeping flow study, an investigation of the laminar flowing, smooth surface films might be conducted. It is very important in these studies that precise definition of the gas-liquid interface be obtained, as well as the elimination of the wall effects.

It is also suggested that a more rigorous statistical treatment of the surface disturbances be obtained. This study could be performed at various angles of inclination, including the vertical. Simultaneous monitoring of the surface configuration at two points, one directly

downstream from the other would be beneficial. A wide flow surface should be used in order to reduce the effects of stationary waves that exist at the side walls.

Extension of the theoretical work of this thesis to include the effects of a random wave pattern would be useful. In addition, a study of the effects of the curved interface, both stationary and when moving, might be informative.

NOMENCLATURE

c	wave velocity, cm/sec.
C	concentration, gm/liter
$\underline{C}$	dimensionless concentration, defined in equation (5) as $(C - C_o)/(C_s - C_o)$
D	molecular diffusion coefficient, $cm^2/sec.$
g	acceleration of gravity, 980 $cm/sec.^2$
h	liquid film thickness, cm
$\bar{h}$	mean liquid film thickness, cm
k	wave number, $2\pi/\lambda$, cm^{-1}
K	parameter composed of constant physical properties of the system, defined as $(D\nu)/(g \sin \beta)$
Q	volumetric flow rate per unit of width, $cm^2/sec.$
Re	Reynolds number, defined as $4Q/\nu$, dimensionless
s	arc length, cm
t	time, seconds
u	velocity component in direction of bulk flow, cm/sec.
v	velocity component normal to direction of bulk flow, cm/sec.
x	coordinate axis, direction of bulk flow, cm
y	coordinate axis, normal to direction of bulk flow, measured from bottom of film, cm.
Y	dimensionless coordinate axis, normal to direction of bulk flow, measured from bottom of film, $Y = y/h$

Subscripts

avg	designates an average value
o	designates value at entrance
s	designates condition at surface
1,2,	relative position in x direction, lower numbers indicating positions closer to entrance

Greek Symbols

α	dimensionless amplitude, defined as amplitude/ mean film thickness
β	angle of inclination, measured from horizontal, degrees
δ	distance of diffusion boundary layer above bottom of liquid film, cm
Δ	dimensionless distance of diffusion boundary layer above bottom of film, defined as δ/h
θ	angle measured from vertical, degrees
ϵ	eddy component of total diffusion coefficient, cm^2/sec.
λ	wave length, cm
ν	kinematic viscosity, cm^2/sec
ρ	density, gm/cm^3
σ	surface tension, dynes/cm
φ	angle of contact between a liquid and a solid surface, measured through the liquid phase, degrees

BIBLIOGRAPHY

1. Belkin, H. H., MacLeod, A. A., Monrad, C. C., and Rothfus, R. R., A.I.Ch.E. Jour., 5 (1959), p. 245.

2. Benjamin, T. B., "Wave Formation in Laminar Flow Down an Inclined Plane," Jour. Fluid Mech., 2 (1957), p. 554

3. Benjamin, T. B., "The Development of Three Dimensional Disturbances in an Unstable Film of Liquid Flowing Down an Inclined Plane," Jour. Fluid Mech., 10 (1961), p 401.

4. Binnie, A. M., "Instability in a Slightly Inclined Water Channel," Jour. Fluid Mech., 5 (1959), p. 561.

5. Bird, R. B., Stewart, W. E., and Lightfoot, E. N., Transport Phenomena. New York: John Wiley and Sons, Inc., 1960.

6. Bois, G. P., Tables of Indefinite Integrals. New York: Dover Publications, Inc., 1961.

7. Bushmanov, V. K., Zh. Eksperim.i Theo., Fiz, 39 (1960), p. 1251. English trans: Soviet Phys-Jour. Exp. and Theo. Phy., 12 (1961), p 873.

8. Childress, H. L., B. S. Thesis, University of Illinois, 1941.

9. Davies, J. T., and Rideal, E. K., Interfacial Phenomena. New York: Academic Press, 1961.

10. Dukler, A. E., and Bergelin, O. P., "Characteristics of Flow in Falling Liquid Films," Chem. Engr. Prog., 48 (1952) p 557.

11. Dukler, A. E., "Dynamics of Vertical Falling Film Systems," Chem. Engr. Prog., 55 (10) (1959), p 62.

12. Emmert, R. E., and Pigford, R. L., "Interfacial Resistance: A Study of Gas Absorption in Falling Liquid Films," Chem. Engr. Prog., 50 (1954), p 87.

13. Fage, A., and Townend, H. C. H., Proc. Roy. Soc. London 135A (1932), p 656.

14. Fallah, A., Hunter, T. G., and Nash, A. W., Jour. Soc. Chem. Ind. (London), 53 (1934), p 369 T.

15. Friedman, S. J., and Miller, C. O., "Liquid Films in the Viscous Flow Region," Ind. Engr. Chem., 33 (1941) p 889.

16. Fulford, G. D., Gas-Liquid Flow in an Inclined Channel. Ph.D. Thesis, University of Birmingham, England, 1962.

17. Fulford, G. D., "The Flow of Liquids in Thin Films," Advances in Chemical Engineering, Vol. 5. New York: Academic Press, 1964.

18. Grimley, S. S., "Liquid Flow Conditions in Packed Towers," Trans. Inst. Chem. Engr., 23 (1945), p 488.

19. Harvey, E. A., The Absorption of CO_2 by a Quiescent Liquid. Ph.D. Thesis, University of London, 1958.

19a. Hodgman, C. D., Handbook of Chemistry and Physics, 40th Edition. Cleveland, Ohio: Chemical Rubber Publishing Co., 1958.

20. Hopf, L., Ann. Physik, 32(4) (1910), p 777.

21. Jackson, M. L., "Liquid Films in Viscous Flow," A.I.Ch.E. Jour. 1 (1955), p 231.

22. Jackson, M. L., Johnson, R. T., and Ceaglski, N. H., "Surface Velocities of Liquid Films in the Streamline Flow Region," Proceedings of the Midwestern Conference on Fluid Dynamics, J. W. Edwards, Ann Arbor, Michigan, 1951.

23. Jepsen, J. C., The Effect of Wave Induced Turbulence on the Rate of Absorption of Gases in Falling Liquid Films. Ph.D. Thesis, University of Oklahoma, 1964.

24. Kamei, S., and Oishi, J., Mem. Fac. Engr. Kyoto Univ., 18 (1956), p 1.

25. Kapitsa, P. L., Zh. Eksperim. Theo. Fiz., 18 (1948), p 3.

26. Lamb, Sir H., Hydrodynamics. New York: Dover Publications, Inc., 1945.

27. Lange, N. A., Handbook of Chemistry, 9th ed. Sandusky, Ohio: Handbook Publishers, Inc., 1956.

28. Levich, V. G., Physicochemical Hydrodynamics. Englewood Cliffs, N. J.: Prentice Hall, Inc., 1962.

29. Lin, C. C., The Theory of Hydrodynamic Stability, Cambridge: Cambridge University Press, 1955.

30. Lu, H. S., Influence of Surface Waves Upon Mass Transfer into Liquid Films Flowing on Inclined Plates. Ph.D. Thesis, University of Oklahoma, 1965.

31. Lynn, S., Straatemeier, J. R., and Kramers, H., "Absorption Studies in the Light of the Penetration Theory," Chem. Engr. Sci., 4(2) (1955), p. 49.

32. Nikuradse, J., Forschungsheft, 361 (1933), p 1.

33. Nusselt, W. Z., Ver. Dtsch. Ing., 60 (1916), p. 569.

34. Pigford, R. L., Counter Diffusion in a Wetted Wall Column. Ph.D. Thesis, University of Illinois, 1941.

35. Pohlhausen, K. Zeit. Angew. Math. Mech., 1 (1921), p. 252.

36. Portalski, S., The Mechanism of Flow in Wetted-Wall Columns. Ph.D. Thesis, University of London, 1960.

37. Portalski, S., "Studies of Falling Film Flow," Chem. Engr. Sci., 18 (1963), p. 787.

38. Portalski, S., "Velocities in Film Flow of Liquids on Vertical Plates," Chem. Engr. Sci., 19 (1964), p. 575.

39. Reiss, L. P. and Hanratty, T. J., "Measurement of Instantaneous Rates of Mass Transfer to a Small Sink on a Wall," A.I.Ch.E. Jour., 8(2) (1962), p. 245.

40. Rundstadler, P. W., Kline, S. J., and Reynolds, W. C. An Experimental Investigation of the Flow Structure of the Turbulent Boundary Layer. AFOSR-TN-5241, Stanford University, 1963.

41. Stirba, C., and Hurt, D. M., "Turbulence in Falling Liquid Films," A.I.Ch.E. Jour., 1(2) (1955), p. 178.

42. Thomas, W. J., and Portalski, S., "Counter Current Flow in Wall Columns," Ind. Engr. Chem., 50 (1958), p. 1086.

43. van Rossum, J. J., "Experimental Investigation of Horizontal Liquid Films," Chem. Engr. Sci., 11 (1959), p. 35.

44. von Karman, T., Trans. Am. Soc. Mech. Engrs., 61 (1939), p. 705.

45. Wicks, Moye III, Ph.D. Thesis in preparation, University of Houston.

46. Wilkes, J. O., and Nedderman, R. M., "The Measurement of Velocities in Thin Films of Liquid," Chem. Engr. Sci., 17 (1962), p. 177.

APPENDICES

APPENDIX A

DERIVATION OF THE SHAPE OF A MENISCUS AT A VERTICAL WALL WHICH IS WETTED BY THE FLUID

If it is desired to calculate the local velocities in the meniscus region as Fulford did, it is necessary to determine the equation that represents the shape of the liquid surface in order to locate the points where the boundary conditions are to be applied. Fulford relied on an expression presented by Levich (28) which was derived from thermodynamic considerations, the radius of curvature, and various approximations. An equivalent expression is here derived from a force balance on the surface of the liquid.

The system is considered as a static liquid adjacent to a vertical wall which it wets at a contact angle φ. The gas phase pressure is P and considered to act everywhere normal to the surface. At any constant depth inside the liquid phase, the pressure is considered constant, and calculable from equilibrium criteria of fluid statics. The surface tension σ is considered to act tangentially to the surface at all points.

An infinitesimal surface element, Δs long and of unit length into the paper, and the acting forces are

shown in Figure 21. θ is the angle between the vertical and the tangent to the surface at any point.

Making a vertical force balance at a distance s along the arc of the surface

$$\sigma \cos \theta \Big|_s - \sigma \cos \theta \Big|_{s + \Delta s} + [P - (y - h)\, \rho g]\, \Delta s \sin \theta -$$

$$P\, \Delta s \sin \theta = 0 \qquad \text{(A-1)}$$

Dividing all terms by Δs and taking the limit as Δs approaches 0

$$\sigma \frac{d \cos \theta}{ds} + (y - h)\, \rho g \sin \theta = 0 \qquad \text{(A-2)}$$

The boundary condition used will be

$$y = h \text{ when } \theta = \frac{\pi}{2} \qquad \text{(A-3)}$$

that is, the liquid surface becomes that of the film thickness when the tangent to the liquid surface is parallel to the bottom of the container.

Carrying out the indicated differentiation in equation (A-2)

$$-\sigma \sin \theta \frac{d\theta}{ds} + (y - h)\, \rho g \sin \theta = 0$$

or

$$d\theta = (y - h) \frac{\rho g}{\sigma} ds \qquad \text{(A-4)}$$

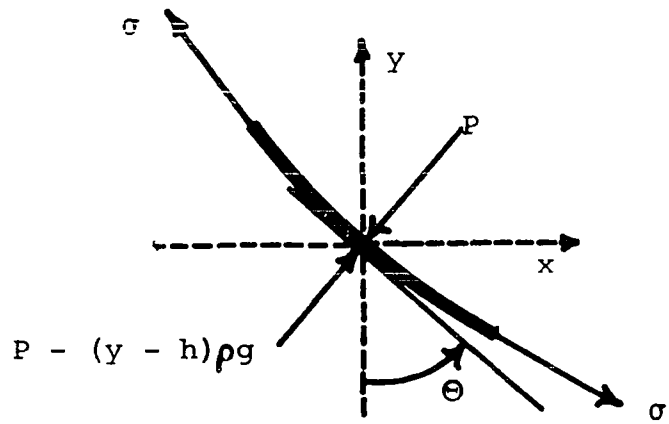

Figure 21

Force Balance on Liquid Surface for Determination of Meniscus Shape

Substituting a well-known expression for the arc length, s, into equation (A-4), and remaining aware of the directional change in x with y (i.e. the negative root)

$$d\theta = -(y-h)\,\frac{\rho g}{\sigma}\left[1 + \left[\frac{dx}{dy}\right]^2\right]^{\frac{1}{2}} dy = -(y-h)\,\frac{\rho g}{\sigma}\,(1 + \tan^2\theta)^{\frac{1}{2}}\,dy$$

or

$$\cos\theta\; d\theta = -(y-h)\,\frac{\rho g}{\sigma}\,dy \qquad \text{(A-5)}$$

Integrating equation (A-5)

$$\sin\theta = -\,(y-h)^2\,\frac{\rho g}{2\sigma} + C_1 \qquad \text{(A-6)}$$

where C_1 may be evaluated at the boundary condition (A-3).

$$C_1 = 1 \qquad \text{(A-7)}$$

Thus equation (A-6) becomes

$$\sin\theta = 1 - (y-h)^2\,\frac{\rho g}{2\sigma} \qquad \text{(A-8)}$$

Another boundary condition may be used to determine the height of the capillary rise on a vertical surface. When the x coordinate is zero, the liquid is at the wall, and the value of θ is the contact angle φ. Thus the height of capillary rise may be calculated as

$$(y-h) = \left[\frac{2\sigma}{\rho g}\,(1 - \sin\varphi)\right]^{\frac{1}{2}} \qquad \text{(A-9)}$$

Proceeding toward determining an expression for the surface configuration, advantage is taken of another well-known expression in terms of the arc length, $dx/ds = \sin\theta$. Rewriting equation (A-8)

$$\frac{dx}{ds} = 1 - (y-h)^2 \frac{\rho g}{2\sigma} \tag{A-10}$$

Substituting an alternative expression from that used in equation (A-5) into equation (A-10)

$$dx = \left[1 - (y-h)^2 \frac{\rho g}{2\sigma}\right] ds = \left[1 - (y-h)^2 \frac{\rho g}{2\sigma}\right]\left[1 + \left[\frac{dy}{dx}\right]^2\right]^{\frac{1}{2}} \tag{A-11}$$

Solving for an expression for dy/dx and remembering that as x increases y decreases

$$\frac{dy}{dx} = -\left\{\left[\frac{1}{1 - (y-h)^2 \frac{\rho g}{2\sigma}}\right]^2 - 1\right\}^{\frac{1}{2}} \tag{A-12}$$

or rewriting

$$\frac{dy}{dx} = \frac{-\left[4(y-h)^2 \rho g\sigma - (y-h)^4 \rho^2 g^2\right]^{\frac{1}{2}}}{2\sigma - (y-h)^2 \rho g} \tag{A-13}$$

or again rewriting and rearranging

$$dx = \frac{2\sigma\, dy}{\rho g(y-h)\left[\frac{4\sigma}{\rho g} - (y-h)^2\right]^{\frac{1}{2}}} + \frac{\rho g(y-h)^2\, dy}{\rho g(y-h)\left[\frac{4\sigma}{\rho g} - (y-h)^2\right]^{\frac{1}{2}}} \tag{A-14}$$

If $(y - h) = z$, then $dz = dy$ and integration is performed with respect to x from 0 to an indefinite upper limit, x, while integrating y from a lower limit of $\left[\frac{2\sigma}{\rho g}(1 - \sin\varphi)\right]^{\frac{1}{2}}$ (see equation (A-9)) to an upper indefinite limit of $(y - h)$

$$x = \int_{\left[\frac{2\sigma}{\rho g}(1 - \sin\varphi)\right]^{\frac{1}{2}}}^{(y-h)} \frac{-2\sigma\, dz}{\rho g z\left[\frac{4\sigma}{\rho g} - z^2\right]^{\frac{1}{2}}} + \int_{\left[\frac{2\sigma}{\rho g}(1 - \sin\varphi)\right]^{\frac{1}{2}}}^{(y-h)} \frac{z\,dz}{\left[\frac{4\sigma}{\rho g} - z^2\right]^{\frac{1}{2}}} \qquad \text{(A-15)}$$

and from appropriate integral tables

$$x = \frac{-2\sigma}{\rho g}\left[\frac{\rho g}{4\sigma}\right]^{\frac{1}{2}} \ln\left[\frac{z}{\left[\frac{4\sigma}{\rho g}\right]^{\frac{1}{2}} + \left[\frac{4\sigma}{\rho g} - z^2\right]^{\frac{1}{2}}}\right]\Bigg|_{\left[\frac{2\sigma}{\rho g}(1 - \sin\varphi)\right]^{\frac{1}{2}}}^{(y-h)}$$

$$- \left[\frac{4\sigma}{\rho g} - z^2\right]^{\frac{1}{2}}\Bigg|_{\left[\frac{2\sigma}{\rho g}(1 - \sin\varphi)\right]^{\frac{1}{2}}}^{(y-h)} \qquad \text{(A-16)}$$

Upon evaluating equation (A-16) at its upper and lower limits and simplifying

$$x = -\left[\frac{\sigma}{\rho g}\right]^{\frac{1}{2}} \ln\left[\frac{\left[\frac{y-h}{2}\right]}{\left[\frac{\sigma}{\rho g}\right]^{\frac{1}{2}} + \left[\frac{\sigma}{\rho g} - \left[\frac{y-h}{2}\right]^2\right]^{\frac{1}{2}}} \cdot \frac{2^{\frac{1}{2}} + (1 + \sin\varphi)^{\frac{1}{2}}}{(1 - \sin\varphi)^{\frac{1}{2}}}\right]$$

$$+ \left[\frac{2\sigma}{\rho g}\right]^{\frac{1}{2}} (1 + \sin\varphi)^{\frac{1}{2}} - \left[\frac{4\sigma}{\rho g} - (y-h)^2\right]^{\frac{1}{2}} \qquad \text{(A-17)}$$

Equation (A-17) is the expression for the shape of a liquid meniscus in the vicinity of a vertical wall. If the liquid is water and the vertical wall glass, the contact angle, φ, between water and glass, measured from the glass to the liquid surface through the water phase, is zero and the equation becomes

$$x = -\left[\frac{\sigma}{\rho g}\right]^{\frac{1}{2}} \ln\left[\frac{1.207\ (y-h)}{\left[\frac{\sigma}{\rho g}\right]^{\frac{1}{2}} + \left[\frac{\sigma}{\rho g} - \left[\frac{y-h}{2}\right]^2\right]^{\frac{1}{2}}}\right] + \left[\frac{2\sigma}{\rho g}\right]^{\frac{1}{2}} - \left[\frac{\sigma}{\rho g} - \left[\frac{y-h}{2}\right]^2\right]^{\frac{1}{2}}$$

(A-18)

A graphical representation of equation (A-18) is given in Figure 22.

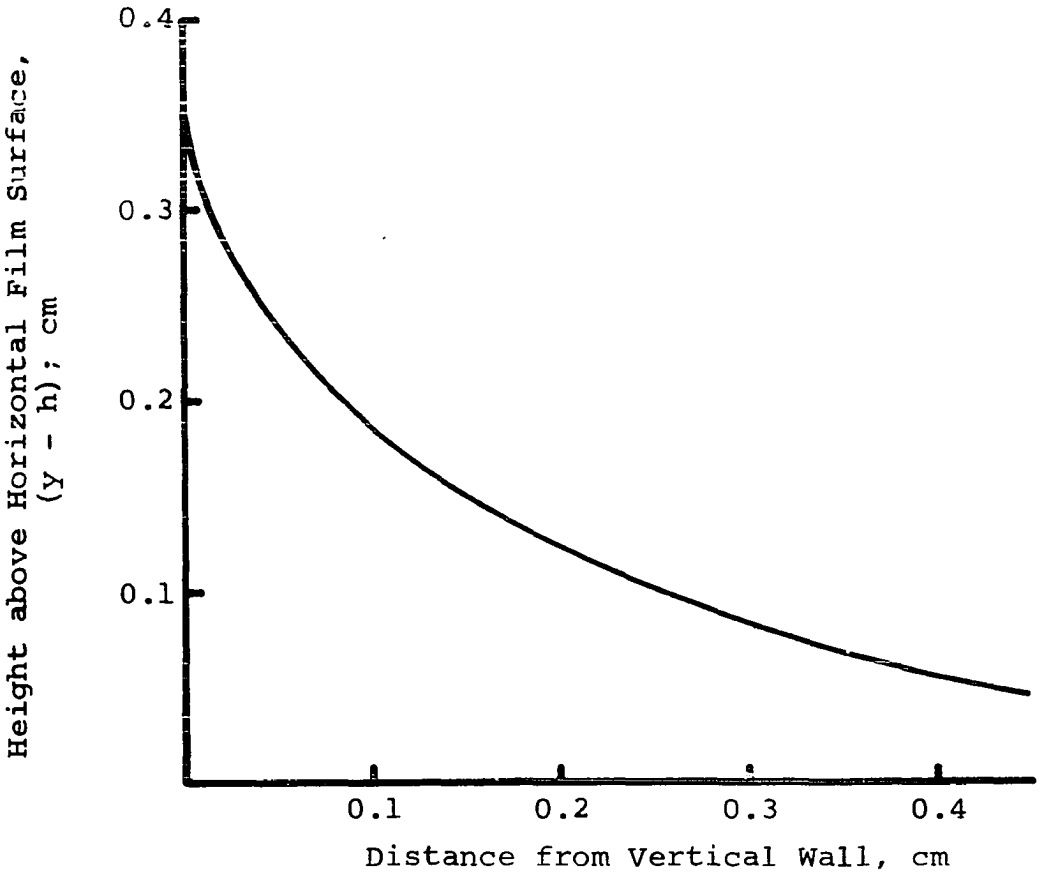

Figure 22

Water Meniscus Shape in Vicinity of a Vertical Glass Wall

APPENDIX B

CORRECTION TO LEVICH'S ESTIMATE OF INCREASE IN MASS TRANSFER IN WAVY FILM FLOW

Levich (28) in his presentation of the corrected Kapitsa (25) theory for wavy film flow down a vertical surface, reports erroneous expressions for the x and y components of the velocity. The error is involved with the substitution of the value of his disturbance amplitude into his derived expressions. The proper expressions for his velocity components (his equations 134.31 and 134.32) should read

$$v_x = 3v_o \left[1 + 0.294 \sin k(x-ct) - 0.0617 \sin^2 k(x-ct)\right]\left[\frac{y}{h} - \frac{y^2}{2h^2}\right] \tag{B-1}$$

and

$$v_y = - 0.882 v_o k \cos k(x-ct) \left[1 - 0.42 \sin k(x-ct)\right]\left[\frac{y^2}{2h} - \frac{y^3}{6h^2}\right] \tag{B-2}$$

These two expressions have been evaluated at the liquid surface, y = h, and substituted into the transient

state, two-dimensional convective diffusion equation. Thus his equation 136.12 should read

$$\frac{\partial C}{\partial t} + \frac{3}{2} v_o \left[1 + 0.294 \sin k(x-ct) - 0.0617 \sin^2 k(x-ct)\right] \frac{\partial C}{\partial x}$$

$$- 0.882 v_o k \cos k(x-ct) \left[1 - 0.42 \sin k(x-ct)\right] \frac{h}{3} = D \frac{\partial^2 C}{\partial y^2} \qquad (B-3)$$

Levich previously presented an incorrect solution for the smooth surface laminar convective diffusion equation with very slight penetration (his equation 136.3)

$$\frac{3}{2} v_o \frac{\partial C}{\partial x} = D \frac{\partial^2 C}{\partial y^2} \qquad (B-4)$$

whose solution should have read

$$\frac{C}{C_s} = 1 - \frac{2}{\sqrt{\pi}} \int_0^{\frac{y}{2}\sqrt{\frac{3v_o}{2Dx}}} e^{-z^2} dz \qquad (B-5)$$

Levich's approach to solving equation (B-3) is to assume a solution of the form

$$C = C_1 + C_2 \qquad (B-6)$$

where C_1 is the solution (B-5) of equation (B-4) which fits the boundary condition $C_1 = C_s$ at $y = 0$. Thus C_2 must fit the condition $C_2 = 0$ at $y = 0$ for the composite solution

to fit the desired condition of saturation at the surface. Levich now agrees that a quasi-steady state solution is satisfactory and treats his expression, here replaced by equation (B-3), by time-smoothing over one period. He apparently makes the further assumption that a time-smoothed product is equal to the product of its time-smoothed components. This assumption allows him to eliminate completely any contribution to C of the convective term $v_y \, \partial C/\partial y$, since the time-smoothed value of v_y is zero. Thus his treatment has at this point been altered to a treatment of the steady state, slight penetration, unidirectional, convective diffusion equation

$$v_x \frac{\partial C}{\partial x} = D \frac{\partial^2 C}{\partial y^2} \tag{B-7}$$

where v_x is represented by time-smoothed equation (B-1) evaluated at $y = h$. The mathematical statement of the equation to be solved is

$$\frac{3}{2} v_o (1 + 0.294 \sin \beta - 0.0617 \sin^2 \beta) \frac{\partial (C_1+C_2)}{\partial x} = D \frac{\partial^2 (C_1+C_2)}{\partial y^2} \tag{B-8}$$

where $\beta = k(x - ct)$

Now since $\frac{1}{2\pi} \int_0^{2\pi} \sin \beta \, d\beta = 0$; $\frac{1}{2\pi} \int_0^{2\pi} \sin^2 \beta \, d\beta = \frac{1}{2}$

and equation (B-4) is valid for C_1, equation (B-8) reduces to

$$\frac{3}{2} v_o(0.9692) \frac{\partial C_2}{\partial x} - \frac{3}{2} v_o(0.0308) \frac{\partial C_1}{\partial x} = D \frac{\partial^2 C_2}{\partial y^2} \qquad \text{(B-9)}$$

An expression for the second term in (B-9) may be obtained by differentiating (B-5) with respect to x,

$$\frac{\partial C_1}{\partial x} = \frac{C_s y}{2x^{3/2}} \sqrt{\frac{3v_o}{2\pi D}} \exp\left[-\frac{3 v_o y^2}{8Dx}\right] \qquad \text{(B-10)}$$

which upon substitution into (B-9) and rearranging yields

$$\frac{\partial^2 C_2}{\partial y^2} - \frac{3(0.9692) v_o}{2D} \frac{\partial C_2}{\partial x} = - \frac{3(0.0308) v_o C_s y}{2Dx^{3/2}} \sqrt{\frac{3v_o}{2\pi D}} e^{\left[-\frac{3v_o y^2}{8Dx}\right]} \qquad \text{(B-11)}$$

Now attempt to define a solution

$$C_2 = B \frac{y}{\sqrt{x}} \exp\left[-\frac{y^2}{4(0.9692)Kx}\right] \qquad \text{(B-12)}$$

where $K = (2D)/(3 \cdot 0.9692 \cdot v_o)$ and B is an unknown constant to be determined such that (B-11) is satisfied. Taking the first partial derivative of (B-12) with respect to x, and the second partial derivative with respect to y

$$\frac{\partial C_2}{\partial x} = \frac{-By}{2x^{3/2}} \exp(\eta) + \frac{By^3}{4(0.9692)Kx^{5/2}} \exp(\eta) \qquad \text{(B-13)}$$

and

$$\frac{\partial^2 C_2}{\partial y^2} = \frac{-6By}{4(0.9692)Kx^{3/2}} \exp(\eta) + \frac{By^3}{4(0.9692)^2K^2x^{5/2}} \exp(\eta) \qquad \text{(B-14)}$$

where $\eta = - y^2/[4(0.9692)Kx]$

Substituting equations (B-13) and (B-14) into equation (B-11) with simplification and rearrangement of terms yields

$$B\left[- 4.0616 + \frac{0.1212y^2}{4(0.9692)Kx}\right] = - 0.0617C_s\sqrt{\frac{3v_o}{2\pi D}} \qquad \text{(B-15)}$$

from which an expression for B is obtained

$$B = \frac{(0.0617)C_s\sqrt{\frac{3v_o}{2\pi D}}}{4.0616 - \frac{0.1212\ y^2}{3.8768\ Kx}} \qquad \text{(B-16)}$$

Equation (B-16) indicates that B is still a function of y^2/x. However, if the element in (B-16) that varies with x and y is evaluated for a CO_2-water system at 25° C with values of y between 0 and 0.2 cm, it is found that this

element's magnitude lies between $10^{-5}/x$ and $0.02/x$. This range represents a small contribution, and thus this portion of the expression for B is neglected.

Thus, with B evaluated approximately, the solution for C_2 is

$$\frac{C_2}{C_s} = \frac{0.0617}{4.06} \sqrt{\frac{3v_o}{2\pi D}} \frac{y}{\sqrt{x}} \exp\left[\frac{-3v_o y^2}{8Dx}\right] \qquad \text{(B-17)}$$

The total flux of solute across the gas-liquid interface is determined from equation (B-5) and (B-17)

$$N_A = -D \left.\frac{\partial C}{\partial y}\right|_{y=0} = -D\left[\left.\frac{\partial C_1}{\partial y}\right|_{y=0} + \left.\frac{\partial C_2}{\partial y}\right|_{y=0}\right] \qquad \text{(B-18)}$$

where $-D \left.\frac{\partial C_1}{\partial y}\right|_{y=0}$ is the flux when no surface disturbances are present, and $-D \left.\frac{\partial C_2}{\partial y}\right|_{y=0}$ is the incremental contribution due to waves. Evaluating equation (B-18)

$$N_A = -D\, C_s\left[-\sqrt{\frac{3v_o}{2\pi Dx}} + \frac{0.0617}{4.0616}\sqrt{\frac{3v_o}{2\pi Dx}}\right] = 0.9848\sqrt{\frac{3v_o}{2\pi Dx}} \qquad \text{(B-19)}$$

Equation (B-19) shows that contrary to Levich's statement that a 15 percent increase in mass transfer is predicted by his analysis when waves are present, a 1.52 percent decrease is indicated.

APPENDIX C

EXAMPLES OF CAPACITOMETER TRACES

Appendix C is composed of one-second portions from the capacitometer traces that were used in the experimental determinations of mean film thickness, mean wave frequency, and mean wave amplitude. A complete capacitometer trace usually represented from 10 to 20-second time periods.

Each trace portion is identified by the angle of inclination and film Reynolds number (Re) at which it was taken and by the micrometer reading corresponding to the metal probe position. In order to determine the film height at any instant in time, subtract from the micrometer reading at the cell bottom, the probe position and the air gap distance that corresponds to the particular visicorder reading. Visicorder readings appear directly on each capacitometer trace portion and the air gap may be read from the appropriate capacitometer calibration curve.

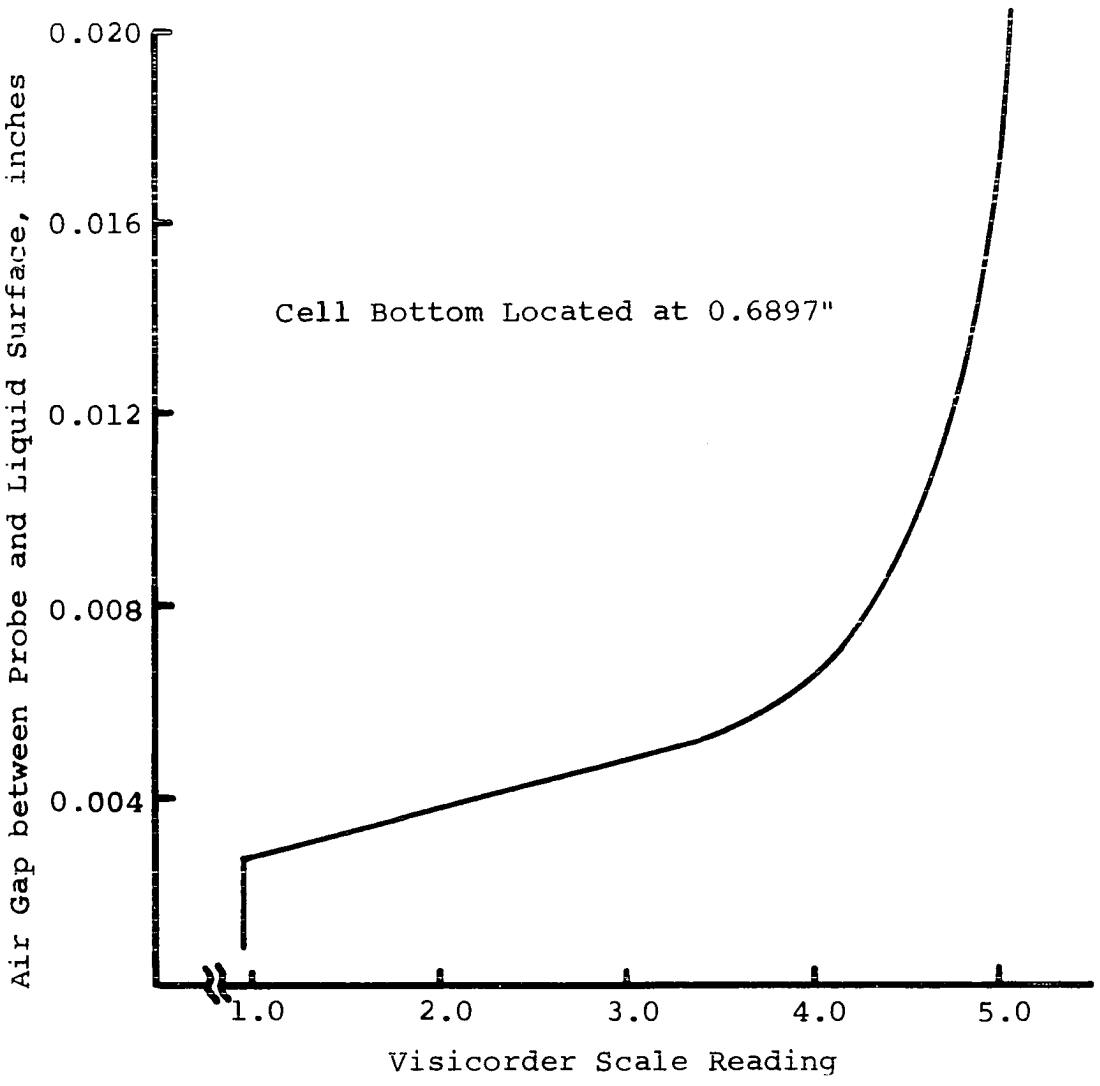

Figure 23

Capacitometer Calibration Curve
for Angles of 1°, 2°, and 3°

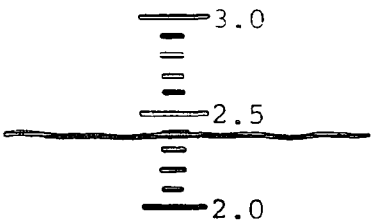

Re= 143
Probe Pos. 0.6620

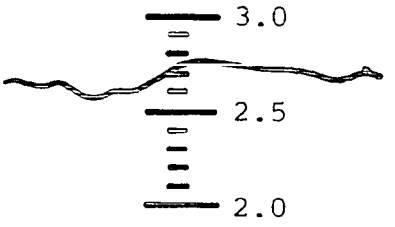

Re= 304
Probe Pos. 0.6540

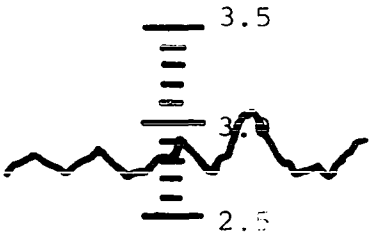

Re= 477
Probe Pos. 0.6480

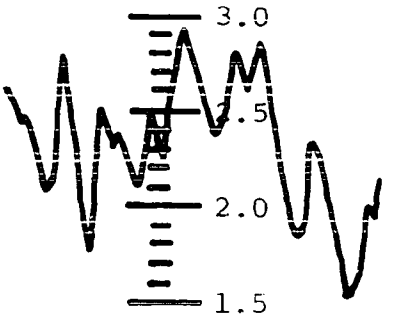

Re= 1069
Probe Pos. 0.6370

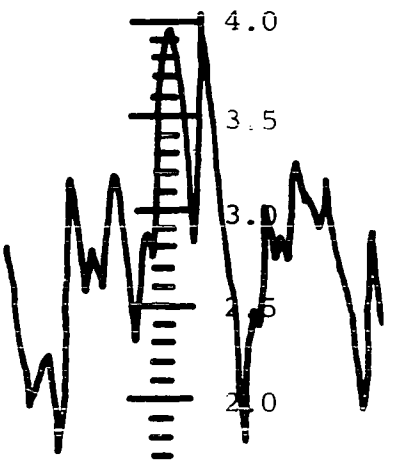

Re= 1480
Probe Pos. 0.6300

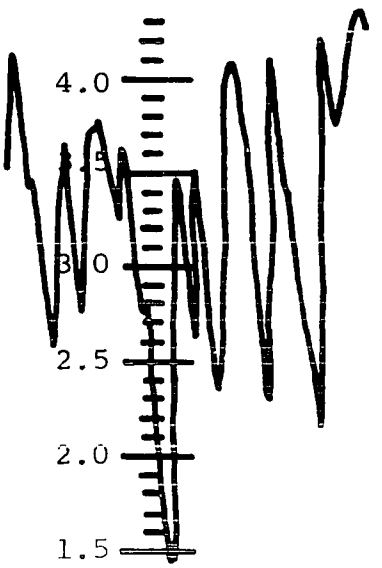

Re= 1870
Probe Pos. 0.6240

Figure 24

One Second Capacitometer Traces at an Angle of 2°

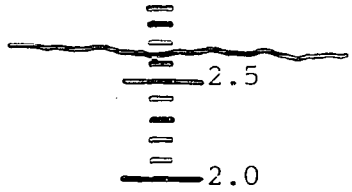

Re= 140
Probe Pos. 0.6650

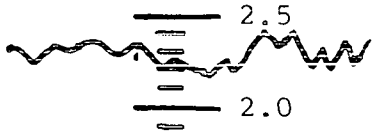

Re= 278
Probe Pos. 0.6590

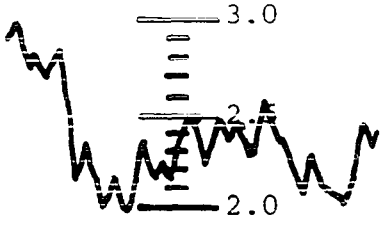

Re= 458
Probe Pos. 0.6530

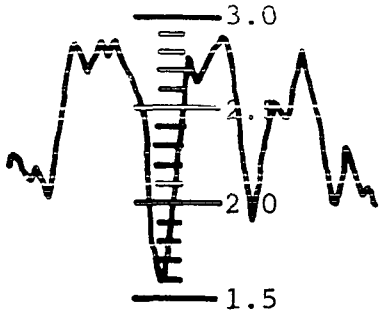

Re= 630
Probe Pos. 0.6490

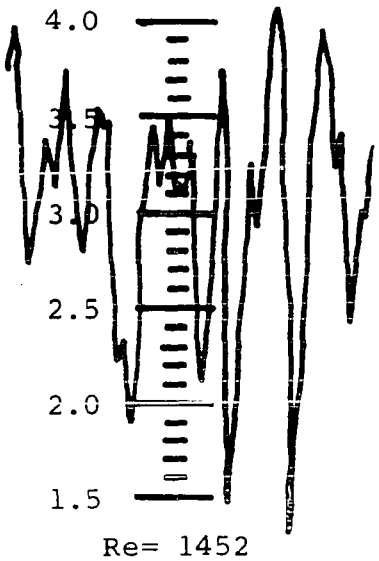

Re= 1452
Probe Pos. 0.6370

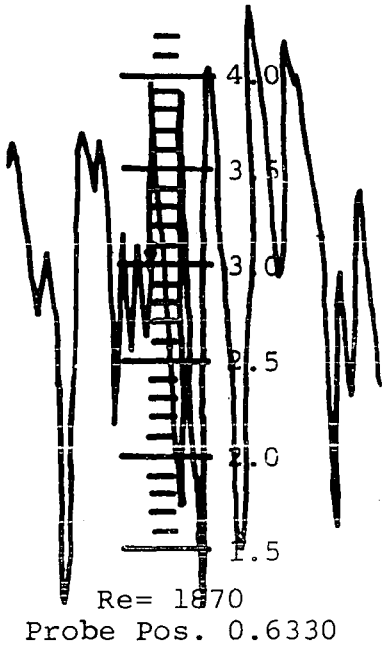

Re= 1870
Probe Pos. 0.6330

Figure 25

One Second Capacitometer Traces at an Angle of 3°

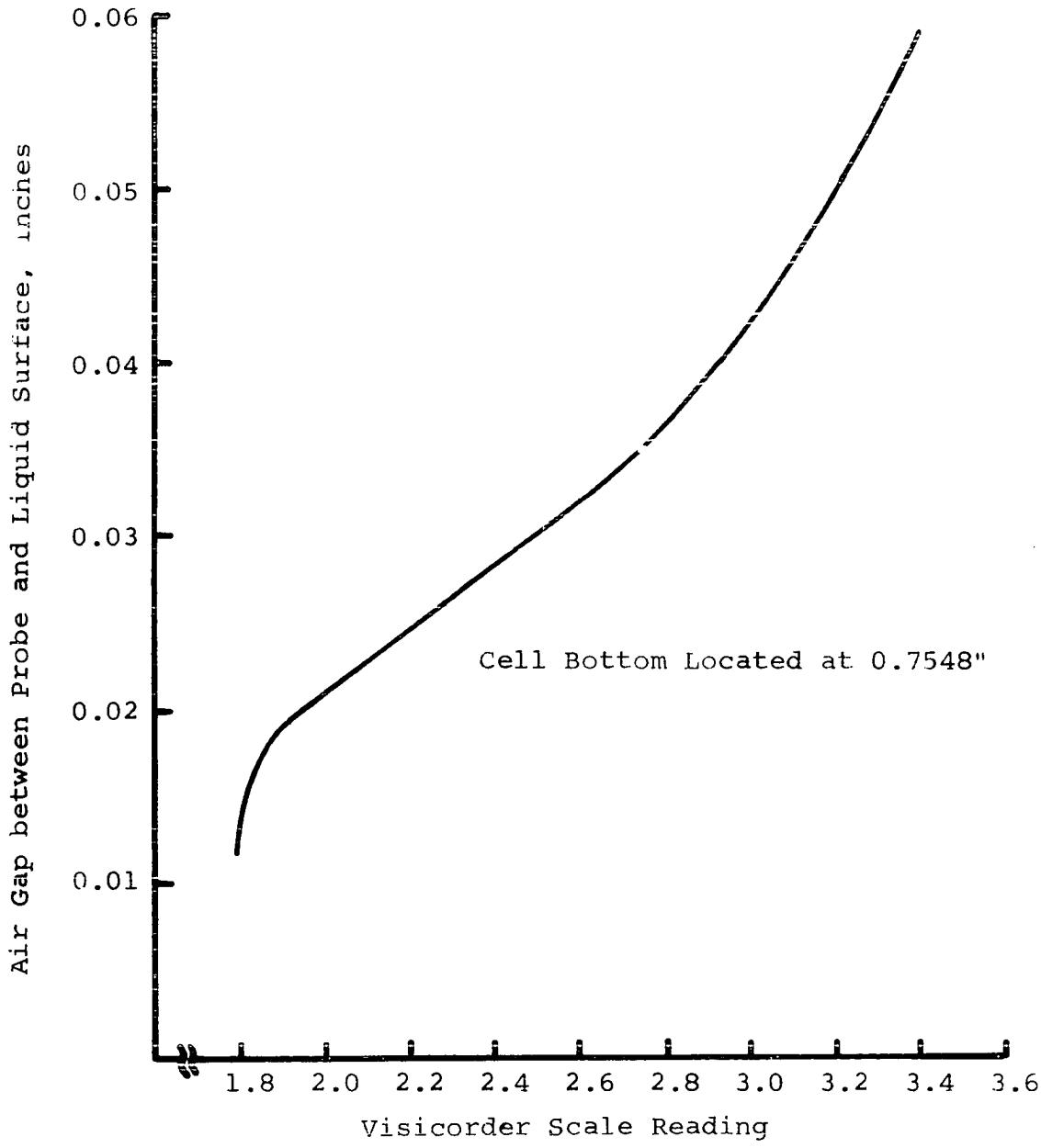

Figure 26

Capacitometer Calibration Curve for Angles of 5°, 10°, 15°, and 25°

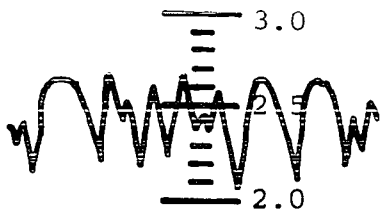

Re= 204
Probe Pos. 0.7100

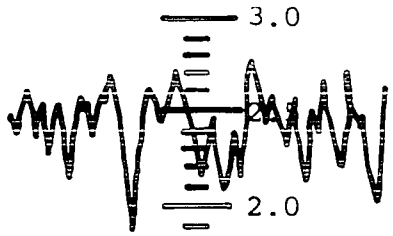

Re= 304
Probe Pos. 0.7080

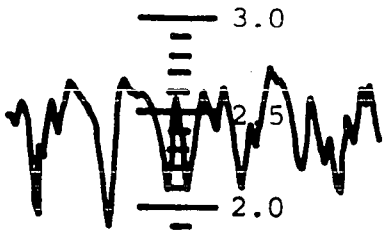

Re= 434
Probe Pos. 0.7060

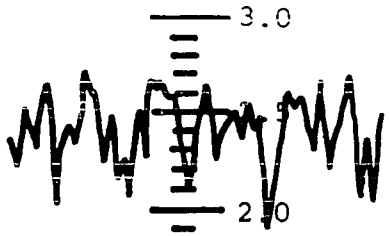

Re= 756
Probe Pos. 0.7030

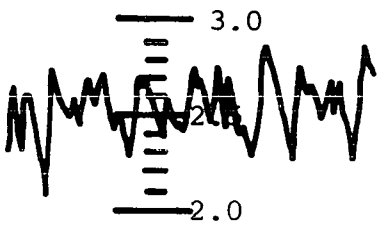

Re= 1160
Probe Pos. 0.6980

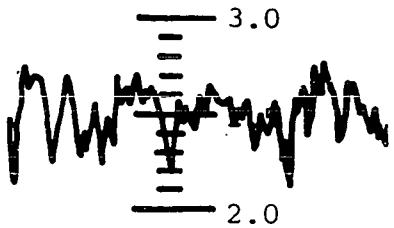

Re= 1526
Probe Pos. 0.6950

Figure 27
One Second Capacitometer Traces at an Angle of 15°

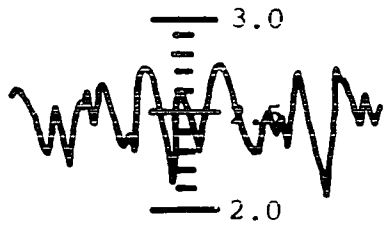

Re= 216
Probe Pos. 0.7120

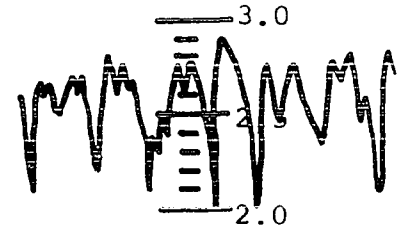

Re= 312
Probe Pos. 0.7080

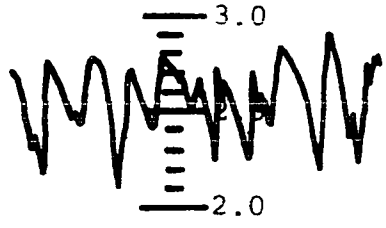

Re= 419
Probe Pos. 0.7060



Re= 703
Probe Pos. 0.6980

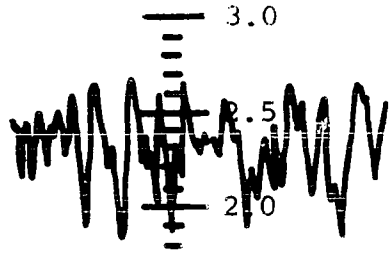

Re= 1072
Probe Pos. 0.7040

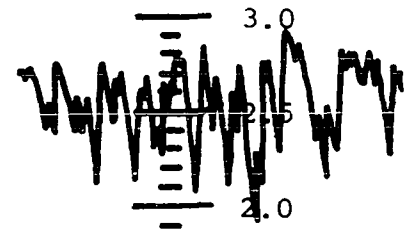

Re= 1385
Probe Pos. 0.7000

Figure 28
One Second Capacitometer Traces at an Angle of 25°

APPENDIX D

EXAMPLES OF INTERFERENCE PROFILES

Appendix D is composed of selected examples of the interference profiles obtained in this study. Included as examples are photographs of the profiles obtained in the quiet pool and flowing film studies.

In addition, Appendix D includes the reduced data of the flowing film interference profiles. Each profile is identified by run number, angle of inclination, liquid film Reynolds number (Re), and the distance in inches from the liquid inlet to where the profile was obtained (Position). Since initially the data were interpreted as concentration profiles, they are presented as the concentration in grams per liter as a function of the height above the bottom plate, in cm.

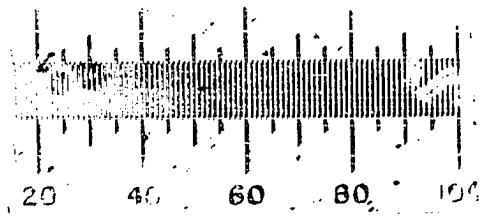

Scale: 200 divisions/cm

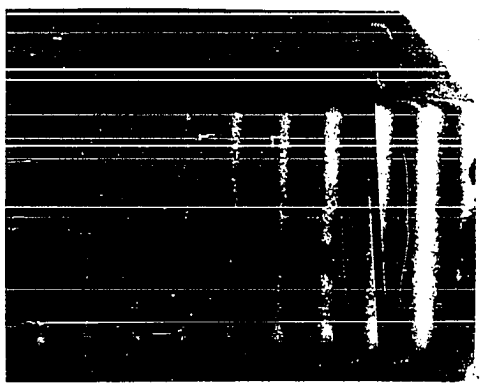

Air saturated water pool

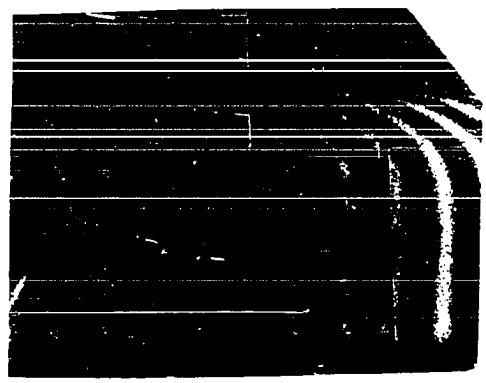

After 1.5 minute exposure to CO_2

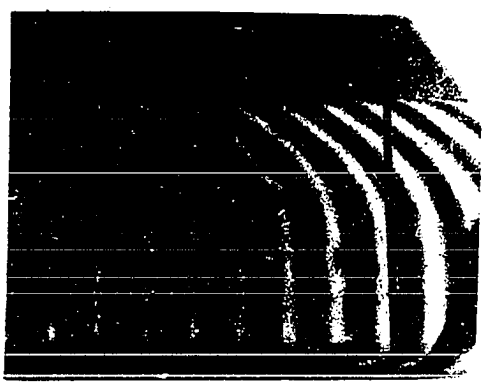

After 2.5 minute exposure to CO_2

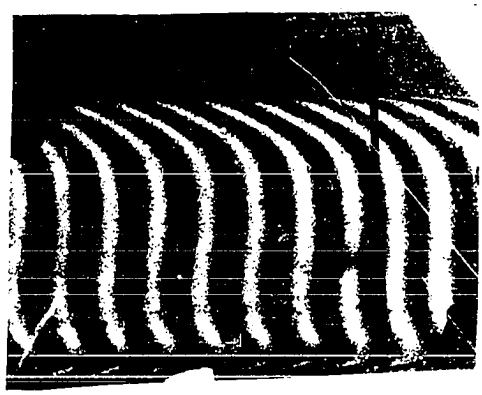

After 3.5 minute exposure to CO_2

Figure 29

Example Interference Profiles from Quiet Pool Studies

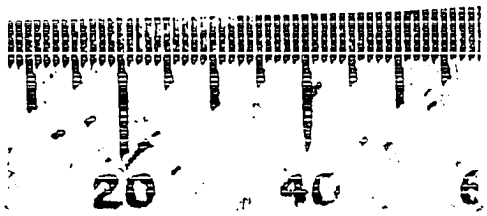

Scale: 200 divisions/cm

Air saturated films | Films exposed to CO_2



Reynolds Number = 304



Reynolds Number = 1069

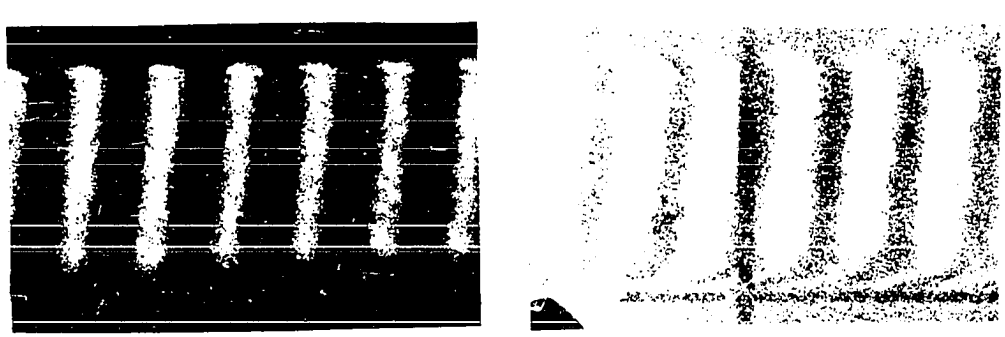

Reynolds Number = 1870

Figure 30. Example Interference Profiles from Flowing Film Studies at an Angle of 2° and a Position 19 inches from Liquid Feed Point

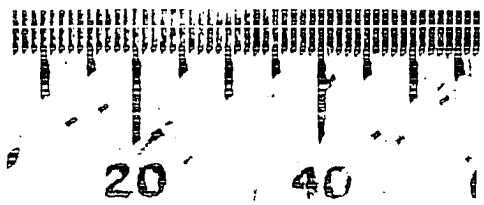

Scale: 200 divisions/cm

Air saturated films | Films exposed to CO_2



Reynolds Number = 304



Reynolds Number = 1069

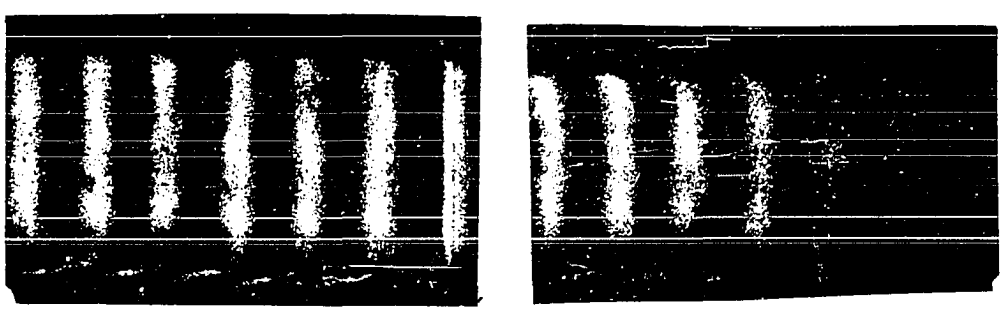

Reynolds Number = 1870

Figure 31. Example Interference Profiles from Flowing Film Studies at an Angle of 2° and a Position 25 Inches from Liquid Feed Point

Run W22-3
Angle 1°
Re = 157
Position 10

y, cm	C, gm/l
0.0000	0
0.0115	0
0.0225	0.0212
0.0346	0.0766
0.0450	0.1942
0.0548	0.4260

Run W22-1
Angle 1°
Re = 328
Position 10

y, cm	C, gm/l
0.0000	0
0.0461	0
0.0600	0.0083
0.0692	0.0953
0.0732	0.2260

Run W23-7
Angle 1°
Re = 507
Position 10

y, cm	C, gm/l
0.0000	0
0.0565	0
0.0801	0.0169
0.0859	0.1260
0.0899	0.2795

Run W23-6
Angle 1°
Re = 701
Position 10

y, cm	C, gm/l
0.0000	0
0.0784	0
0.0962	0.0394
0.1026	0.2140

Run W23-5
Angle 1°
Re = 1103
Position 10

y, cm	C, gm/l
0.0000	0
0.1049	0
0.1188	0.0432
0.1239	0.1350

Run W23-3
Angle 1°
Re = 1550
Position 10

y, cm	C, gm/l
0.0000	0
0.1165	0
0.1384	0.0084
0.1453	0.1598

Run W23-2
Angle 1°
Re = 1940
Position 10

y, cm	C, gm/l
0.0000	0
0.1366	0
0.1643	0.0168
0.1706	0.0925

Run W24-3
Angle 1°
Re = 157
Position 19

y, cm	C, gm/l
0.0000	0
0.0116	0
0.0247	0.0161
0.0399	0.1460
0.0530	0.4123
0.0598	0.6050

Run W24-1
Angle 1°
Re = 328
Position 19

y, cm	C, gm/l
0.0000	0
0.0462	0
0.0578	0.0203
0.0672	0.1220
0.0761	0.3455
0.0808	0.5000

Run W25-7
Angle 1°
Re = 507
Position 19

y, cm	C, gm/l
0.0000	0
0.0220	0
0.0457	0.0095
0.0646	0.0517
0.0777	0.0891
0.0876	0.2960
0.0961	0.6190

Run W25-6
Angle 1°
Re = 701
Position 19

y, cm	C, gm/l
0.0000	0
0.0189	0.0048
0.0394	0.0286
0.0593	0.0524
0.0793	0.0524
0.0919	0.0954
0.1008	0.2810
0.1066	0.4760

Run W25-5
Angle 1°
Re = 1103
Position 19

y, cm	C, gm/l
0.0000	0
0.0740	0
0.0935	0.0268
0.1113	0.0895
0.1223	0.1970
0.1283	0.3760

Run W25-3
Angle 1°
Re = 1550
Position 19

y, cm	C, gm/l
0.0000	0
0.1045	0
0.1244	0.0144
0.1336	0.1294
0.1454	0.3020

Run W25-1
Angle 1°
Re = 1940
Position 19

y, cm	C, gm/l
0.0000	0
0.1155	0
0.1386	0.0324
0.1507	0.0740
0.1591	0.1800
0.1659	0.3530

Run W28-3
Angle 1°
Re = 157
Position 25

y, cm	C, gm/l
0.0000	0
0.0163	0
0.0304	0.0372
0.0462	0.1288
0.0588	0.3320
0.0677	0.5550
0.0746	0.7940

Run W28-1
Angle 1°
Re = 328
Position 25

y, cm	C, gm/l
0.0000	0
0.0567	0
0.0709	0.1168
0.0850	0.4155
0.0947	0.7920

Run W29-7
Angle 1°
Re = 507
Position 25

y, cm	C, gm/l
0.0000	0
0.0667	0
0.0819	0.0195
0.0945	0.1655
0.1034	0.4020
0.1102	0.8170

Run W29-6
Angle 1°
Re = 701
Position 25

y, cm	C, gm/l
0.0000	0
0.0651	0
0.0856	0.0128
0.0982	0.0256
0.1087	0.1088
0.1176	0.3625
0.1239	0.5720

Run W29-5
Angle 1°
Re = 1103
Position 25

y, cm	C, gm/l
0.0000	0
0.1102	0
0.1281	0.0503
0.1402	0.2450
0.1507	0.6750

Run W29-4
Angle 1°
Re = 1550
Position 25

c, cm	C, gm/l
0.0000	0
0.0614	0
0.0934	0.0159
0.1203	0.0320
0.1389	0.0384
0.1460	0.0761
0.1570	0.2140
0.1638	0.4130

Run W29-3
Angle 1°
Re = 1940
Position 25

y, cm	C, gm/l
0.0000	0
0.1449	0
0.1591	0.0322
0.1690	0.1540

Run Z2-3
Angle 2°
Re = 143
Position 19

y, cm	C, gm/l
0.0000	0
0.0056	0.0169
0.0113	0.0473
0.0180	0.0890
0.0265	0.2125
0.0335	0.3280
0.0415	0.4910
0.0473	0.6850

Run Z2-1
Angle 2°
Re = 304
Position 19

y, cm	C, gm/l
0.0000	0
0.0170	0
0.0283	0.0318
0.0397	0.1212
0.0509	0.3540
0.0594	0.6090
0.0655	0.9140

Run Z3-7
Angle 2°
Re = 477
Position 19

y, cm	C, gm/l
0.0000	0
0.0170	0
0.0359	0.0182
0.0511	0.0670
0.0587	0.1097
0.0689	0.3265
0.0772	0.6760
0.0831	1.0000

Run Z3-5
Angle 2°
Re = 655
Position 19

y, cm	C, gm/l
0.0000	0
0.0426	0
0.0587	0.0672
0.0729	0.3360
0.0855	0.9550

Run Z3-3
Angle 2°
Re = 1069
Position 19

y, cm	C, gm/l
0.0000	0
0.0478	0
0.0609	0.0049
0.0764	0.0702
0.0890	0.3415
0.0949	0.4980

Run Z3-1
Angle 2°
Re = 1480
Position 19

y, cm	C, gm/l
0.0000	0
0.0747	0
0.0881	0.0087
0.0996	0.1710
0.1114	0.6650

Run Z4-7
Angle 2°
Re = 1870
Position 19

y, cm	C, gm/l
0.0000	0
0.0714	0
0.1003	0.0273
0.1140	0.1620
0.1212	0.3680

Run Z4-1
Angle 2°
Re = 143
Position 25

y, cm	C, gm/l
0.0000	0
0.0105	0
0.0242	0.0882
0.0360	0.3260
0.0426	0.4980
0.0491	0.7205

Run Z5-7
Angle 2°
Re = 304
Position 25

y, cm	C, gm/l
0.0000	0
0.0295	0
0.0406	0.0553
0.0524	0.2020
0.0623	0.5000

Run Z5-5
Angle 2°
Re = 477
Position 25

y, cm	C, gm/l
0.0000	0
0.0406	0
0.0544	0.0204
0.0636	0.1412
0.0695	0.3825

Run Z5-3
Angle 2°
Re = 655
Position 25

y, cm	C, gm/l
0.0000	0
0.0439	0
0.0583	0.0415
0.0688	0.1620
0.0780	0.4810

Run Z5-1
Angle 2°
Re = 1069
Position 25

y, cm	C, gm/l
0.0000	0
0.0518	0
0.0622	0.0066
0.0832	0.0569
0.0904	0.1550

Run Z6-7
Angle 2°
Re = 1480
Position 25

y, cm	C, gm/l
0.0000	0
0.0662	0
0.0819	0.0050
0.0970	0.0196
0.1048	0.1469

Run Z6-5
Angle 2°
Re = 1870
Position 25

y, cm	C, gm/l
0.0000	0
0.0734	0
0.0898	0.0088
0.1022	0.0525
0.1094	0.1926

Run X1-3
Angle 2°
Re = 143
Position 10

y, cm	C, gm/l
0.0000	0
0.0110	0
0.0215	0.0346
0.0299	0.1355
0.0373	0.3235
0.0420	0.5000

Run X1-1
Angle 2°
Re = 304
Position 10

c, cm	C, gm/l
0.0000	0
0.0315	0
0.0399	0.0238
0.0478	0.1055
0.0541	0.2760

Run X2-7
Angle 2°
Re = 477
Position 10

y, cm	C, gm/l
0.0000	0
0.0399	0
0.0509	0.0094
0.0572	0.0408
0.0640	0.1692

Run X2-6
Angle 2°
Re = 655
Position 10

y, cm	C, gm/l
0.0000	0
0.0394	0
0.0530	0.0243
0.0651	0.0336
0.0735	0.0793
0.0782	0.1860

Run X2-5
Angle 2°
Re = 1069
Position 10

y, cm	C, gm/l
0.0000	0
0.0184	0
0.0368	0.0130
0.0525	0.0225
0.0730	0.0350
0.0824	0.0444
0.0914	0.0725
0.0971	0.1900

Run X2-1
Angle 2°
Re = 1480
Position 10

y, cm	C, gm/l
0.0000	0
0.0945	0
0.1034	0.0090
0.1087	0.0515

Run X2-2
Angle 2°
Re = 1870
Position 10

y, cm	C, gm/l
0.0000	0
0.1087	0
0.1223	0.0120
0.1286	0.0632

Run X3-3
Angle 2°
Re = 143
Position 19

y, cm	C, gm/l
0.0000	0
0.0110	0
0.0205	0.0441
0.0284	0.1543
0.0357	0.3310
0.0446	0.5630

Run X3-1
Angle 2°
Re = 304
Position 19

y, cm	C, gm/l
0.0000	0
0.0304	0
0.0399	0.0414
0.0483	0.2225
0.0541	0.3860

Run X4-7
Angle 2°
Re = 477
Position 19

y, cm	C, gm/l
0.0000	0
0.0242	0
0.0368	0.0131
0.0478	0.0291
0.0578	0.0840
0.0646	0.1908

Run X4-6
Angle 2°
Re = 655
Position 19

y, cm	C, gm/l
0.0000	0
0.0289	0
0.0446	0.0101
0.0556	0.0384
0.0667	0.1152
0.0746	0.2812

Run X4-5
Angle 2°
Re = 1069
Position 19

y, cm	C, gm/l
0.0000	0
0.0766	0
0.0845	0.0389
0.0914	0.1523

Run X4-1
Angle 2°
Re = 1480
Position 19

y, cm	C, gm/l
0.0000	0
0.0530	0
0.0735	0.0063
0.0919	0.0188
0.0992	0.0469
0.1071	0.1598

Run X4-2
Angle 2°
Re = 1870
Position 19

y, cm	C, gm/l
0.0000	0
0.0220	0.0062
0.0457	0.0155
0.0672	0.0217
0.0850	0.0435
0.1034	0.0560
0.1118	0.1182

Run X7-3
Angle 2°
Re = 143
Position 25

y, cm	C, gm/l
0.0000	0
0.0089	0.0049
0.0184	0.0318
0.0273	0.1220
0.0368	0.2615
0.0457	0.4845
0.0504	0.6280
0.0551	0.8410

Run X7-1
Angle 2°
Re = 304
Position 25

y, cm	C, gm/l
0.0000	0
0.0262	0
0.0378	0.0167
0.0467	0.0473
0.0556	0.1780
0.0625	0.3680
0.0688	0.5950

Run X8-7
Angle 2°
Re = 477
Position 25

y, cm	C, gm/l
0.0000	0
0.0294	0
0.0452	0.0216
0.0567	0.0577
0.0667	0.1921
0.0735	0.3505
0.0777	0.4320

Run X8-6
Angle 2°
Re = 655
Position 25

y, cm	C, gm/l
0.0000	0
0.0158	0
0.0304	0.0023
0.0457	0.0046
0.0625	0.0159
0.0730	0.0974
0.0798	0.2310
0.0856	0.3980

Run X8-5
Angle 2°
Re = 1069
Position 25

y, cm	C, gm/l
0.0000	0
0.0346	0
0.0536	0.0149
0.0704	0.0273
0.0808	0.0396
0.0892	0.0890
0.0956	0.1527

Run X8-1
Angle 2°
Re = 1480
Position 25

y, cm	C, gm/l
0.0000	0
0.0252	0
0.0494	0.0133
0.0709	0.0221
0.0914	0.0264
0.0987	0.0353
0.1050	0.0706
0.1129	0.1878

Run X8-2
Angle 2°
Re = 1870
Position 25

y, cm	C, gm/l
0.0000	0
0.0898	0
0.1071	0.0135
0.1171	0.0495
0.1239	0.1416

Run Y1-3
Angle 3°
Re = 140
Position 10

y, cm	C, gm/l
0.0000	0
0.0167	0
0.0251	0.0384
0.0324	0.2470
0.0413	0.6150

Run Y1-1
Angle 3°
Re = 278
Position 10

y, cm	C, gm/l
0.0000	0
0.0366	0
0.0439	0.0107
0.0491	0.1272
0.0548	0.3280

Run Y2-7
Angle 3°
Re = 458
Position 10

y, cm	C, gm/l
0.0000	0
0.0387	0
0.0554	0.0529
0.0611	0.1860
0.0684	0.4300

Run Y2-6
Angle 3°
Re = 630
Position 10

y, cm	C, gm/l
0.0000	0
0.0522	0
0.0627	0.0071
0.0684	0.0641
0.0742	0.3235

Run Y2-4
Angle 3°
Re = 1032
Position 10

y, cm	C, gm/l
0.0000	0
0.0146	0
0.0303	0.0024
0.0462	0.0188
0.0606	0.0361
0.0779	0.0866
0.0826	0.1474
0.0888	0.3820

Run Y2-1
Angle 3°
Re = 1870
Position 10

y, cm	C, gm/l
0.0000	0
0.1102	0
0.1181	0.2160

Run Y3-3
Angle 3°
Re = 140
Position 19

y, cm	C, gm/l
0.0000	0
0.0094	0.0552
0.0199	0.1401
0.0282	0.3530
0.0345	0.5970
0.0402	0.8010

Run Y3-1
Angle 3°
Re = 278
Position 19

y, cm	C, gm/l
0.0000	0
0.0084	0
0.0172	0.0019
0.0198	0.0059
0.0392	0.0560
0.0455	0.1911
0.0517	0.3675

Run Y4-7
Angle 3°
Re = 458
Position 19

y, cm	C, gm/l
0.0000	0
0.0366	0
0.0455	0.0187
0.0491	0.0458
0.0559	0.2140

Run Y4-6
Angle 3°
Re = 630
Position 19

y, cm	C, gm/l
0.0000	0
0.0402	0
0.0534	0.0083
0.0596	0.0228
0.0648	0.1250

Run Y4-5
Angle 3°
Re = 1032
Position 19

y, cm	C, gm/l
0.0000	0
0.0298	0
0.0481	0.0243
0.0627	0.0425
0.0758	0.0445
0.0846	0.1395

Run Y4-1
Angle 3°
Re = 1452
Position 19

y, cm	C, gm/l
0.0000	0
0.0204	0.0125
0.0418	0.0424
0.0601	0.0721
0.0841	0.0956
0.0904	0.1332
0.0977	0.2260

Run Y4-2
Angle 3°
Re = 1870
Position 19

y, cm	C, gm/l
0.0000	0
0.0225	0.0081
0.0418	0.0260
0.0674	0.0585
0.0946	0.0763
0.1040	0.1024
0.1129	0.1707

Run Y7-3
Angle 3°
Re = 140
Position 25

y, cm	C, gm/l
0.0000	0
0.0094	0.0056
0.0193	0.0655
0.0293	0.2870
0.0392	0.6240

Run Y7-1
Angle 3°
Re = 278
Position 25

y, cm	C, gm/l
0.0000	0
0.0099	0.0031
0.0199	0.0094
0.0293	0.0500
0.0376	0.1277
0.0434	0.3420

Run Y8-7
Angle 3°
Re = 458
Position 25

y, cm	C, gm/l
0.0000	0
0.0329	0
0.0423	0.0063
0.0491	0.1010

Run Y8-6
Angle 3°
Re = 630
Position 25

y, cm	C, gm/l
0.0000	0
0.0392	0
0.0460	0.0096
0.0517	0.0158

Run Y8-5
Angle 3°
Re = 1032
Position 25

y, cm	C, gm/l
0.0000	0
0.0120	0.0361
0.0261	0.0656
0.0408	0.0754
0.0585	0.1113
0.0658	0.1968

Run Y8-1
Angle 3°
Re = 1452
Position 25

y, cm	C, gm/l
0.0000	0
0.0366	0
0.0528	0.0080
0.0716	0.0080
0.0815	0.0828

Run Y8-2
Angle 3°
Re = 1870
Position 25

y, cm	C, gm/l
o.0000	0
0.0601	0
0.0815	0.0325
0.0899	0.1030